AD-A251 152

On the Estimation of a Moving Ship's Velocity and Hull Geometry Information from its Wave Spectra

Zhijian Wu
Department of Atmospheric, Oceanic and Space Sciences

Contract Number N00014-86-K-0684
Technical Report No. 91-1

September 1991

DTIC
ELECTE
JUN 1 1992
S C D

DISTRIBUTION STATEMENT A
Approved for public release;
Distribution Unlimited

92-13789

92 5 [illegible] 015

Statement A per telecon Dr. Edwin Rood
ONR/Code 1132
Arlington, VA 22217-5000

NWW 6/1/92

NTIS GRA&I
DTIC TAB
Unannounced
Justification
By
Distribution/
Availability Codes
Dist | Avail and/or Special
A-1

ABSTRACT

ON THE ESTIMATION OF A MOVING SHIP'S VELOCITY AND HULL GEOMETRY INFORMATION FROM ITS WAVE SPECTRA

by

Zhijian Wu

Chairperson: Guy A. Meadows

The wake generated by a moving ship may extend for many tens of kilometers in the open ocean, and can be remotely sensed. Through indirect methods, the detection of a ship and its related characteristics, is generally obtained by measuring the ship generated waves or their spectra. From the viewpoint of remote sensing, interesting problems exist related to the detection of a ship's presence and the acquisition of dynamic and static information about it. This problem can be divided into two basic aspects. First, how to obtain a moving ship's wave spectra from remotely sensed images, and second, how to extract the desired ship information from the imaged wave spectra. This thesis concentrates on the latter aspect, in particular, how to estimate a moving ship's direction, speed, length and hull shape from its wave spectra.

The extraction of ship information is based on the relations of the ship's wave spectra, wave amplitude function and hull geometry. In this thesis, an analytic rep-

resentation of wave elevation is introduced with the use of the Hilbert transform, and the derivation is given for the calculation of the wave amplitude function from the Fourier spectrum of one and two dimensional complex-valued wave elevations. Methods and formulas are given for estimating a ship's speed and direction from the spectrum of a two-dimensional wave patch, a single wave cut or two wave cuts. A theoretical model of the wave amplitude function is developed, and three methods are designed for the estimation of a ship's length from the wave amplitude function. Under the assumption of thin-ship theory, an inversion technique to predict the geometry of a ship's hull from the wave amplitude function or its magnitude is developed through the application of a spectral method and the constrained maximum likelihood method. Examples comparing theoretically calculated data and tow tank experimental data are given to demonstrate the methods developed and estimate performance.

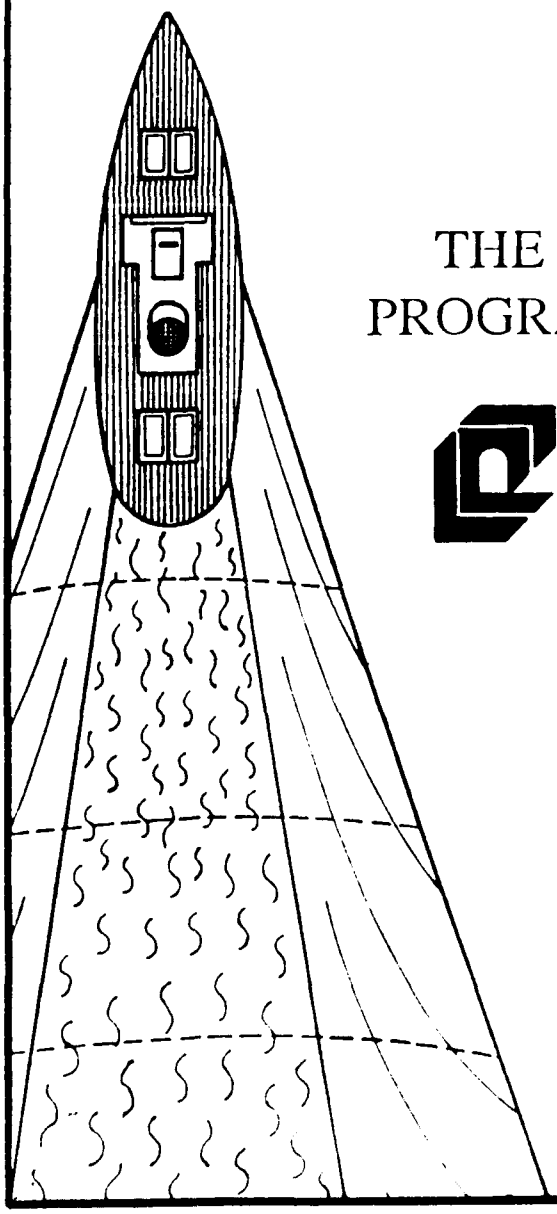

THE UNIVERSITY OF MICHIGAN PROGRAM IN SHIP HYDRODYNAMICS

COLLEGE OF ENGINEERING

NAVAL ARCHITECTURE & MARINE ENGINEERING

AEROSPACE ENGINEERING

MECHANICAL ENGINEERING & APPLIED MECHANICS

SHIP HYDRODYNAMIC LABORATORY

SPACE PHYSICS RESEARCH LABORATORY

ERIM

To my wife
and
my parents

ACKNOWLEDGEMENTS

I wish to thank Professor Guy A. Meadows for serving as the chairman of my dissertation committee. Without his guidance, encouragement and support this thesis could not be completed. His influence on my academic career at the University of Michigan has been substantial.

I would also like to thank Professor Robert F. Beck for his encouragement and suggestion on the selection of my topic and for his support during the research. Thanks also go to Professors Stanley J. Jacobs, John F. Vesecky, and John P. Boyd for their guidance, comments and suggestions. In addition, I am grateful to Professor Leslie A. Olsen and Teaching Assistant Kirstin Fredrickson for their advice on writing.

This work was supported under the Program for Ship Hydrodynamics at the University of Michigan, funded by the University Research Initiative of the Office of Naval Research, Contract No. N000184-86-K-0684. This support has made this work possible.

Finally, I would like to express my appreciation to my wife Debra for her understanding and inspiration, and to my parents, brother and sisters for their moral support.

TABLE OF CONTENTS

DEDICATION ii

ACKNOWLEDGEMENTS iii

LIST OF FIGURES vii

LIST OF TABLES xii

CHAPTER

I. INTRODUCTION 1

II. SHIP WAVE SPECTRA 6

2.1 Ship Wave Elevation and its Analytic Representation 6
2.2 Spectra of Wave Elevation and Slope 10

III. ESTIMATION OF THE WAVE AMPLITUDE FUNCTION FROM WAVE SPECTRA 14

3.1 Estimation from 2-D Wave Fields 16
3.1.1 Loci of Ship Wave Spectra 16
3.1.2 Calculation of the Wave Amplitude Function 19
3.2 Estimation from 1-D Wave Cuts 24
3.3 Effect of Data Sampling Intervals 31
3.3.1 Maximum Resolvable Wave Angles in 1-D Cases . . 32
3.3.2 Maximum Resolvable Wave Angles in 2-D Cases . . 33
3.3.3 Sampling Intervals for a Real Ship and its Model . . 36

IV. ESTIMATION OF A MOVING SHIP'S SPEED AND DIRECTION 39

4.1 Presence of a Moving Ship in Ambient Ocean Waves 39
4.2 Estimation of a Ship's Speed and Direction from 2-D Wave Spectra 43

4.3 Estimation of a Ship's Speed and Direction from 1-D Wave Spectra 50
4.3.1 One-cut Method 51
4.3.2 Two-cut Method 55

V. ESTIMATION OF SHIP LENGTH 60

5.1 Relationship between a Ship's Hull and its Wave Amplitude Function 61
5.2 Periodic Character of the Ship Wave Amplitude Function . . 63
5.2.1 Approximation of $A(K_x)$ for larger ν 68
5.2.2 Periodic Character and the Ship Length Estimation 74
5.2.3 Periodic Character and the Shape of a Ship's Bow and Stern 77
5.2.4 Ship Length Estimation from the Magnitude of $A(K_x)$ 80
5.2.5 Examples of Ship Hulls 83
5.3 Methods of Determination of Ship Length 86
5.3.1 Spectrum Method 88
5.3.2 Zero-Crossing Method 93
5.3.3 Frequency Demodulation Method 96
5.4 Estimation of the Quapaw Hull Length 100

VI. EXTRACTION OF SHIP HULL GEOMETRY INFORMATION 110

6.1 Spectral method 112
6.2 Selection of Basis Functions 114
6.3 Effects of Singularity and Data Error on Linear Inversion . . 120
6.3.1 Effects of the Ill-condition of Matrices 120
6.3.2 Effects of Data Noise 123
6.4 Constrained Linear Inversion 126
6.5 Application of Bayes Theorem to Inverse Problems 130
6.6 Non-Linear inversion 134
6.7 Examples of Ship Hull Estimations 139
6.7.1 Evaluation of Hull Surface Models 140
6.7.2 Estimation of Hull Shape from the Wave Amplitude Function 144
6.7.3 Estimation of Hull Shape from the Magnitude of the Wave Amplitude Function 153

VII. CONCLUSIONS AND RECOMMENDATIONS 162

APPENDIX **166**

BIBLIOGRAPHY 169

LIST OF FIGURES

Figure

1.1 A scheme to extract ship information from remote sensing images. . 2

2.1 Reference coordinate system. The mean water surface is at $z = 0$. . 7

3.1 Loci of wave spectra in the spatial frequency (u, v) plane for different ship speeds U. 18

3.2 1-D wave cut in the ship wave field. 25

3.3 Curves of $\frac{\Phi(\theta)}{K_0 U_p}$ versus θ for different wave cut angles α. 26

3.4 Curves of $\frac{\Phi'(\theta)}{K_0 U_p}$ versus θ for different wave cut angles α. 27

3.5 Maximum resolvable wave angle from 1-D or 2-D wave spectra versus $\frac{\Delta}{U^2}$. 34

4.1 (a) Pseudo image of the wave elevation calculated from WAVEAMP for Quapaw hull model with direction $\alpha = 10°$ and speed U=2.229 m/s. The crest appears dark and the trough bright. (b) Pseudo image of the Fourier transform $H(u, v)$ of the wave elevation from (a). 40

4.2 (a) Pseudo image of the Quapaw ship wave elevation in a random sine ambient wave. (b) Pseudo image of the Fourier transform of the wave elevation from (a). 41

4.3 Two coordinate systems in spatial domain: the ship reference coordinate system xoy and image coordinate system $x_m o_m y_m$ 45

4.4 Two coordinate systems in frequency domain: the ship reference coordinate system uov and image coordinate system $u_m o_m v_m$ 45

4.5 Scheme for estimating a moving ship's direction and speed from its wave spectrum 49

4.6 Contour plot of the Fourier transform $H_m(u_m, v_m)$ of the Quapaw's wave elevation. 50

4.7 Relations between the wave angle θ, cut angle α and frequency f_p at peaks. (a) α versus θ; (b) $\frac{2\pi f_p}{K_0 U_p}$ versus θ; (b) $\frac{2\pi f_p}{K_0 U_p}$ versus α; (b) $\frac{f_{p1}}{f_{p2}}$ versus α. 52

4.8 (a) Wave elevation cut calculated from WAVEAMP for the Quapaw model with wave cut angle $\alpha = 10°$, speed $U = 2.229$ m/s, and $(x_{m0}, y_{m0}) = (-48.5087, -20.5690)$; (b) Magnitude of the Fourier transform (dotted line) of the wave elevation from (a), and two peaks (solid lines) where $f - |\Phi(\theta)| = 0$. 54

4.9 Wave elevation cuts from tow tank experiments for the Quapaw model. 57

4.10 Magnitude of the FFT of wave cuts, RUN5-B and RUN5-C, and their phase difference $\Delta\phi_H$. 58

5.1 $p_{R_2}(\nu)$ and the approximation errors of $p_{R_{2i}}$. 69

5.2 $p_{I_1}(\nu)$ and the approximation errors of $p_{I_{2i+1}}$. 69

5.3 $q_{R_0}(\nu)$ and the approximation errors of $q_{R_{2i}}$. 70

5.4 $q_{I_1}(\nu)$ and the approximation errors of $q_{I_{2i+1}}$. 70

5.5 Hull waterline curve $y = \pm\zeta(x, z_0)$. 79

5.6 Spectrum method for the estimation of ship length 88

5.7 A Wigley-Cosine hull model and its waterline curves $y = \pm\zeta(x, z)$ at $z = -0.3, -0.2, -0.1, 0.0$ meters. 89

5.8 (a) Wave amplitude function of the Wigley-Cosine hull model; (b) Frequency variation of A_R and A_I and their approximation. 90

5.9 Signal waveforms in the ship length estimation from A_R for the Wigley-Cosine hull model using the spectrum method. The estimated ship length is $\hat{L} = 4.825$ m with a relative error of 2.6%. . . . 91

5.10 Zero-crossing method for the estimation of ship length. 93

5.11 Signal waveforms in the ship length estimation from A_I for the Wigley-Cosine hull model using the zero-crossing method. The estimated ship length is $\hat{L}_{zc} = 5.042\ m$ with a relative error of 1.8%. . . 94

5.12 Frequency demodulation method for the estimation of ship length. . 96

5.13 Signal waveforms in the ship length estimation from A_m for the Wigley-Cosine hull model using the frequency demodulation method. The estimated ship length is $\hat{L}_{fd} = 4.949$ meters with a relative error of 0.08%. 98

5.14 Quapaw hull model and its waterline curves $y = \pm\zeta(x, z)$ at $z = -0.3, -0.2, -0.1, -0.001$ meters. 101

5.15 (a) Magnitude of the FFT of the wave elevation for data RUN3-C; (b) magnification of plot (a); (c) the magnitude of the wave amplitude function $|A(K_x)|$ calculated from (a); (d) the spectrum of detrended $|A(K_x)|$. 102

5.16 Quapaw hull length estimation from the tow tank wave cut RUN3-A at $y = 1.219\ m$ using three methods. The estimated ship length is $\hat{L}_{sp} = 4.746\ m$ ($\epsilon_L = 4.2\%$) for the spectrum method, $\hat{L}_{zc} = 5.240\ m$ ($\epsilon_L = 5.8\%$) for the zero-crossing method, and $\hat{L}_{fd} = 4.959\ m$ ($\epsilon_L = 0.1\%$) for the frequency demodulation method. 107

5.17 Quapaw hull length estimation from the tow tank wave cut RUN3-B at $y = 1.524\ m$ using three methods. The estimated ship length is $\hat{L}_{sp} = 4.812\ m$ ($\epsilon_L = 2.8\%$) for the spectrum method, $\hat{L}_{zc} = 5.190\ m$ ($\epsilon_L = 4.8\%$) for the zero-crossing method, and $\hat{L}_{fd} = 4.946\ m$ ($\epsilon_L = 0.1\%$) for the frequency demodulation method. 108

5.18 Quapaw hull length estimation from the tow tank wave cut RUN3-C at $y = 1.8288\ m$ using three methods. The estimated ship length is $\hat{L}_{sp} = 5.347\ m$ ($\epsilon_L = 8.0\%$) for the spectrum method, $\hat{L}_{zc} = 5.290\ m$ ($\epsilon_L = 6.8\%$) for the zero-crossing method, and $\hat{L}_{fd} = 5.078\ m$ ($\epsilon_L = 2.5\%$) for the frequency demodulation method. 109

6.1 Elements λ_i of the diagonal matrices decomposed from (a) $\mathbf{W}_R$ and (b) $\mathbf{W}_I$ with $K = 135$ and $L_1 = 6$ associated with $M = 4$ and $N = 3$; (c) $\mathbf{W}_R$ and (d) $\mathbf{W}_I$ with $K = 135$ and $L_1 = 18$ associated with $M = 6$ and $N = 6$. 121

6.2 Kernel function $e^{s(\theta)z}$ with $F_n = 0.32$ and $\frac{H}{L} = 0.10$ 122

6.3 Relations (a) between N_c and H/L and (b) between N_c and F_n with $M = 4$, $N = 3$ and $K = 135$. 124

6.4 The relative overall r.m.s. residual error ϵ_{ro} of the Wigley-Cosine hull and the Quapaw model in the hull approximation using $N \times N$ basis functions. 143

6.5 Curves of ϵ_{ro} and ϵ_{res} versus γ_s for the modified Wigley hull with $M = N = 6$. No error and noise are present in the input data. . . . 146

6.6 (a) the real part, (b) imaginary part, and (c) the magnitude of the wave amplitude function of the modified Wigley hull, given the parameters $L = 100$ m, $H = 10$ m, $B = 10$ m, and $U = 10$ m/s. The dotted lines represent the wave amplitude function with no noise, and solid lines the one with 10% noise. 147

6.7 The modified Wigley hull recovered from the wave amplitude function with no noise using the constrained ML method, given the parameters $L = 100$ m, $H = 10$ m, $B = 10$ m, $U = 10$ m/s, $M = 6$, $N = 6$, $\gamma_c = 0.$ and $\gamma_s = 10^{-6}$ 148

6.8 The modified Wigley hull recovered from the wave amplitude function with 10% noise using the constrained ML method, given the parameters $L = 100$ m, $H = 10$ m, $B = 10$ m, $U = 10$ m/s, $M = N = 6$, $\gamma_c = 10^{-1}$ and $\gamma_s = 3800$. 149

6.9 (a) The real part, (b) imaginary part, and (c) the magnitude of the wave amplitude function of the Wigley-Cosine hull, given the parameters $L = 100$ m, $H = 10$ m, $B = 10$ m, and $U = 10$ m/s. The dotted lines represent the wave amplitude function with no noise, and solid lines the one with 10% noise. 150

6.10 The Wigley-Cosine hull recovered from the wave amplitude function with 10% noise using the constrained ML method, given the parameters $L = 100$ m, $H = 10$ m, $B = 10$ m, $U = 10$ m/s, $M = N = 6$, and $\gamma_s = 100$. 151

6.11 Curves of ϵ_{ro} and ϵ_{res} verses γ_s given $\gamma_c = 10^{-3}$ and 10^{-2}, and the parameters $L = 100$ m, $H = 10$ m, $B = 10$ m, $U = 10$ m/s, $M = N = 6$, a 10% noise or error in the input data. In the subscripts of ϵ, "mw" represents the modified Wigley hull, "wc" the Wigley-Cosine hull, "a" denotes $\gamma_c = 10^{-1}$, "b" $\gamma_c = 10^{-2}$. 152

6.12 The Wigley-Cosine hull recovered from the magnitude of the wave amplitude function with no noise using the conjugate gradient method, given the parameters $L = 100$ m, $H = 10$ m, $B = 10$ m, $U = 10$ m/s and $M = N = 6$, and $\gamma_s = 0$. 156

6.13 The Wigley-Cosine hull recovered from the magnitude of the wave amplitude function with 10% noise, given the parameters $L = 100$ m, $H = 10$ m, $B = 10$ m, $U = 10$ m/s, $M = 6$, $N = 6$, and $\gamma_s = 100$. 157

6.14 The magnitude of the wave amplitude function obtained from the data RUN5-A and RUN5-B for the Quapaw model with $L = 4.953$ m, $H = 0.362$ m, $B = 0.978$ m, and $U = 2.229$ m/s. 158

6.15 The Quapaw hull estimated from the data RUN5-A using the constrained ML method with $M = 6$, $N = 6$, and $\gamma_s = 100$. 159

6.16 The Quapaw hull estimated from the data RUN5-B using the constrained ML method with $M = 6$, $N = 6$, and $\gamma_s = 100$. 160

6.17 Error performance of the Quapaw hull estimated from the data RUN5-A and RUN5-B, given $M = N = 6$. The subscript "a" represents RUN5-A, and "b" RUN5-B. 161

LIST OF TABLES

Table

4.1 Ship speed estimated from the Quapaw's wave cuts using the two-cut method. 59

5.1 Quapaw hull length estimated from the three wave cuts of RUN3 using the spectrum method, zero-crossing method and frequency demodulation method. The unit of the ship length in the table is *meters*, and the true hull length is 4.953 meters. 106

6.1 The Wigley-Cosine hull's relative overall r.m.s. residual error ϵ_{ro} in the hull approximation using $M \times N$ basis functions. 141

6.2 The Quapaw's relative overall r.m.s. residual error ϵ_{ro} in the hull approximation using $M \times N$ basis functions. 142

6.3 The error performance of the Wigley-Cosine Hull estimated from the magnitude of the wave amplitude function with $M = N = 6$. 154

CHAPTER I

INTRODUCTION

Although a ship's length is bounded within a range of values, the wake it generates in the open ocean may extend for many tens of kilometers. Through indirect methods, the detection of a ship and its related characteristics, is generally obtained by measuring the ship generated waves or their spectra. From the viewpoint of remote sensing, interesting problems exist related to the detection of a ship's presence and the acquisition of dynamic and static information about it. For example, a ship's velocity, size and hull shape are desired characteristics. Figure 1.1 illustrates a scheme for obtaining this information about a ship from remotely sensed images. This problem can be divided into two basic aspects, one is how to obtain a moving ship's wave spectra from remotely sensed images, the second is how to extract the desired ship information from the wave spectra. This work concentrates on the latter aspect, in particular, how to estimate a moving ship's direction, speed, length and hull shape from its wave spectra.

Ship generated surface gravity wave patterns can be remotely detected using several techniques, including visible photography, infrared sensing and microwave radars. Several radar remote sensing techniques can be used to estimate ocean surface directional wave properties, for example, the Ocean Wave Spectrometer (ROWS), the

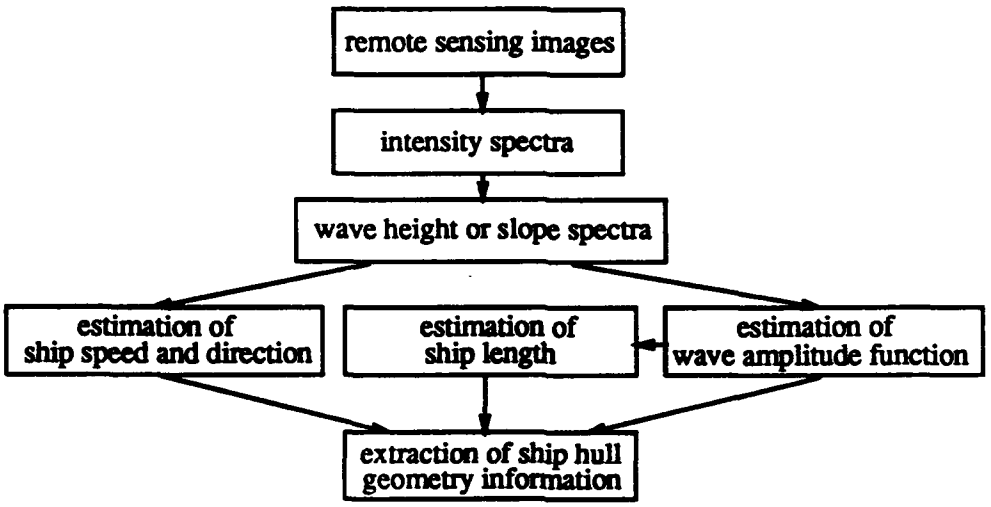

Figure 1.1: A scheme to extract ship information from remote sensing images.

Three-Frequency Airborne Radar (TRIFAR) and Synthetic Aperture Radar (SAR) [1]. Vesecky et al. have studied remote sensing of ocean waveheight spectrum using SAR [2]-[4], and Monaldo et al. have studied the transformation of surface wave slope- and height-variance spectra from radar images [5] in recent years. These techniques may find their applications in the detection of ship characteristics from remotely sensed images. Ship wave spectra have distinct features which are different from those of ambient ocean waves. Tuck et al. have studied the Fourier spectra of real ship wave elevations and indicated the possibility of utilizing this information to estimate ship speed [6]. The estimation of ship hull geometry information from ship waves or their spectra can be considered as an inverse Kelvin wake problem, and has been explored by Kuhn, Newman et al. recently [7]-[9].

Since the inverse Kelvin wake problem is relatively new, little directly related published work exists. The study of this problem will naturally rely, to a great extent, on the existing theories and results on the forward Kelvin wake problem, i.e.,

predicting the wave field due to the geometry of the ship. The forward problem has been studied for several decades with the desire to predict the ship wake and reduce the ship wave resistance to a ship [15]-[28].

Mathematically, the inverse Kelvin wake problem has some characteristics similar to inverse problems in other areas. Thus, the methods developed in those areas will be helpful in finding solutions of this inverse Kelvin wake problem [46]-[54].

In this work, the study of the estimation of a moving ship's speed, direction and hull geometry characteristics from its wave spectra is based on the recognition of the relations among the wave spectra, the wave amplitude function and the ship hull shape. On the spectrum diagram the wave number distribution contains the ship's speed information, the position of spectrum loci contains the ship's direction information, and the magnitude of the wave spectra contains the ship's hull geometry information.

In the following, Chapter 2 and Chapter 3 serve as the theoretical foundation of the study. Based on basic ship wave theory and Fourier theory, Chapter 2 discusses ship generated free waves and their Fourier spectra. An analytic representation of wave elevation is introduced with the use of the Hilbert transform. The concept of complex wave elevation with this analytic representation is helpful in simplifying the derivation of of the wave amplitude function from the wave spectra.

In Chapter 3, the derivation is given for the estimation of the wave amplitude function from the spectra of one and two dimensional complex-valued wave elevations. The spectrum loci on a spectrum diagram, a distinct characteristic of ship wave spectra, are important for the estimation of the ship speed and direction, and thus are mathematically described. The formulas to calculate the wave amplitude function are given in detail. The effects of sampling intervals on the resolution of

wave angles and the wave amplitude function, and the relation between the sampling intervals for a real ship and its model must be understood and considered in tow tank experimental studies or other practical applications. Thus, one section is included for these contents.

With the fundamentals and formulas given in Chapter 2 and Chapter 3, the following chapters develop the theory and methodology for the estimation of a ship's velocity, length and hull surface shape. Chapter 4 first shows the discovery of the presence of a moving ship in an ambient random wave field through a simple example. The methods and formulas for calculating a ship's speed and direction from the spectrum of a two-dimensional wave patch, a single wave cut or two wave cuts are then discussed in detail. The examples with theoretically calculated data and tow tank experimental data are given to demonstrate the methods and the estimation performance.

In Chapter 5, a theoretical model of the wave amplitude function is developed for the estimation of a ship's length from the wave amplitude function. This model explicitly reveals the periodic character inherent in the real and imaginary part and even in the magnitude of the wave amplitude function. It also shows the relation between a ship's length and the periodicity, and the effects of the bow and stern's shape on the periodic character. With this understanding, three methods, the spectrum method, zero-crossing method and frequency demodulation method, are designed to estimate ship length. Examples are given for each method and the results are compared.

Chapter 6 develops a technique to extract a ship's hull geometry shape from the wave amplitude function or from its magnitude under the assumption of the thin-ship theory. The spectral method is used in converting the continuous inverse

problem to a discrete problem, and the selection of basis functions are discussed. The ill-condition of matrices in the resulting equations, noise in input parameters and the wave amplitude function have severe effects on the solution as analyzed in the chapter. To reduce the effects to a minimum, Bayes estimation theory is applied to the inverse problem, and the constraints are considered in both linear and nonlinear cases. The maximum likelihood method with constraints is found to be especially useful in the examples of mathematically well-defined hulls and that of a sea-going tug, the USS Quapaw.

The final chapter, Chapter 7, summarizes the research conducted in this study and gives some recommendations for further efforts.

CHAPTER II

SHIP WAVE SPECTRA

The extraction of ship information is based on the relations of the ship's wave spectra, wave amplitude function and hull geometry. The wave spectra have relations with wave elevation and slopes through Fourier transform. Ship wave numbers contain the desired ship speed information, the position of spectrum loci in spatial frequency space or wavenumber space contains the ship direction information, and the magnitude of wave spectra contains the hull geometry information.

In this chapter, an analytic representation of wave elevation is introduced to simplify the mathematical manipulation in wave spectra later, and then the relation between elevation and slope spectra is discussed for stationary ship wave motions.

2.1 Ship Wave Elevation and its Analytic Representation

Propagating waves and the signals they carry can be modeled as functions of space and time, and they can be analyzed by using multidimensional Fourier transform methods. For general cases, if $s(\mathbf{x}, t)$ represents a signal that is a function of spatial position $\mathbf{x} = (x, y, z)$ and time t, and $S(\mathbf{k}, \omega)$ represents its four-dimensional wavenumber frequency spectrum, then $s(\mathbf{x}, t)$ and $S(\mathbf{k}, \omega)$ can be expressed in terms

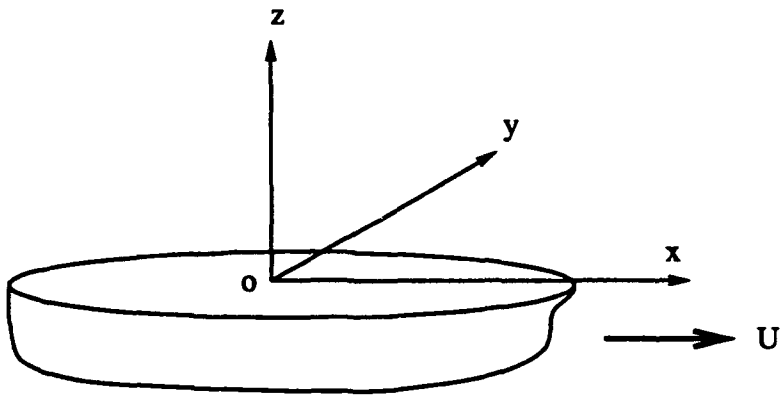

Figure 2.1: Reference coordinate system. The mean water surface is at $z = 0$.

of each other in the following equations [10] :

$$S(\mathbf{k},\omega) = \int_{-\infty}^{\infty}\int_{-\infty}^{\infty} s(\mathbf{x},t)e^{-\mathrm{j}(\omega-\mathbf{k}\cdot\mathbf{x})}d\mathbf{x}dt \tag{2.1}$$

$$s(\mathbf{x},t) = \frac{1}{4\pi}\int_{-\infty}^{\infty}\int_{-\infty}^{\infty} S(\mathbf{k},\omega)e^{\mathrm{j}(\omega-\mathbf{k}\cdot\mathbf{x})}d\mathbf{k}d\omega \tag{2.2}$$

where $\mathrm{j} = \sqrt{-1}$, and $\mathbf{k}\cdot\mathbf{x}$ represents the inner product of the wavenumber $\mathbf{k}$ and the position vector $\mathbf{x}$. The space-time signal $s(\mathbf{x},t)$ can be considered as the superposition of numerous elemental propagating waves $\exp\{\mathrm{j}(\omega - \mathbf{k}\cdot\mathbf{x}\}$ weighted by $S(\mathbf{k},\omega)$.

In the problems below, the wave field is generated by a moving ship in deep water and it can be described as a three-dimensional problem, i.e, x and y in space and t in time. Additionally, the assumption of linearized free-surface boundary condition is made. Now, consider a reference system moving with the ship in the positive x-direction with speed U, as shown in Figure 2.1, then the wave elevation $\eta(x,y,t)$ can be expressed in the following form [14]

$$\eta(x,y,t) = Re\{\int_0^{\infty} d\omega \int_0^{2\pi} d\theta\, A(\omega,\theta)\, e^{-\mathrm{j}K(x\cos\theta+y\sin\theta)+\mathrm{j}(\omega-KU\cos\theta)t}\} \ . \tag{2.3}$$

Here, θ is the wave angle, $A(\omega, \theta)$ is called the wave amplitude function, and $K(\omega)$ is the wave number corresponding to a given frequency ω in accordance with the dispersion relation for infinite depth

$$K = \frac{\omega^2}{g} \tag{2.4}$$

where g denotes the acceleration of gravity. For real problems, the wave elevation is always real; thus, the operation, $Re\{\cdot\}$, to take the real part is used in (2.3).

It will be more convenient, however, if the real operation in (2.3) can be left out in the complicated mathematical manipulation. For this purpose, the complex-valued wave elevation is introduced here with the use of the Hilbert transform. The Hilbert transform of a real-valued signal $\chi(t)$ is another real-valued signal, which is defined by the convolution integral of $\chi(t)$ and $\frac{1}{\pi t}$ [11]. That is, if the Hilbert transform of $\chi(t)$ is denoted by $\check{\chi}(t)$, then

$$\check{\chi}(t) = \mathcal{H}\{\,\chi(t)\,\} = \int_{-\infty}^{\infty} \frac{\chi(\tau)}{\pi(t-\tau)} d\tau \ . \tag{2.5}$$

An analytic signal $\tilde{\chi}(t)$ associated with $\chi(t)$ is defined by

$$\tilde{\chi}(t) = \chi(t) + \mathrm{j}\,\check{\chi}(t) \tag{2.6}$$

and it can be expressed with a magnitude function $a(t)$ and a phase function $\varphi(t)$, where $a(t)$ describes the envelope of the original function $\chi(t)$, and $\varphi(t)$ describes the instantaneous phase of $\chi(t)$. Thus, $\tilde{\chi}(t)$ can be written in the form

$$\tilde{\chi}(t) = a(t)\, e^{\mathrm{j}\varphi(t)} \tag{2.7}$$

where

$$\begin{aligned} a(t) &= [\chi(t) + \check{\chi}(t)]^{\frac{1}{2}} \\ \varphi(t) &= \tan^{-1}[\,\frac{\check{\chi}(t)}{\chi(t)}\,] \ . \end{aligned}$$

A useful property of an analytic signal $\tilde{\chi}(t)$ is the Fourier transform relations among $\chi(t)$, $\check{\chi}(t)$ and $\tilde{\chi}(t)$. Let $X(f)$, $\check{X}(f)$ and $\tilde{X}(f)$ be the Fourier transforms of $\chi(t)$, $\check{\chi}(t)$ and $\tilde{\chi}(t)$, respectively. Then, it can be proved that

$$\check{X}(f) = -\mathrm{j}\, sgn(f)\, X(f) \tag{2.8}$$

$$\tilde{X}(f) = [1 + sgn(f)]\, X(f) = \begin{cases} 2X(f) & \text{for } f > 0 \\ X(f) & \text{for } f = 0 \\ 0 & \text{for } f < 0 \end{cases} \tag{2.9}$$

where $sgn(f)$ is a sign function which is defined as $sgn(f) = 1$ if $f > 0$, $sgn(f) = 0$ if $f = 0$ and $sgn(f) = -1$ if $f < 0$. From these relations, $\check{X}(f)$ and $\tilde{X}(f)$ can be obtained once $X(f)$ is available.

Now, consider two analytic signals associated with the real signals

$$f_1(\tau) = Re\{\, Ae^{-\mathrm{j}\Omega\tau} \,\} \tag{2.10}$$

$$f_2(\tau) = Re\{\, Ae^{\mathrm{j}\Omega\tau} \,\} \tag{2.11}$$

where A is complex and independent of τ, and Ω is real. With the help of the following Hilbert transform relations of sine and cosine with constants c_1 and c_2:

$$\mathcal{H}\{\, \cos(c_1\tau + c_2) \,\} = \sin(c_1\tau + c_2)$$

$$\mathcal{H}\{\, \sin(c_1\tau + c_2) \,\} = -\cos(c_1\tau + c_2)$$

the analytic signals of $f_1(\tau)$ and $f_2(\tau)$ are given by

$$\tilde{f}_1(\tau) = \begin{cases} A^* e^{\mathrm{j}\Omega\tau} & \text{for } \Omega \geq 0 \\ Ae^{-\mathrm{j}\Omega\tau} & \text{for } \Omega < 0 \end{cases} \tag{2.12}$$

$$\tilde{f}_2(\tau) = \begin{cases} Ae^{\mathrm{j}\Omega\tau} & \text{for } \Omega \geq 0 \\ A^* e^{-\mathrm{j}\Omega\tau} & \text{for } \Omega < 0 \end{cases} \tag{2.13}$$

where A^* denotes the conjugate of A.

By applying the above concept for an analytic signal to the wave elevation given in (2.3), the complex-valued wave elevation, i.e., the analytic representation of the wave elevation can be derived. In terms of formula (2.12), the analytic representation of $\eta(x,y,t)$ is now given by

$$\begin{aligned}\tilde{\eta}(x,y,t) &= \eta(x,y,t) + \mathrm{j}\,\check{\eta}(x,y,t) \\ &= \int_0^\infty d\omega \int_{-\frac{\pi}{2}}^{\frac{\pi}{2}} d\theta\, A^*(\omega,\theta)\, e^{\mathrm{j}K(x\cos\theta + y\sin\theta) - \mathrm{j}(\omega - KU\cos\theta)t} \\ &\quad + \int_0^\infty d\omega \int_{\frac{\pi}{2}}^{\frac{3\pi}{2}} d\theta\, A(\omega,\theta)\, e^{-\mathrm{j}K(x\cos\theta + y\sin\theta) + \mathrm{j}(\omega - KU\cos\theta)t} \qquad (2.14)\end{aligned}$$

where the Hilbert transform is taken with respect to x. The above analytic representation of wave elevation and the property of the Hilbert Transform in (2.9) will be helpful in the following mathematical derivation.

2.2 Spectra of Wave Elevation and Slope

Equation (2.3) describes a non-steady wave motion, that is, the wave elevation changes not only with the spatial position but also with time. If the motion is steady state in the reference system moving with the ship, however, expression (2.3) must be independent of time. Thus,

$$KU\cos\theta - \omega = 0 \qquad (2.15)$$

and the phase velocity of each admissible wave component can be obtained from (2.15),

$$V_p \triangleq \frac{\omega}{K} = U\cos\theta \ . \qquad (2.16)$$

From (2.4) and (2.15), the wave number $K(\theta)$ can be related to the ship speed and wave angle θ in the form

$$K(\theta) = \frac{g}{U^2 \cos^2 \theta} \quad . \tag{2.17}$$

The restriction (2.15) can be used to eliminate the variable t. By retaining the wave angle θ and by noting that (2.15) and (2.16) require that $\cos\theta > 0$, the free-wave distribution of a given ship for the deep-water case now can be expressed from (2.3) in its real form

$$\eta(x,y) \;=\; Re\{\int_{-\frac{\pi}{2}}^{\frac{\pi}{2}} A(\theta)\, e^{-j[K_x(\theta)\,x + K_x(\theta)\,y]} d\theta\,\} \tag{2.18}$$

where

$$\begin{aligned} K_x(\theta) &= K(\theta)\cos\theta \\ K_y(\theta) &= K(\theta)\sin\theta\,. \end{aligned}$$

Note that θ must now range from $-\frac{\pi}{2}$ to $\frac{\pi}{2}$ because of the requirement $\cos\theta > 0$. The analytic representation of wave elevation now becomes

$$\tilde{\eta}(x,y) \;=\; \int_{-\frac{\pi}{2}}^{\frac{\pi}{2}} A^*(\theta)\, e^{j[K_x(\theta)\,x + K_x(\theta)\,y]} d\theta \tag{2.19}$$

where the Hilbert transform is taken with respect to x. Additionally, the wave elevation spectrum is given for the real wave elevation by

$$H(u,v) = \mathcal{F}\{\,\eta(x,y)\,\} = \int_{-\infty}^{\infty}\int_{-\infty}^{\infty} \eta(x,y) e^{-j2\pi(ux+vy)} dx dy \tag{2.20}$$

and for the complex wave elevation by

$$\tilde{H}(u,v) = \mathcal{F}\{\,\tilde{\eta}(x,y)\,\} = \int_{-\infty}^{\infty}\int_{-\infty}^{\infty} \tilde{\eta}(x,y) e^{-j2\pi(ux+vy)} dx dy \tag{2.21}$$

where u and v are the spatial frequencies associated with x and y, respectively.

The relation between the wave elevation and its spectrum has been now established through Fourier relations. Theoretically, thus, the ship information can be recovered from either the wave elevation itself or its spectrum. In some real situations such as in remote sensing, however, the available information on ship waves may not be the wave elevation or its spectra but wave slopes or the slope spectra. Therefore, a brief investigation of the relations among them is made below.

The surface wave slope vector $\tilde{\mathbf{s}}$ is defined by the gradient of the wave elevation, i.e.,

$$\tilde{\mathbf{s}}(x,y) = \nabla\tilde{\eta} \;=\; \tilde{\eta}_x(x,y)\,\hat{x} + \tilde{\eta}_y(x,y)\,\hat{y} \tag{2.22}$$

where ∇ denotes the gradient operation, $\hat{x}$ and $\hat{y}$ denote the unit vector in $x-$ and $y-$ directions, and $\tilde{\eta}_x$ and $\tilde{\eta}_y$ are the partial derivatives of wave elevation with respect to x and y, respectively. In terms of the properties of Fourier transform, the spectra of the slope components are given by

$$\tilde{H}_x(u,v) \;=\; \mathcal{F}\{\,\tilde{\eta}_x(x,y)\,\} = \mathrm{j}2\pi u\tilde{H}(u,v) \tag{2.23}$$

$$\tilde{H}_y(u,v) \;=\; \mathcal{F}\{\,\tilde{\eta}_y(x,y)\,\} = \mathrm{j}2\pi v\tilde{H}(u,v) \tag{2.24}$$

and the vector slope spectrum is given by

$$\tilde{\mathbf{S}}(u,v) = \mathcal{F}\{\,\tilde{\mathbf{s}}(x,y)\,\} = \mathrm{j}2\pi(u\hat{x} + v\hat{y})\tilde{H}(u,v) \quad . \tag{2.25}$$

A slope component in any direction $\hat{\mathbf{n}}$, denoted by $\tilde{\mathbf{s}}_n(x,y)$, can be obtained from the directional derivatives of wave elevation, that is,

$$\tilde{s}_n(x,y) = \hat{\mathbf{n}}\cdot\tilde{\mathbf{s}}(x,y) \quad . \tag{2.26}$$

Thus, its spectrum is

$$\tilde{S}_n(u,v) = \hat{\mathbf{n}}\cdot\mathcal{F}\{\,\tilde{\mathbf{s}}(x,y)\,\} = \mathrm{j}2\pi\,[\,\hat{\mathbf{n}}\cdot(u\hat{x} + v\hat{y})\,]\,\tilde{H}(u,v) \quad . \tag{2.27}$$

In terms of the above relations, slope spectra can be obtained once elevation spectra are available. Similarly, elevation spectra is also obtainable from slope spectra, except at zero frequency since the denominator will be zero at zero frequency . The zero frequency component of the elevation spectra represents the average value of wave elevation, and it is not very important in many real situations. Because of the relation between slope spectra and elevation spectra, the discussion in later chapters will focus only on the elevation spectra.

CHAPTER III

ESTIMATION OF THE WAVE AMPLITUDE FUNCTION FROM WAVE SPECTRA

In this chapter, ship wave spectrum patterns are discussed and the relationship between the wave amplitude functions and wave spectra is derived. As stated in the last chapter, the ship generated stationary wave elevation and its spectrum are entirely dependent on wave numbers and the wave amplitude function. Generally speaking, the wave elevation or wave spectra can be directly measured or remotely sensed, but the wave amplitude function can not. As will be seen in the following chapters, however, dynamic and static information about a moving ship, such as speed and hull geometry, is strongly reflected in wave numbers and the wave amplitude function. Thus, recovering the wave amplitude function from wave spectra is an important procedure for obtaining this information.

The wave pattern analysis, especially the estimation of the wave amplitude function, also plays an important role in the ship wave resistance analysis because of its direct relation with wave resistances. For the purpose of analyzing the ship wave resistances, different derivation methods to calculate the wave amplitude function were introduced in the last twenty years [15]-[22]. Ship wave patterns not only contain the information that can be extracted to estimate ship wave resistances, but

also contain other useful ship information, thus, ship wave pattern analysis is also an important means for remotely sensing ship information [6].

In this chapter, the explicit and succinct expressions for the wave amplitude function are established from one- or two-dimensional wave spectra based on the analytic representation of wave elevation. The distinct characteristics of ship wave spectra can be observed in these derivations, and they become the basis for the estimation of ship speed and direction in the next chapter. The effect of sampling intervals on the wave angle and wave amplitude function is also discussed for practical use of this formulas. In this chapter, the first section discusses two dimensional wave fields; the second section discusses one dimensional wave cuts; and the final section discusses the effect of sample intervals.

Before discussing the estimation of the wave amplitude function, it is helpful to review briefly some formulas about the δ function, which can be found in reference [41],

$$\delta(x) = \delta(-x) \tag{3.1}$$

$$\delta(x,y) = \delta(x)\delta(y) \tag{3.2}$$

$$f(x)\delta(x-a) = f(a)\delta(x-a) \tag{3.3}$$

$$\int \delta(x-y)\delta(y-a)dy = \delta(x-a) \tag{3.4}$$

$$\delta(q(x)) = \sum_j \frac{1}{|q'(x_j)|}\delta(x-x_j) \tag{3.5}$$

where x_j is the root of $q(x) = 0$, and its derivative $q'(x_j) \neq 0$.

3.1 Estimation from 2-D Wave Fields

As seen in Chapter 2, the ship generated surface wave can be described as a two-dimensional (2-D) wave field. The two-dimensional wave or spectrum data can be obtained either in tow tank experiments [23], [30], or possibly by remote sensing methods [5], [31]. The most distinct signature contained in ship wave spectra, different from general ocean wave patterns, is the locus in the spatial frequency plane. The first subsection below discusses the properties of the wave spectra. The second subsection discusses the relation between the wave amplitude function and the wave spectra, the discrete forms for calculating the wave amplitude function and the effect of truncated errors.

3.1.1 Loci of Ship Wave Spectra

In this subsection, discussion starts from the complex-valued wave elevation. From Chapter 2, a stationary wave elevation is given by

$$\tilde{\eta}(x,y) = \eta(x,y) + \mathrm{j}\,\check{\eta}(x,y) = \int_{-\frac{\pi}{2}}^{\frac{\pi}{2}} A^*(\theta)\, e^{\mathrm{j}[K_x(\theta)\,x + K_x(\theta)\,y]} d\theta \tag{3.6}$$

where the wave angle θ ranges from $-\frac{\pi}{2}$ to $\frac{\pi}{2}$ and the wave amplitude function $A(\theta)$ is complex.

To obtain the wave elevation spectrum, the Fourier transform of the wave elevation is taken and it follows that

$$\begin{aligned}
\tilde{H}(u,v) &= \int_{-\infty}^{\infty}\int_{-\infty}^{\infty} \tilde{\eta}(x,y) e^{-\mathrm{j}2\pi(ux+vy)} dx dy \\
&= \int_{-\frac{\pi}{2}}^{\frac{\pi}{2}} A^*(\theta)\{\int_{-\infty}^{\infty}\int_{-\infty}^{\infty} e^{-\mathrm{j}2\pi[(u-\frac{K_x(\theta)}{2\pi})x+(v-\frac{K_y(\theta)}{2\pi})y]} dx dy\} d\theta \\
&= \int_{-\frac{\pi}{2}}^{\frac{\pi}{2}} A^*(\theta)\delta(u - \frac{K_x(\theta)}{2\pi})\delta(v - \frac{K_y(\theta)}{2\pi}) d\theta\,. \qquad (3.7)
\end{aligned}$$

Now, let

$$g_1(\theta) = u - \frac{K_x(\theta)}{2\pi} \tag{3.8}$$

$$g_2(\theta) = v - \frac{K_y(\theta)}{2\pi} \tag{3.9}$$

and let θ_1 and θ_2 be the roots of $g_1(\theta)$ and $g_2(\theta)$, respectively. Then, in terms of the δ formulas, (3.7) becomes

$$\begin{aligned} \tilde{H}(u,v) &= \int_{-\frac{\pi}{2}}^{\frac{\pi}{2}} A^*(\theta) \frac{\delta(\theta-\theta_1)}{|g_1'(\theta_1)|} \frac{\delta(\theta-\theta_2)}{|g_2'(\theta_2)|} d\theta \\ &= \frac{A^*(\theta_1)}{|g_1'(\theta_1)|\,|g_2'(\theta_2)|} \delta(\theta_1-\theta_2) \end{aligned} \tag{3.10}$$

where g_1' and g_2' represent the derivatives of g_1 and g_2, respectively, with respect to θ. In terms of (3.10), thus, the wave spectrum $\tilde{H}(u,v)$ is combined with a number of impulses with intensity $\frac{A^*(\theta_1)}{|g_1'(\theta_1)||g_2'(\theta_2)|}$ at position $\theta_1 = \theta_2$. Here, θ_1 or θ_2 is solved from $g_1(\theta) = 0$ and $g_2(\theta) = 0$, that is,

$$u = \frac{K_x(\theta)}{2\pi} \tag{3.11}$$

$$v = \frac{K_y(\theta)}{2\pi} \ . \tag{3.12}$$

This set of parametric equations represent a locus on the (u,v)-plane, or the wave spatial frequency plane and describe the distribution of ship wave components on this plane. That is, only the spectrum values on this locus are non-zero. Besides, the spatial frequencies u and v in the domain of the Fourier transform are consistent very well with the ship wave numbers, K_x and K_y, in the $x-$ and $y-$ directions. Thus, the locus on the spatial frequency plane contains ship information.

The wave angle θ and the wave number $K(\theta)$ can be expressed as functions of u and v. By solving (3.11) and (3.12), it follows that

$$\theta = \tan^{-1}(\frac{v}{u}) \tag{3.13}$$

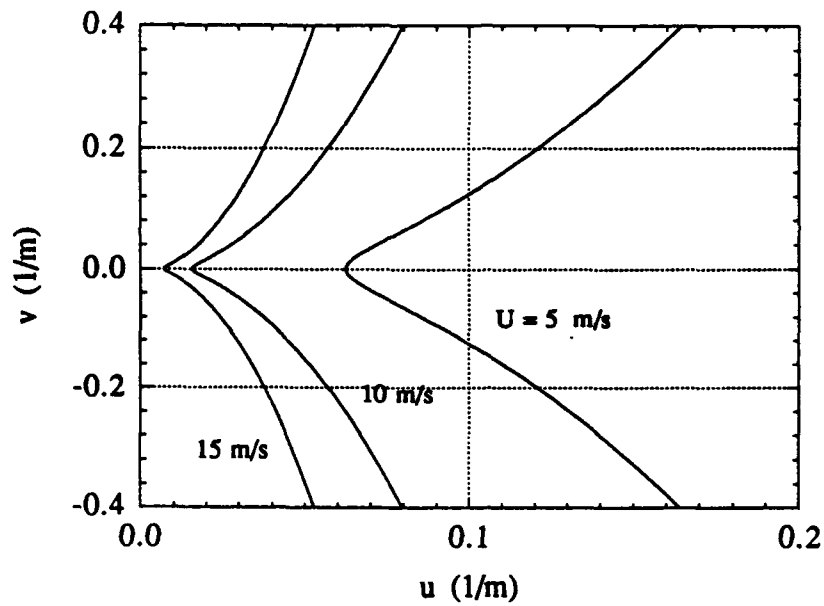

Figure 3.1: Loci of wave spectra in the spatial frequency (u, v) plane for different ship speeds U.

$$K(\theta) = \frac{K_0}{\cos^2\theta} = 2\pi(u^2+v^2)^{\frac{1}{2}} \tag{3.14}$$

where

$$K_0 \triangleq \frac{g}{U^2} \quad . \tag{3.15}$$

The locus of ship wave elements can be also expressed by one equation. For this, canceling θ in (3.13) and (3.14), it follows that

$$u^4 - (\frac{K_0}{2\pi})^2(u^2+v^2) = 0 \quad . \tag{3.16}$$

The loci on the (u, v) plane for different moving speeds are plotted in Figure 3.1. As shown in the figure, the wave components are located in the first and fourth quadrants of the (u, v) wave spatial frequency plane since the wave angles θ are in $[-\frac{\pi}{2}, \frac{\pi}{2}]$ and $u > 0$.

3.1.2 Calculation of the Wave Amplitude Function

In this subsection, an explicit and succinct expression for the wave amplitude function is established from two-dimensional continuous or discrete wave spectra.

Since the wave spectrum is combined with the δ functions as shown in (3.10), it is possible to obtain the expression of $A(\theta)$ by integrating both sides of (3.10), resulting in

$$A^*(\theta_1) = |g_1'(\theta_1)|\,|g_2'(\theta_1)| \int_{-\frac{\pi}{2}}^{\frac{\pi}{2}} \tilde{H}(u,v)d\theta_2 \ . \tag{3.17}$$

However, this result complicates further manipulation, because the integral is with respect to θ_2 and the integrand is a function of u and v, although there is the relations among u, v and θ_2.

An alternative method is to start the derivation directly from (3.7) and integrate with respect to u since $\tilde{H}(u,v)$ is a function of u and v. In terms of the properties of the δ function, (3.7) can be written as

$$\tilde{H}(u,v) = A^*(\theta_0) \int_{-\frac{\pi}{2}}^{\frac{\pi}{2}} \delta(u - \frac{K_x(\theta)}{2\pi})\delta(v - \frac{K_y(\theta)}{2\pi})d\theta \tag{3.18}$$

where $\theta_0 = \theta_0(u,v)$ satisfies (3.11) and (3.12). In order to simplify this expression, let

$$R(\theta) = \frac{K_y(\theta)}{2\pi} = K_0 \frac{\sin\theta}{2\pi\cos^2\theta}$$

then (3.18) becomes

$$\begin{aligned} \tilde{H}(u,v) &= A^*(\theta_0) \int_{-\frac{\pi}{2}}^{\frac{\pi}{2}} \delta(u - R\cot\theta)\delta(v - R)d\theta \\ &= A^*(\theta_0) \int_{-\infty}^{\infty} \frac{1}{R'(\theta)}\delta(u - Rh(R))\delta(R - v)dR \\ &= \frac{A^*(\theta_0)}{R'(\theta_0)}\delta(u - vh(v)) \end{aligned} \tag{3.19}$$

where $h(R) \triangleq \cot\theta$ and the derivative R' is given by

$$R'(\theta) = \frac{dR(\theta)}{d\theta} = K_0 \frac{1+\sin^2\theta}{2\pi\cos^3\theta} \ . \tag{3.20}$$

Note that $u - Rh(R) = 0$ and $R - v = 0$ are equivalent to (3.11) and (3.12); thus, the last step in (3.19) is valid. Here, $R\,h(R)$ is given by

$$\begin{aligned} R\,h(R) &= R\cot\theta \\ &= \sqrt{\frac{K_0}{8\pi}(K_0 + \sqrt{K_0^2 + 16\pi^2 R^2})} \ . \end{aligned} \tag{3.21}$$

To cancel the δ function on the right side of (3.19), integrate both sides of (3.19) with respect to u. The result is

$$\int_{-\infty}^{\infty} \tilde{H}(u,v)du = \frac{A^*(\theta_0)}{R'(\theta_0)} \ . \tag{3.22}$$

Since $\tilde{H}(u,v)$ is combined with δ functions as shown in (3.19), it is possible to write $\tilde{H}(u,v)$ into the δ function with its intensity $\tilde{H}_{int}(u,v)$, i.e., $\tilde{H}(u,v) = \tilde{H}_{int}(u,v)\delta(u - vh(v))$. Thus, the integral of the left hand side of (3.22) is equal to $\tilde{H}_{int}(vh(v),v)$, and it represents the intensity of the spectrum on the locus. Hence, the wave amplitude function can be written from (3.22) in the form

$$\begin{aligned} A(\theta(u,v)) &= R'(\theta(u,v))\,\tilde{H}^*_{int}(u,v) \\ &= K_0 \frac{1+\sin^2\theta(u,v)}{2\pi\cos^3\theta(u,v)}\,\tilde{H}^*_{int}(u,v) \ . \end{aligned} \tag{3.23}$$

Note that u is retained, and θ's subscript "0" is omitted in (3.23) for simplicity, but remember that u and v must be on the locus, that is, must satisfy (3.11) and (3.12).

The wave amplitude function is an even function of the wave angle when the ship wave is symmetric in the y-direction. This can be proved in terms of the above relations. From (3.13), the wave angle is a odd function of v, i.e., $\theta(u,v) = -\theta(u,-v)$. When the ship wave is symmetric in the y-direction, that is, $\eta(x,y) = \eta(x,-y)$ the

wave spectrum is even with respect to v, i.e., $H(u,v) = H(u,-v)$, according to the Fourier transform properties. Thus, $\tilde{H}(u,v) = \tilde{H}(u,-v)$ too. It is found from (3.23) that the amplitude function $A(\theta)$ is even with respect to θ, that is, $A(\theta) = A(-\theta)$, when the wave elevation is even with respect to y. For many ship types, the hull is symmetric with respect to the ship central plane, thus the ship wave is symmetric with respect to the centerline, and the wave amplitude function is even with respect to wave angles.

There are different ways of obtaining the wave spectrum in real applications. One way is from the wave elevation or slopes, that is, the wave spectrum is calculated by taking the Fourier transform of the observed wave data. Another possibility is to obtain the wave elevation spectra indirectly. For instance, the wave spectrum can be estimated from radar images. In practical applications, the data are discrete; thus, the discrete formula is useful for real situations and a discussion is given below.

To derive the discrete formulas, some definitions of discrete variables are given first. If we let n_1 and n_2 be the discrete forms of x and y, and Δx and Δy the interval sizes in the $x-$ and $y-$directions in the spatial domain, and let k_1 and k_2 be the discrete forms of u and v , and Δu, Δv the interval sizes in the $u-$ and $v-$ directions in the spatial frequency domain, then $x = n_1\Delta x$, $y = n_2\Delta y$, $u = k_1\Delta u$, and $v = k_2\Delta v$.

Under the assumption that $\tilde{\eta}(x,y)$ is very small outside the range of $-\frac{L_1}{2} \leq x \leq \frac{L_1}{2}$ and $-\frac{L_2}{2} \leq y \leq \frac{L_2}{2}$, the infinite-range Fourier transform can be approximated by its Fourier transform with finite ranges L_1 and L_2 in the $x-$ and $y-$directions, i.e.,

$$\begin{aligned} \tilde{H}(u,v) &= \int_{-\infty}^{\infty}\int_{-\infty}^{\infty} \tilde{\eta}(x,y) e^{-j2\pi(ux+vy)} dxdy \\ &\approx \int_{-\frac{L_1}{2}}^{\frac{L_1}{2}}\int_{-\frac{L_2}{2}}^{\frac{L_2}{2}} \tilde{\eta}(x,y) e^{-j2\pi(ux+vy)} dxdy \quad . \end{aligned} \tag{3.24}$$

After discretization, (3.24) can be expressed in the form

$$\tilde{H}(k_1,k_2) \approx \Delta x \Delta y \sum_{n_1=-\frac{N_1}{2}}^{\frac{N_1}{2}-1} \sum_{n_2=-\frac{N_2}{2}}^{\frac{N_2}{2}-1} \tilde{\eta}(k_1,k_2)\exp[-j2\pi(\frac{k_1 n_1}{N_1}+\frac{k_2 n_2}{N_2})] \quad (3.25)$$

$$k_1 = -\frac{N_1}{2},...,-1,0,1,2,...,\frac{N_1}{2}-1$$
$$k_2 = -\frac{N_2}{2},...,-1,0,1,2,...,\frac{N_2}{2}-1;$$

where N_1 and N_2 are the number of data points in the $x-$ and $y-$ directions.

The right hand side of (3.25) can be computed using powerful FFT algorithms. Once the discrete Fourier transform of wave elevation has been found, the algorithm for recovering the wave amplitude function can be established from (3.23) in the discrete form

$$\begin{aligned} A(\theta(k_1,k_2)) &= R'(\theta(k_1,k_2))\tilde{H}^*(k_1,k_2)\Delta u \\ &= K_0 \frac{1+\sin^2\theta(k_1,k_2)}{2\pi\cos^3\theta(k_1,k_2)}\tilde{H}^*(k_1,k_2)\Delta u \end{aligned} \quad (3.26)$$

where $K_0 = \frac{g}{U^2}$, $\Delta u = \frac{1}{\Delta x N_1}$, and θ, k_1 and k_2 satisfy

$$\theta(k_1,k_2) = \tan^{-1}(\frac{k_2}{k_1}) \quad (3.27)$$

$$(\Delta u\, k_1)^2 + (\Delta v\, k_2)^2 = [\frac{K(\theta)}{2\pi}]^2 = (\frac{K_0}{2\pi\cos^2\theta})^2 . \quad (3.28)$$

That is, the spectrum values can only be taken from those on the spectrum locus. Equation (3.26) does not contain the summation operation because there is only one non-zero value of $\tilde{H}(u,v)$ for each v. Once the discrete spatial frequency spectrum $\tilde{H}(k_1,k_2)$ of the ship wave elevation $\tilde{\eta}(x,y)$ is obtained, the ship wave amplitude function can be extracted from it.

In practical cases, the real-valued ship wave elevation $\eta(n_1,n_2)$ or its spatial frequency spectrum $H(k_1,k_2)$ is available. According to the definition of $\tilde{\eta}(x,y)$

and the properties of the Hilbert transform, the spectra $H(k_1, k_2)$ and $\tilde{H}(k_1, k_2)$ are related by

$$\tilde{H}(k_1, k_2) = \begin{cases} 2H(k_1, k_2) & \text{for } k_1 > 0 \\ H(k_1, k_2) & \text{for } k_1 = 0 \\ 0 & \text{for } k_1 < 0 \end{cases} \tag{3.29}$$

Thus, the wave amplitude function also can be expressed by the spectrum $H(k_1, k_2)$, that is,

$$A(\theta(k_1, k_2)) \;=\; K_0 \frac{1 + \sin^2\theta(k_1, k_2)}{\pi \cos^3\theta(k_1, k_2)} H^*(k_1, k_2)\Delta u \tag{3.30}$$

with $k_1 > 0$. Note that the value at $k_1 = 0$ is not considered in the above formula, since when $k_1 = 0$, $\theta = \pm\frac{\pi}{2}$ and $\cos\theta = 0$. This will result in the infinity of $A(\theta(k_1, k_2))$.

In the above discussion, it has been assumed that the truncation error caused by the finite data length in the $x-$ and $y-$ directions can be neglected, and thus the FFT algorithm is used to obtain the wave spectrum, and then the wave amplitude function is recovered from it. In some situations, however, the truncation error is too large to be neglected. In this case, the wave amplitude function may be recovered by using an inversion technique. It is assumed that the truncated wave elevation is represented by

$$\tilde{\eta}_T(x, y) = \tilde{\eta}(x, y)\, g_T(x, y) \tag{3.31}$$

where the two-dimensional gate function $g_T(x, y)$ is defined as

$$g_T(x, y) = \begin{cases} 1 & \text{for } -\frac{L_1}{2} \le x \le \frac{L_1}{2},\ -\frac{L_2}{2} \le y \le \frac{L_2}{2} \\ 0 & \text{otherwise} \end{cases} \quad . \tag{3.32}$$

Its Fourier transform is given by

$$G_T(u, v) = L_1 L_2 S_a(\pi L_1 u) S_a(\pi L_2 v) \tag{3.33}$$

where $S_a(\xi) \triangleq \sin\xi/\xi$ is called the sampling function. By using the convolution property and the result in (3.7), the spectrum of the truncated wave elevation in (3.31) is given by

$$\tilde{H}_T(u,v) = L_1 L_2 \int_{-\frac{\pi}{2}}^{\frac{\pi}{2}} A^*(\theta) S_a(\pi L_1(u - \frac{K_x(\theta)}{2\pi})) S_a(\pi L_2(v - \frac{K_y(\theta)}{2\pi})) d\theta \ . \quad (3.34)$$

Thus, if $\tilde{H}_T(u,v)$ is known, the wave amplitude $A(\theta)$ can be founded by solving this integral equation.

3.2 Estimation from 1-D Wave Cuts

In many real situations, two-dimensional wave elevation data or spectra may not be available, but one-dimensional (1-D) wave cuts or spectra may be obtained by some remote sensing means or by field measurements. In this section, the relation between one-dimensional wave spectra and the wave amplitude function is discussed based on the complex-valued wave elevation cuts. Then, a special example is given, in which the wave cut is measured by a stationary sensor, and the wave amplitude function is recovered from its FFT spectrum.

The derivation of the wave amplitude function from wave spectra includes three steps. First, the one-dimensional wave cut is expressed as a function of time according to a pair of wave cut path equations; then the spectrum is obtained by taking the Fourier transform of the wave elevation; finally, the wave amplitude function is expressed in terms of the spectrum. Now, consider a general case shown in Figure 3.2, where a wave cut is taken in the ship generated wave field by a sensor moving with a uniform speed U_p in a direction making an angle α with the positive x-axis, i.e., the direction that the ship is moving. In the reference system moving with the ship at constant speed U, the wave cut path can be described by a pair of parametric

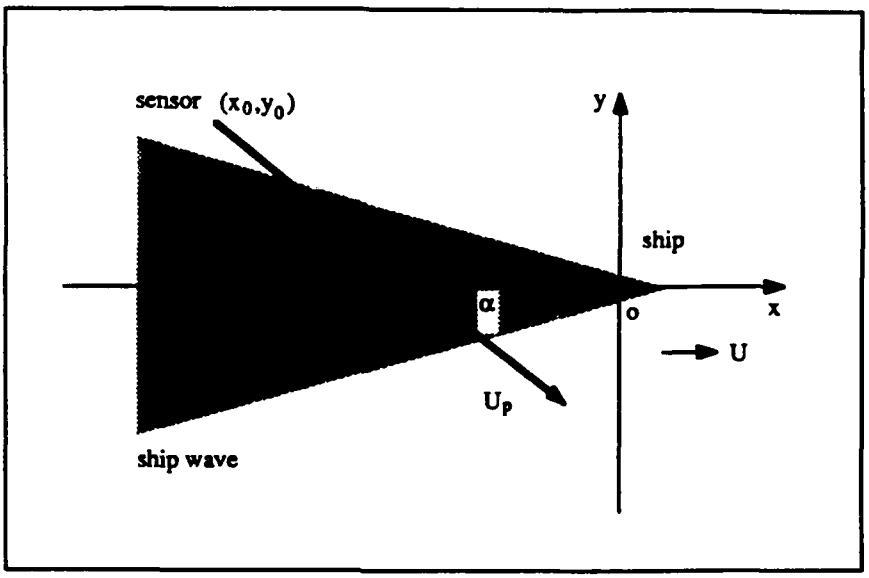

Figure 3.2: 1-D wave cut in the ship wave field.

equations

$$x(t) = x_0 + (U_p \cos\alpha - U)\, t \tag{3.35}$$

$$y(t) = y_0 + U_p \sin\alpha\, t \tag{3.36}$$

where t is a parameter representing the measurement time, and (x_0, y_0) is the sensor's initial position in the given coordinate system at $t = 0$. If the sensor is mounted on an airplane or satellite, the sensor's speed U_p will be much larger than the ship's traveling speed U. In some cases, however, the sensor is considered to be fixed in a position to measure the wave cuts when a ship passes through, for instance, in tow tank experiments. When $U_p \cos\alpha > U$, $x(t)$ increases with t, otherwise it decreases with t.

The complex-valued wave elevation cut can be derived by substituting (3.35) and (3.36) into (2.18) and then by taking the Hilbert transform. Its form is given by

$$\tilde{\eta}(t) \triangleq \tilde{\eta}(x(t), y(t)) = \{ \int_{-\frac{\pi}{2}}^{\frac{\pi}{2}} A^*(\theta) e^{j\Phi_0(\theta)}\, e^{j2\pi\Phi(\theta)t} d\theta \}^{*\Phi} \tag{3.37}$$

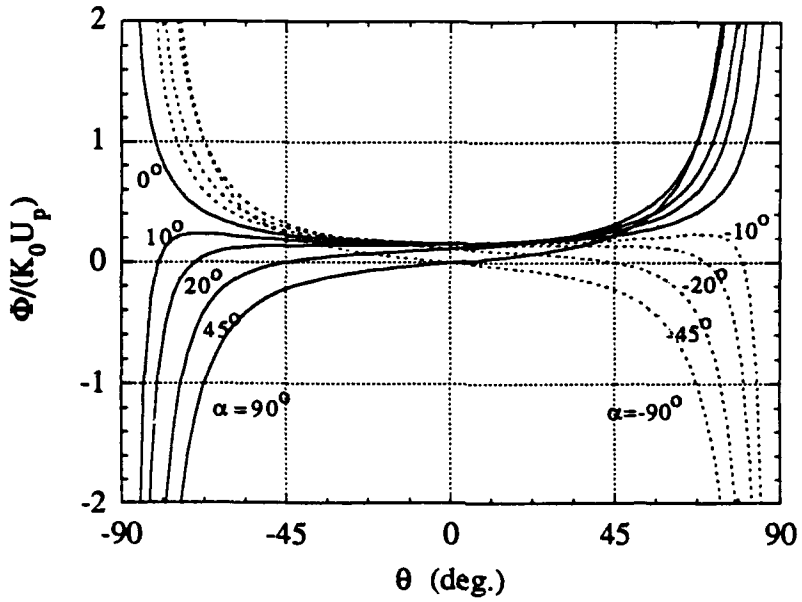

Figure 3.3: Curves of $\frac{\Phi(\theta)}{K_0 U_p}$ versus θ for different wave cut angles α.

where $\{.\}^{*\blacklozenge}$ specifically defines a conditional conjugate operation, that is, no operation is taken when $\Phi(\theta) \geq 0$, but the conjugate operation is taken when $\Phi(\theta) < 0$. $\Phi_0(\theta)$ and $\Phi(\theta)$ are defined by

$$\Phi_0(\theta) \triangleq K_x(\theta)x_0 + K_y(\theta)y_0 \tag{3.38}$$

$$\Phi(\theta) \triangleq \frac{1}{2\pi}\left[K_x(\theta)(U_p\cos\alpha - U) + K_y(\theta)U_p\sin\alpha\right]. \tag{3.39}$$

With the above wave cut expression, the wave spectrum is obtained by taking the Fourier transform of $\tilde{\eta}(t)$ with respect to t:

$$\begin{aligned}\tilde{H}(f) &= \mathcal{F}\{\tilde{\eta}(t)\} = \int_{-\infty}^{\infty}\tilde{\eta}(t)e^{-j2\pi ft}\,t \\ &= \int_{-\frac{\pi}{2}}^{\frac{\pi}{2}}\{A^*(\theta)\,e^{j\Phi_0(\theta)}\}^{*\blacklozenge}\,\delta(f-|\Phi(\theta)|)\,d\theta \\ &= \frac{1}{|\Phi'(\theta_0)|}\{A^*(\theta_0)\,e^{j\Phi_0(\theta_0)}\}^{*\blacklozenge}\end{aligned} \tag{3.40}$$

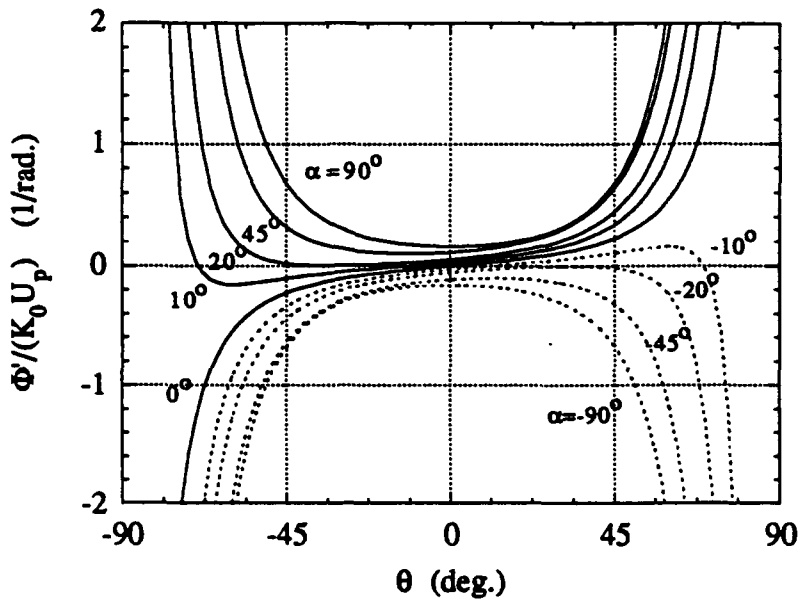

Figure 3.4: Curves of $\frac{\Phi'(\theta)}{K_0 U_p}$ versus θ for different wave cut angles α.

where θ_0 must satisfy the equation

$$f - |\Phi(\theta)| = 0 \tag{3.41}$$

and must be such that $\Phi'(\theta_0) \neq 0$. Here, the derivative, $\Phi'(\theta)$, is calculated from (3.39) and is given by

$$\Phi'(\theta) = \frac{g}{2\pi U^2 \cos^2\theta}[(U_p \cos\alpha - U)\sin\theta + U_p \sin\alpha \sec\theta(\sin^2\theta + 1)] \ . \tag{3.42}$$

When $U_p \cos\alpha \gg U$, $\Phi(\theta)$ and $\Phi'(\theta)$ can be approximated by

$$\Phi(\theta) \approx \frac{K_0 U_p}{2\pi} \frac{\cos(\theta - \alpha)}{\cos^2\theta} \tag{3.43}$$

$$\Phi'(\theta) \approx \frac{K_0 U_p}{2\pi \cos^2\theta}[\cos\alpha \sin\theta + \sin\alpha \sec\theta(\sin^2\theta + 1)] \tag{3.44}$$

where $K_0 = \frac{g}{U^2}$. These forms are similar to the ones given by Tuck, Collins and Wells [6]. The curves of θ versus $\frac{\Phi(\theta)}{K_0 U_p}$ and $\frac{\Phi'(\theta)}{K_0 U_p}$ are plotted in Figure 3.3 and Figure 3.4 for the above approximate relations.

By rewriting (3.40), the wave amplitude function $A(\theta)$ now can be expressed in the form

$$A(\theta) = |\Phi'(\theta)| \, \{ \tilde{H}^*(f) \}^{*} \, e^{j\Phi_0(\theta)} \tag{3.45}$$

where the subscript of θ is omitted for simplicity, but keep in mind that θ must satisfy (3.41). When the ship wave is symmetric to the ship central line, the wave amplitude function is an even function of θ, thus the calculation may be taken only for $0 \leq \theta \leq \frac{\pi}{2}$ or $-\frac{\pi}{2} \leq \theta \leq 0$. Because of the fact that $\tilde{H}(f) = 0$ for $f < 0$, only the positive frequency components needs to considered in the above calculation. The valid wave angle can be found for each positive f by solving (3.41) or by estimating from curves in Figure 3.3 and Figure 3.4. In terms of (3.45), the wave amplitude function can be calculated if the wave cut spectrum $\tilde{H}(f)$ has been obtained together with the parameters U, U_p, α, and the initial position (x_0, y_0). The methods for obtaining the ship speed U and the wave cut angle α will be presented in the next chapter.

As an example, a special case now is considered in which a sensor is assumed fixed in position and the wave elevation is measured as the wave field is generated when the ship passes, as is typically done in tow tank wave measurement experiments. Both U_p and α are zero for this case. $0 \leq \cos\theta \leq 1$ when θ ranges from $-\frac{\pi}{2}$ to $\frac{\pi}{2}$, thus, now $\Phi(\theta) = -\frac{g}{2\pi U \cos\theta} < 0$. For this case, the wave amplitude function in (3.45) and the f constraint condition in (3.41) become

$$A(\theta) \;=\; \tilde{H}(f)\frac{g|\sin(\theta)|}{2\pi U^2 \cos^2\theta} e^{j\Phi_0(\theta)} = \tilde{H}(f)\frac{|K_y(\theta)|}{2\pi} e^{j\Phi_0(\theta)} \tag{3.46}$$

$$f - \frac{g}{2\pi U \cos\theta} = 0 \ . \tag{3.47}$$

Since frequency f is positive, its minimum value that can be considered in the estimation of the wave amplitude function from the spectrum is $f_{min} = \frac{g}{2\pi U}$ in terms of

(3.47). Given a value of f larger than f_{min}, there are corresponding values for wave angle θ and $\tilde{H}(f)$. Hence, $A(\theta)$ can be evaluated in terms of (3.46).

Usually, the spectrum $\tilde{H}(f)$ is obtained from the FFT of discrete wave cut data or mapped from other discrete spectra. Therefore, f is discrete. For the wave elevation cut, if the data length is N and the sample interval is Δt, then the discrete positive frequency is given by

$$f_k = \frac{k}{N\Delta t} \qquad k = k_0, k_0+1, ..., \frac{N}{2} \tag{3.48}$$

where k_0 denotes the smallest integer larger than $\frac{gN\Delta t}{2\pi U}$. The corresponding discrete wave angle is given by

$$\theta_k = \cos^{-1}(\frac{gN\Delta t}{2\pi kU}) \qquad k = k_0, k_0+1, ..., \frac{N}{2} \ . \tag{3.49}$$

From this formula, it is found that the data length should be large in order to obtain a good resolution for small wave angles. The minimum resolvable wave angle is dependent on $\cos^{-1}\frac{gN\Delta t}{2\pi k_0 U}$; the possible maximum resolvable wave angle is dependent on the sample interval, which will be discussed in the next section.

The above derivation is based on the assumption of the time sequential wave cut data. In some applications, however, the path of a wave cut may be described by a path equation $y = y_0 + \tan\alpha\, x$, for instance, the one-dimensional wave data is cut from two-dimensional wave data in the x and y spatial domain. For this case, the wave elevation is given in the form of $\tilde{\eta}(x) \triangleq \tilde{\eta}(x, y(x))$, its spectrum can be obtained by taking the Fourier transform with respect to x. Then similar procedures to calculate the wave amplitude function can proceed. For instance, the

wave amplitude function for a wave cut $\tilde{\eta}(x, y_0)$ is given by

$$A(\theta) = \tilde{H}(u)\frac{g|\sin(\theta)|}{2\pi U^2\cos^2\theta}e^{j\frac{g\sin(\theta)}{U^2\cos^2\theta}y_0} = \tilde{H}(u)\frac{|K_y(\theta)|}{2\pi}e^{jK_y(\theta)y_0} \tag{3.50}$$

$$u - \frac{g}{2\pi U^2\cos\theta} = 0 \ . \tag{3.51}$$

where y_0 is a constant and $\tilde{H}(u)$ is Fourier transform with respect to variable x.

Similar to the two-dimensional case, it is assumed in the above discussion that the truncation error caused by finite data length can be neglected. In some situations, however, the truncation error is too large to be neglected, and thus some remedy methods are needed. One method is to extend the truncated wave cut according to the theoretical ship wave asymptotic behavior as given in [20]. Another possibility, which will be discussed here, is the use of an inversion technique to recover the wave amplitude function from truncated wave spectra, which is similar to the two-dimensional case discussed in Section 3.1.

In the second method, it is assumed that the data length is T, and that the truncated wave cut is represented by $\tilde{\eta}_T(t) = \tilde{\eta}(t)\, g_T(t - \frac{T}{2})$, where the gate function is defined as $g_T(t) = 1$ while $\frac{T}{2} \leq t \leq \frac{T}{2}$ and zero otherwise. The Fourier transform of the one-dimensional gate function is $T\, S_a(\pi T f)$. By taking the Fourier transform of $\tilde{\eta}_T$, the spectrum of the truncated wave cut is given in the form

$$\tilde{H}_T(f) = Te^{-j\pi Tf}\int_{-\frac{\pi}{2}}^{\frac{\pi}{2}}\{A^*(\theta)e^{j\Phi_0(\theta)}\}^{*} * e^{j\pi T|\Phi(\theta)|}S_a(\pi T(f - |\Phi(\theta)|))\, d\theta \tag{3.52}$$

When $\tilde{H}_T(f)$ is known, $A(\theta)$ can be found by solving this integral equation. Though, the calculation will be more complicated than the method neglecting truncated errors.

So far, the first section and this section have discussed the methods to recover the wave amplitude function from either one- or two-dimensional wave spectra. Generally speaking, the calculation for one-dimensional data is simpler and performance

is better than those for two-dimensional data if the one-dimensional data contain enough required ship information. The reason that the accuracy may be degraded in two-dimensional discrete cases is that the spectrum consists of discrete sample pixels, the impulse on the locus can not be always located on these sampling points, and a slight deviation from the locus may result in a large error for that impulse value. However, the advantage of using two-dimensional data is that it is much easier to remove the background noise, such as a rough wind generated wave, and it is also easier to estimate a ship's speed and direction from two-dimensional wave fields than from one-dimensional wave cuts. For the above reasons, it is suggested that the signal processing and the estimation of ship speed and direction proceed in the two-dimensional basis, but the wave amplitude function be recovered from one-dimensional data that are extracted from the two-dimensional data.

3.3 Effect of Data Sampling Intervals

The wave amplitude function is a function of the wave angle. Theoretically, the wave angle ranges from $-\frac{\pi}{2}$ to $\frac{\pi}{2}$ for ship generated surface waves. In most situations, however, the data we obtained are discrete, and the range of the wave angle is dependent on the sample interval and the ship speed as will be seen below. The following two subsections discuss the effect of sampling intervals on the maximum resolvable wave angles in one and two-dimensional cases, based on Nyquist's sampling theory. The final subsection discusses the relationship between the wave sampling intervals for a real ship and its model, because ship models and tow tank experimental data are usually used.

3.3.1 Maximum Resolvable Wave Angles in 1-D Cases

The maximum resolvable wave angle from a one-dimensional wave spectrum is determined in this subsection, based on Nyquist's sampling theory and the relation between the wave angle and wavelength.

To apply Nyquist's sampling theory to the ship wave sampling problem, the wavelength expression is given first here. For a ship moving at speed U, the wave number K and wave angle θ have the following relation from Chapter 2:

$$K = \frac{g}{U^2 \cos^2 \theta} \, . \tag{3.53}$$

According to the definition of wavelength λ and (3.53), it follows that

$$\begin{aligned} \lambda &\triangleq \frac{2\pi}{K} \\ &= \frac{2\pi}{g} U^2 \cos^2 \theta \\ &= 0.641 U^2 \cos^2 \theta \ . \end{aligned} \tag{3.54}$$

According to Nyquist's sampling theory, in order to reconstruct a signal from its sampling values without aliasing error, the sampling interval Δ in the spatial domain must be such that

$$\Delta \leq \frac{1}{2} \lambda_{min} \tag{3.55}$$

where λ_{min} is the shortest wavelength that the signal contains. If the data sampling is taken in the time domain mentioned in Section 3.2, then $\Delta = U_p \Delta t$. Applying this sampling criterion to the above ship wave problem, it follows that

$$\Delta \leq \frac{\pi}{g} U^2 \cos^2 \theta \ . \tag{3.56}$$

Some comments can be made here in terms of (3.56). Since the wavelength ranges from 0 to $\frac{2\pi}{g} U^2$, corresponding to the wave angle in $[-\frac{\pi}{2}, \frac{\pi}{2}]$, the sampling interval

must be from 0 to $\frac{\pi}{g}U^2$. Thus, the sampling interval must approach zero, in order to cover the wave angle approaching $\pm\frac{\pi}{2}$. In practice, the determination of the sampling interval depends on many other facts, and the interval can not be very small. For any sampling interval Δ larger than zero, the signal components with the wave angle close to $\pm\frac{\pi}{2}$ will inevitably have some distortion. However, if the intensities of these components are very small when the wave angle approaches $\pm\frac{\pi}{2}$, this distortion may be neglected in real applications.

If the sampling interval Δ is given, then the minimum wavelength which can be resolved from the sampling signal is determined by $\lambda_{min} = 2\Delta$; additionally, if the ship speed U is also given, the maximum wave angle which can be resolved from the sampling signal is given from (3.56) by

$$\theta_{max} = \cos^{-1}(\sqrt{\frac{g\Delta}{\pi U^2}}) \tag{3.57}$$

Thus, the available signal components in the wave spectrum will be in the range of $\theta = \theta_{min}$ to $\theta = \theta_{max}$, where θ_{min} has been discussed in Section 3.2 and is given by $\cos^{-1}\frac{gN\Delta}{2\pi k_0 U U_p}$ if $\Delta = U_p\Delta t$ is considered.

For easy reference with different ship speed parameters, the curve of maximum resolvable wave angles from one-dimensional wave spectra versus $\frac{\Delta}{U^2}$ is plotted in Figure 3.5. As an example for a one-dimensional case, given $\Delta = 12.5$ meters and $U = 10$ meters/second, it follows the maximum resolvable wave angle $\theta_{max} = 51.36°$, and the minimum resolvable wavelength $\lambda_{min} = 25$ meters.

3.3.2 Maximum Resolvable Wave Angles in 2-D Cases

The above discussion about one-dimensional cases can be extended directly to two-dimensional cases. In order to reconstruct a two-dimensional signal from its

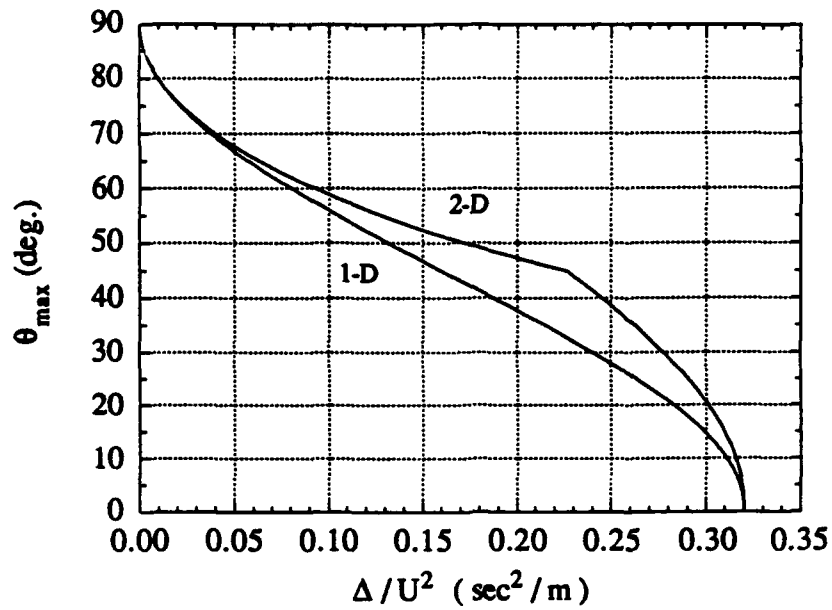

Figure 3.5: Maximum resolvable wave angle from 1-D or 2-D wave spectra versus $\frac{\Delta}{U^2}$.

sampling values without aliasing error, the following conditions must be satisfied, according to Nyquist's sampling theory:

$$\begin{aligned} \Delta_x &\leq \frac{1}{2}\lambda_{x_{min}} = \frac{1}{2u_{max}} \\ \Delta_y &\leq \frac{1}{2}\lambda_{y_{min}} = \frac{1}{2v_{max}} \end{aligned} \tag{3.58}$$

where Δ_x and Δ_y are the spatial sampling intervals in the $x-$ and $y-$directions, respectively. $\lambda_{x_{min}} = \frac{1}{u_{max}}$ and $\lambda_{y_{min}} = \frac{1}{v_{max}}$ are the minimum wavelengths contained in the two-dimensional signal in the $x-$ and $y-$directions. u_{max} and v_{max} denote the maximum spatial frequency components that the signal contains. If sampling intervals Δ_x and Δ_y are given, the spectrum components that can be presented are in the range $[-u_m, u_m]$ and $[-v_m, v_m]$ in the spatial frequency (u, v) plane, where $u_m = \frac{1}{2\Delta_x}$ and $v_m = \frac{1}{2\Delta_y}$.

According to the results discussed in Section 3.1, the non-zero spectrum components for ship waves are always located on a locus on the (u, v) spatial frequency plane, as represented by

$$u = \frac{g}{2\pi U^2 \cos\theta} \tag{3.59}$$

$$v = \frac{g \sin\theta}{2\pi U^2 \cos^2\theta} \ . \tag{3.60}$$

The locus will have an intersection point with the edge $u = u_m$ or $v = v_m$. The maximum resolvable wave angle can be determined from the intersection point. If the locus has an intersection point with $u = u_m$, then the maximum resolvable wave angle can be obtained by solving $u = u_m$ and (3.59),

$$\begin{aligned} \theta_{max} &= \cos^{-1}\left(\frac{g}{2\pi u_m U^2}\right) \\ &= \cos^{-1}\left(\frac{g\Delta_x}{\pi U^2}\right) \ . \end{aligned} \tag{3.61}$$

If the locus has a intersection point with $v = v_m$, then the maximum resolvable wave angle can be obtained by solving $v = v_m$ and

$$\begin{aligned} \theta_{max} &= \sin^{-1}\{\frac{1}{2}[-\frac{g}{2\pi U^2 v_m} + \sqrt{(\frac{g}{2\pi U^2 v_m})^2 + 4}]\} \\ &= \sin^{-1}\{\frac{1}{2}[-\frac{g\Delta_y}{\pi U^2} + \sqrt{(\frac{g\Delta_y}{\pi U^2})^2 + 4}]\} \ . \end{aligned} \tag{3.62}$$

In most cases, the sampling intervals in the $x-$ and $y-$directions are set to be the same, i.e. $\Delta_x = \Delta_y = \Delta$. It can be proved that in the first quadrant of the (u,v) plane, the locus is under the line $u = v$ for $0 \leq \theta \leq \frac{\pi}{4}$, and is above the line $u = v$ for $\frac{\pi}{4} < \theta \leq \frac{\pi}{2}$. From (3.59) and (3.60),

$$u - v = \frac{g}{2\pi U^2 \cos\theta}(1 - tan\theta)$$

thus,

$$u \geq v \qquad \text{if } 0 \leq \theta \leq \frac{\pi}{4} \tag{3.63}$$

$$u < v \qquad \text{if } \frac{\pi}{4} < \theta \leq \frac{\pi}{2} \ . \tag{3.64}$$

From (3.64), it can be concluded for the cases of $\Delta_x = \Delta_y = \Delta$ that when $\theta_{max} \leq \frac{\pi}{4}$, the locus has an intersection point with $u = u_m$ and when $\frac{\pi}{4} < \theta_{max} \leq \frac{\pi}{2}$, the locus has an intersection point with $v = v_m$, and Δ can be expressed from (3.60) in the form

$$\Delta = \begin{cases} \frac{\pi}{g} U^2 \cos\theta_{max} & \text{if } 0 \leq \theta_{max} \leq \frac{\pi}{4} \\ \frac{\pi}{g} U^2 \cos\theta_{max} \cot\theta_{max} & \text{if } \frac{\pi}{4} < \theta_{max} \leq \frac{\pi}{2} \end{cases} \tag{3.65}$$

Figure 3.5 also gives the maximum resolvable wave angle curves versus the ratio of the ship speed U and the sampling interval $\Delta = \Delta_x = \Delta_y$. From Figure 3.5, we find that the sampling intervals must be small enough to recover the wave components with large wave angles. Considering the above example again for a two-dimensional case, given $\Delta = 12.5$ meters, $U = 10$ meters/second, then $\theta_{max} = 55.47°$ in terms of formula (3.62).

3.3.3 Sampling Intervals for a Real Ship and its Model

This subsection discusses the relation between the wave sampling intervals for a real ship and its model. For this purpose, a non-dimensional parameter F_n, called the Froude number, is introduced here. With physical length L, speed U and gravitational acceleration g, F_n is defined by

$$F_n = \frac{U}{\sqrt{gL}} \ . \tag{3.66}$$

It is widely used in the ship wave resistance analysis. According to studies of ship wave resistance, the wave resistance of two geosims with the same hull shape are the same when their Froude numbers are equal [21].

If applying the above result to a real ship with length L and moving speed U and its model with the same hull shape but length L_m and moving speed U_m, then the following ratio can be obtained when their Froude numbers are equal:

$$\frac{U_m^2}{U^2} = \frac{L_m}{L} \tag{3.67}$$

To express the sampling interval relation, let the sampling intervals corresponding to the real ship and its model be denoted by Δ and Δ_m, respectively. The ratio of the two sampling intervals can be connected to the above ratio in the relation

$$\frac{\Delta_m}{\Delta} = \frac{U_m^2}{U^2} = \frac{L_m}{L} \tag{3.68}$$

for either the one-dimensional case in (3.57) or the two-dimensional case in (3.65). This tells us that when the Froude number is kept the same, the sampling interval corresponding to the ship model can be taken as $\Delta_m = \frac{L_m}{L}\Delta$.

So far, this section has discussed the effect of sampling intervals on the maximum resolvable wave angles in one and two-dimensional cases, and the relation between the wave sampling intervals for a real ship and its model. In summary, from the viewpoint of analysis of ship wave spectra and extraction of ship geometry information, the determination of sampling intervals depends mainly on the ship speed and ship length. The smaller the sampling interval, the smaller the distortion of wave spectra, the larger the maximum resolvable wave angle. Additionally, it will be seen in Chapter 4 that the smaller the sampling interval, the more periodic zero points are available in the wave amplitude function. Therefore, the sampling interval should be selected as small as possible. In practice, however, the resolution and properties of data acquisition systems and their operation position, such as SAR, greatly limit the small sampling intervals to be used. Other limitations may be the data storage and data processing, but they are less critical compared to the former. For the wave gen-

erated by a ship model, the sampling interval can be taken as the one proportional to the ratio of the lengths of the model and real ship.

CHAPTER IV

ESTIMATION OF A MOVING SHIP'S SPEED AND DIRECTION

From the viewpoint of remotely sensing a ship moving in the open ocean, interesting problems exist related to the detection of the ship's actual presence, and the acquisition of its dynamic and static information, for instance, the ship's direction and speed and the ship's size and hull shape. These problems will be discussed in the following chapters based on the knowledge given in the previous chapters. This chapter focuses on the estimation of a ship's direction and speed from one dimensional and two dimensional wave spectra. Before this discussion, the problem of the presence of a moving ship in ambient ocean waves is briefly discussed.

4.1 Presence of a Moving Ship in Ambient Ocean Waves

Although a ship's length is bounded within a range of values, the wake it generates in the open ocean may extend for many tens of kilometers. In the indirect methods, the detection of a ship and its related characteristics is obtained by measuring ship generated waves or their spectra.

One important feature of the ship wake, different from that of ambient ocean waves, is its wave spectrum. As analyzed in Chapter 2 the spectrum of the complex-valued wave elevation, $\tilde{H}(u,v)$, has one locus on the spectrum diagram, and the

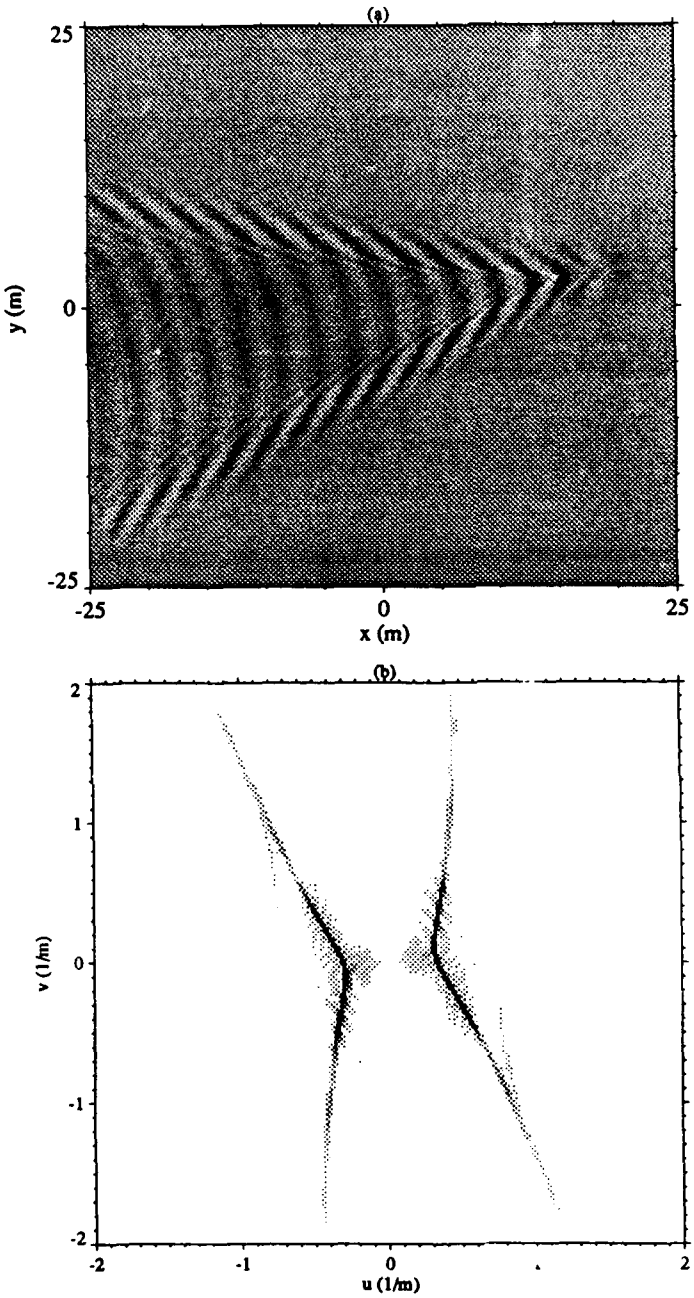

Figure 4.1: (a) Pseudo image of the wave elevation calculated from WAVEAMP for the Quapaw hull model with direction $\alpha = 10°$ and speed U=2.229 m/s. The crest appears dark and the trough bright. (b) Pseudo image of the Fourier transform $H(u, v)$ of the wave elevation from (a).

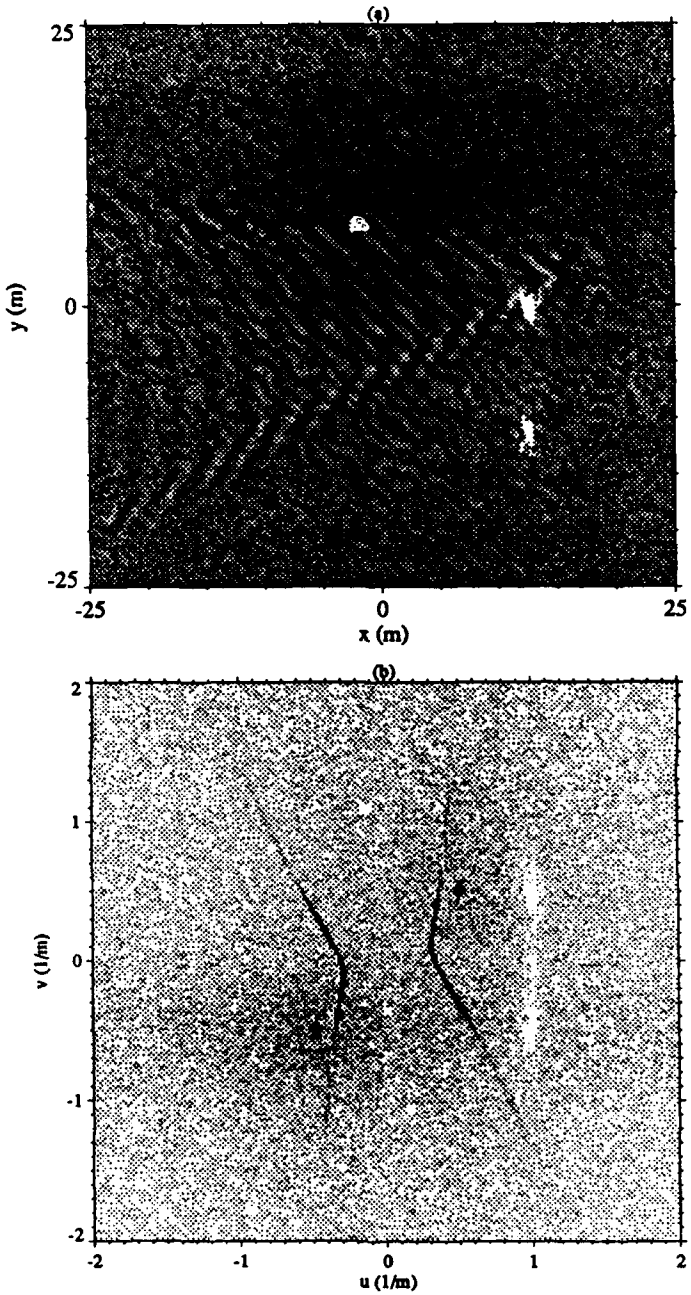

Figure 4.2: (a) Pseudo image of the Quapaw ship wave elevation in a random sine ambient wave. (b) Pseudo image of the Fourier transform of the wave elevation from (a).

spectrum of the real-valued wave elevation, $H(u, v)$, has two loci on the spectrum diagram. Because of the distinct spectrum characteristics, it is usually easier to detect the presence of a moving ship from the sea noise background in the spectral domain than in the spatial domain.

To understand this point, let us examine a simple example of a ship wave plus a random sine ambient wave. This is meant to simulate a ship in a swell background. The ship wave without any ambient waves and background noise is shown as a pseudo image in Figure 4.1(a) together with its FFT spectrum in Figure 4.1(b). In Figure 4.1(a), the origin of the coordinate system has a translation and rotation relative to the ship center, the origin of the ship reference system defined in Chapter 2. This difference results in a rotation of the loci on the spectrum diagram, but it dose not change the shape of the loci. Further discussion about it will be given in the next section.

This ship wake is calculated using WAVEAMP, a program to compute the Kelvin wave elevation [29], for a 1:12 scale model of a seagoing tug, the USS Quapaw, which has a length of 4.953 meters and a speed U of 2.229 meters/second with an angle of 10° relative to the x-axis. The ship wave height has a maximum value 0.231 , mean 0.007 and standard deviation 0.013 meters. The ship wave involved in a random sine ambient wave is displayed in Figure 4.2(a) together with its FFT spectrum in Figure 4.2(b). The random sine wave has a simple model, $A_b sin(K_x x + K_y y)$, where A_b K_x and K_y are random variables generated point by point by a computer program. A_b originally has a Gaussian distribution with mean 0.05 meters and standard deviation 0.05 meters, denoted as $\mathcal{N}(0.05, 0.05)$, and K_x and K_y originally have a Gaussian distribution $\mathcal{N}(3.14, 1.0)$ in rad./meter. They are smoothed using a median filter with a 9-point window size, equivalent to 1.8 by 1.8 meters. The smoothed A_b, K_x and

K_y have means close to their original means, but have different standard deviations of 0.014 meters, 0.28 rad./meter and 0.28 rad./meter, respectively. Finally, they are used to calculate the random sine wave and are added to the ship wave.

From this example, it can be found that in the spatial domain, the ship wave, particularly the wave on the left of the ship, has been corrupted by the random sine wave because of their close wave direction, but the loci can be still recognized clearly from the spectrum. In real situations with severe background noise, conventional or special signal processing may be used to enhance the desired ship wave signal.

4.2 Estimation of a Ship's Speed and Direction from 2-D Wave Spectra

This section discusses the estimation of a moving ship's speed and direction from its two dimensional wave spectrum. The discussion will begin with two kinds of spatial coordinate systems and their corresponding spectrum coordinate systems, and then the formulas for estimating the speed and direction are derived.

In the following, the discussion will focus on the estimation from the magnitude of a Fourier spectrum, instead of the one from a power spectrum, since a power spectrum and the magnitude of a Fourier spectrum have a direct relation and are equivalent when the spectrum locus position is used to estimate a ship's speed and direction.

It has been shown in Chapter 2 that under the steady state assumption, the ship speed U, wave angle θ and wave number $K(\theta)$ have a direct relation

$$K(\theta) = \frac{g}{U^2 \cos^2 \theta} \quad . \tag{4.1}$$

This relation indicates that the ship speed depends only on the wave number, or the wave length at a given wave angle. Theoretically, once the wave number $K(\theta)$

is available, the determination of ship speed becomes a trivial problem. However, the determination of the wave number and wave angle needs prior information about the ship's direction. If this information is not available, then the problem becomes complicated, and both the ship's direction and speed need to be determined simultaneously.

To determine the ship's direction, two coordinate systems in the spatial domain, shown in Figure 4.3, are considered in this section. One is the reference system moving with a ship as defined in Chapter 2; another is the image coordinate system whose origin is the imaging center and the positive x-direction is the sensor's direction. If xoy denotes the ship reference coordinate system and $x_m o_m y_m$ the image coordinate system, then their relation is given as

$$x_m = x_{m0} + x\cos\alpha - y\sin\alpha \tag{4.2}$$

$$y_m = y_{m0} + x\sin\alpha + y\cos\alpha \tag{4.3}$$

or

$$x = (x_m - x_{m0})\cos\alpha + (y_m - y_{m0})\sin\alpha \tag{4.4}$$

$$y = -(x_m - x_{m0})\sin\alpha + (y_m - y_{m0})\cos\alpha \tag{4.5}$$

where (x_{m0}, y_{m0}) is the coordinate of the origin o of the ship reference system in the image coordinate system and where α is the angle between axes ox and $o_m x_m$, which represents the ship's direction relative to the sensor's direction. With the relations, the ship wave $\eta(x, y)$ expressed in the ship reference system can be expressed in the image coordinate system as

$$\begin{aligned}\eta_m(x_m, y_m) = \; & \eta[\,(x_m - x_{m0})\cos\alpha + (y_m - y_{m0})\sin\alpha, \\ & -(x_m - x_{m0})\sin\alpha + (y_m - y_{m0})\cos\alpha\,] \quad .\end{aligned} \tag{4.6}$$

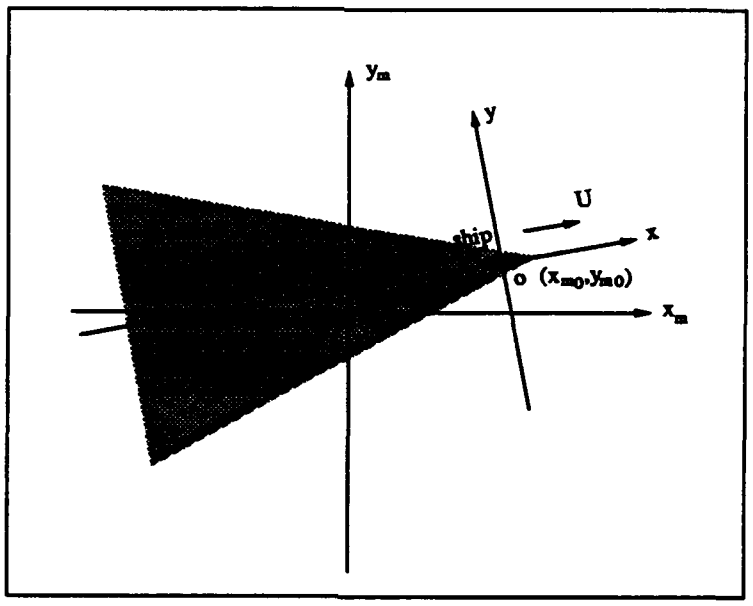

Figure 4.3: Two coordinate systems in spatial domain: the ship reference coordinate system xoy and image coordinate system $x_m o_m y_m$

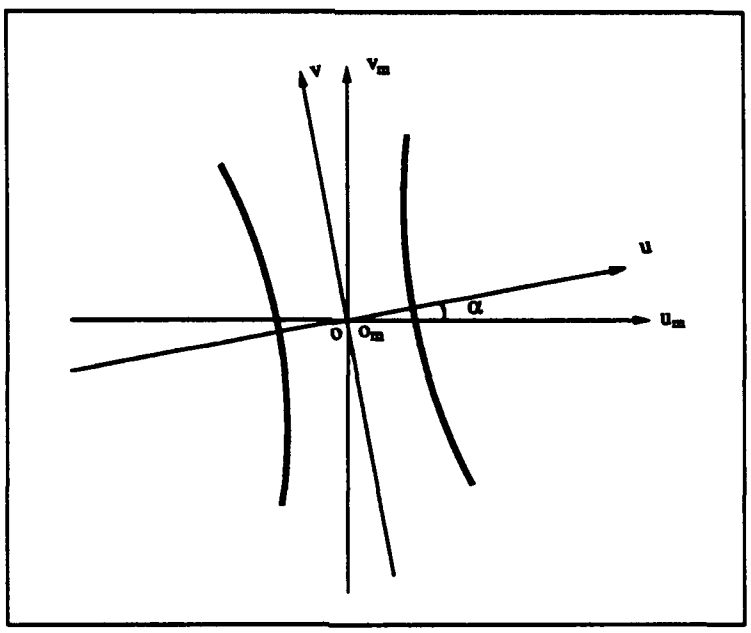

Figure 4.4: Two coordinate systems in frequency domain: the ship reference coordinate system uov and image coordinate system $u_m o_m v_m$

Corresponding to the the above spatial domain coordinate relations, the spectrum domain coordinate relations can be established through the Fourier transform relation. The Fourier transform of $\eta(x,y)$ has been given in (2.20), i.e., $H(u,v) = \mathcal{F}\{\,\eta_m(x,y)\,\}$. The Fourier transform of $\eta_m(x_m,y_m)$ is given as

$$H_m(u_m,v_m) = \mathcal{F}\{\,\eta_m(x_m,y_m)\,\} = \int_{-\infty}^{\infty}\int_{-\infty}^{\infty} \eta_m(x_m,y_m)e^{-j2\pi(u_m x_m + v_m y_m)}dx_m dy_m$$

$$\begin{aligned}
&= \int_{-\infty}^{\infty}\int_{-\infty}^{\infty} \eta[\,(x_m - x_{m0})\cos\alpha + (y_m - y_{m0})\sin\alpha, \\
&\quad -(x_m - x_{m0})\sin\alpha + (y_m - y_{m0})\cos\alpha\,]e^{-j2\pi(u_m x_m + v_m y_m)}dx_m dy_m \\
&= [\int_{-\infty}^{\infty}\int_{-\infty}^{\infty} \eta(x,y)e^{-j2\pi[x(u_m\cos\alpha + v_m\sin\alpha) + y(-u_m\sin\alpha + v_m cos\alpha)]}dxdy\,] \\
&\quad \cdot e^{-j2\pi(u_m x_{m0} + v_m y_{m0})} \\
&= H(\,u_m\cos\alpha + v_m\sin\alpha, -u_m\sin\alpha + v_m cos\alpha\,)e^{-j2\pi(u_m x_{m0} + v_m y_{m0})}\,. \qquad (4.7)
\end{aligned}$$

From the above relation of the Fourier transforms $H_m(u_m,v_m)$ and $H(u,v)$, the coordinate relation in the spectrum domain is given as

$$u = u_m\cos\alpha + v_m\sin\alpha \qquad (4.8)$$

$$v = -v_m\sin\alpha + v_m\cos\alpha \qquad (4.9)$$

or

$$u_m = u\cos\alpha - v\sin\alpha \qquad (4.10)$$

$$v_m = u\sin\alpha + v\cos\alpha\ . \qquad (4.11)$$

In terms of the above expressions, the following comments can be made:

(1) The spectrum domain coordinate system uov, corresponding to xoy, has a rotation, with an angle α, relative to the spectrum domain coordinate system $u_m o_m v_m$, corresponding to $x_m o_m y_m$. Thus, if α is determined, then the ship's direction relative to the sensor's direction can be obtained.

(2) The translation (x_{m0}, y_{m0}) between the two spatial coordinate systems reflects only on the phase of $H_m(u_m, v_m)$. Thus, it is not important to know the translation since the wave number and wave angle are determined from the magnitude of the Fourier spectrum or the power spectrum.

(3) When $\alpha = 0$, then $|H_m(u_m, v_m)| = |H(u_m, v_m)|$, the wave number components and the spatial frequencies have simple relations, i.e., $K_x = 2\pi u_m$ and $K_y = 2\pi v_m$, and the wave angle is given as $\theta = tan^{-1}\frac{v_m}{u_m}$. For this case, the speed can be calculated by directly measuring the position of the locus points in the spectrum diagram.

(4) According to the spectrum coordinate relation, it follows $u_m^2 + v_m^2 = u^2 + v^2$; thus, the wave number K is invariant with the coordinate system transform, that is,

$$K = 2\pi\sqrt{u_m^2 + v_m^2} = 2\pi\sqrt{u^2 + v^2} \quad . \tag{4.12}$$

With the above relations and the conclusions, the general formulas to determine a moving ship's direction and speed are derived in the following. First, consider the ship's wave spectrum locus in the uov coordinate system. From (4.1), $Kcos^2\theta = \frac{g}{U}$; thus, for any two locus points, it follows

$$\sqrt{K_1}cos\theta_1 = \sqrt{K_2}cos\theta_2 \tag{4.13}$$

where the subscript, 1 or 2, indicates that the wave number and angle are obtained from the given point 1 or 2. Since $\cos\theta = \frac{u}{\sqrt{u^2+v^2}} = \frac{2\pi u}{K}$, (4.13) can be rewritten as

$$\sqrt{K_2}u_1 = \sqrt{K_1}u_2 \quad . \tag{4.14}$$

In the $u_m o_m v_m$ coordinate system, (4.14) becomes

$$\sqrt{K_2}(u_{m1}\cos\alpha + v_{m1}\sin\alpha) = \sqrt{K_1}(u_{m2}\cos\alpha + v_{m2}\sin\alpha) \tag{4.15}$$

and, thus, the angle α can be estimated from

$$\hat{\alpha} = -tan^{-1}\frac{\sqrt{K_1}u_{m2} - \sqrt{K_2}u_{m1}}{\sqrt{K_1}v_{m2} - \sqrt{K_2}v_{m1}} \quad . \tag{4.16}$$

Similarly, the ship speed can be calculated from

$$\hat{U} = \sqrt{\frac{g}{K_j cos^2\theta_j}} = \sqrt{\frac{g}{2\pi}} \frac{\sqrt{K_j}}{|u_{mj} cos\hat{\alpha} + v_{mj} \sin \hat{\alpha}|} \tag{4.17}$$

where $j = 1$ or 2.

In real situations, the ship wave spectrum is discrete, and thus the locus points on the spectrum diagram will not always exactly locate on the sampling grids. This results in errors on some locus points when they are read from the spectrum diagram. To remove this effect on the calculation of the ship's speed and direction, many pairs of locus points can be used to calculate the ship's direction and speed, and then their average is taken as the estimate of the direction and speed. Specifically, consider there are M pairs of locus points available. The angle α is calculated with each pair of points, and the average of the calculated angles $\hat{\alpha}_i$, $i = 1, ..., M$ is then considered as the estimate of α, i.e.,

$$\bar{\alpha} = \frac{1}{M} \sum_{i=1}^{M} \hat{\alpha}_i \quad . \tag{4.18}$$

The average of $\hat{U}_i$, $i = 1, ..., 2M$ is considered to be the estimate of the ship speed , that is,

$$\begin{aligned} \bar{U} &= \frac{1}{2M} \sum_{i=1}^{2M} \hat{U}_i \\ &= \frac{1}{2M} \sum_{i=1}^{2M} \sqrt{\frac{g}{2\pi}} \frac{\sqrt{K_i}}{|u_{mi} cos\bar{\alpha} + v_{mi} \sin \bar{\alpha}|} \quad . \end{aligned} \tag{4.19}$$

The formulas for estimating a moving ship's direction and speed from a two dimensional wave spectrum have been derived above. The scheme for the estimation is now shown in Figure 4.5. In real situations, ship waves are involved in a random sea background. Thus, a wave spectrum contains not only the ship wave components but also the noise components. To remove the random noise and other undesired

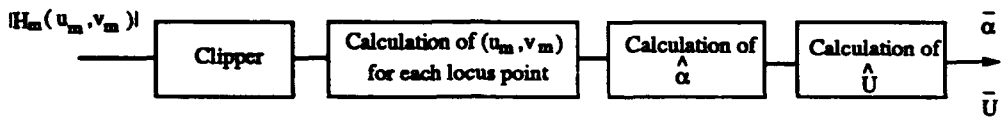

Figure 4.5: Scheme for estimating a moving ship's direction and speed from its wave spectrum

components, digital processing techniques may be used. The clipper shown in the figure is used for the this purpose.

Theoretically, the two dimensional Fourier transform of the ship generated wave is composed of δ-functions; thus, there are many infinite-size impulses located on the loci of the spectrum diagram as discussed in Chapter 3. When the finite wave patch is sensed as in real situations, they are on the order of $O(L_c)$ [6], where L_c denotes the characteristic length of the finite patch. For the case of high signal to noise ratio, a simple processing method can be used. For instance, a clipper is used to remove the background noise components. This processing is helpful in determining the position of each locus point. From the positions (u_{mi}, v_{mi}) of locus points, the ship's direction and speed finally are calculated. The algorithm can be implemented in software with a fast and accurate estimation performance.

To demonstrate the above method, consider here an example of the Quapaw's wave elevation field, shown in Figure 4.1(a). It is assumed in the calculation that the ship's direction and speed are $\alpha = 10°$ and $U = 2.229$ meters/second, and that the sampling intervals in the x- and y-directions are 0.2 meters. The ship's direction and speed are estimated from the spectrum of the wave field, whose contour plot is shown in Figure 4.6. Note that the subscript "m" has been used in this figure to

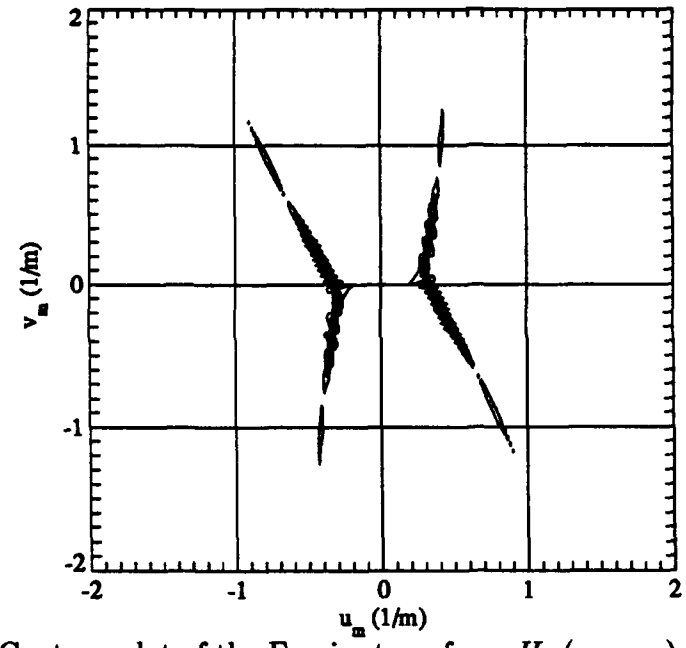

Figure 4.6: Contour plot of the Fourier transform $H_m(u_m, v_m)$ of the Quapaw's wave elevation.

emphasize the image coordinate system. A total of 183 locus points are evaluated for the right locus on the spectrum with a threshold of $\mu_H + \sigma_H$, where μ_H and σ_H are the mean and standard deviation of the spectrum intensity. According to the computer calculation, the estimated direction is $\hat{\alpha} = 9.999°$ with a relative error of 0.006% and a r.m.s. error of 0.233°; the estimated speed is $\hat{U} = 2.230$ meters/second with a relative error of 0.03% and a r.m.s. error of 0.019 meters/second.

4.3 Estimation of a Ship's Speed and Direction from 1-D Wave Spectra

This section discusses the estimation of a moving ship's speed and direction from its one dimensional wave spectrum. The expression for the spectrum of a wave cut making an angle with the positive x-axis has been given in (3.40). The wave cut spectrum has two peaks under certain conditions, and the frequency positions of the two peaks can be used to estimate the ship's direction and speed, as suggested by

Tuck et al [6]. For this one-cut method, the formulas for estimating the direction and speed are given here first, and then another method, called the two-cut method, is introduced for estimating the ship speed from two wave cuts parallel to the ship's central line. Examples are also given to demonstrate the two methods.

4.3.1 One-cut Method

The discussion begins with the wave cut spectrum and its properties. The spectrum expression for a wave cut have been given in (3.40), that is,

$$\tilde{H}(f) = \frac{1}{|\Phi'(\theta)|} \{ A^*(\theta)\, e^{j\Phi_0(\theta_0)} \}^{*\bullet}$$

with a constraint condition for θ, $f - |\Phi(\theta)| = 0$, as in (3.41). This condition indicates θ is a function of frequency f; thus, there may exist some frequencies such that $\Phi'(\theta) = 0$, and hence there may exist some singularities for the spectrum. For the finite length wave cut, this will cause some sharp peaks on its spectrum diagram. The peak height is proportional to the square root of the data record length [6]. The frequency points of the peaks on the wave cut spectrum can be determined by two equations, (3.41) and

$$\Phi'(\theta) = 0 \quad . \tag{4.20}$$

Here, Φ depends on the wave angle θ as well as the wave cut angle α. Substituting the approximation of Φ given in (3.43), $\Phi(\theta) \approx \frac{K_0 U_p}{2\pi} \frac{\cos(\theta-\alpha)}{\cos^2\theta}$, into (4.20) and then solving the resulting equation together with $f - |\Phi(\theta)| = 0$ yields the relation between θ and α:

$$\alpha = tan^{-1} \frac{\sin 2\theta}{\cos 2\theta - 3} \quad . \tag{4.21}$$

The curve of α versus θ is plotted in Figure 4.7 (a). It is found from the figure or calculation that $|sin^{-1}\frac{1}{3}|(= 19.5°)$ is the maximum wave cut angle for the peaks to exist.

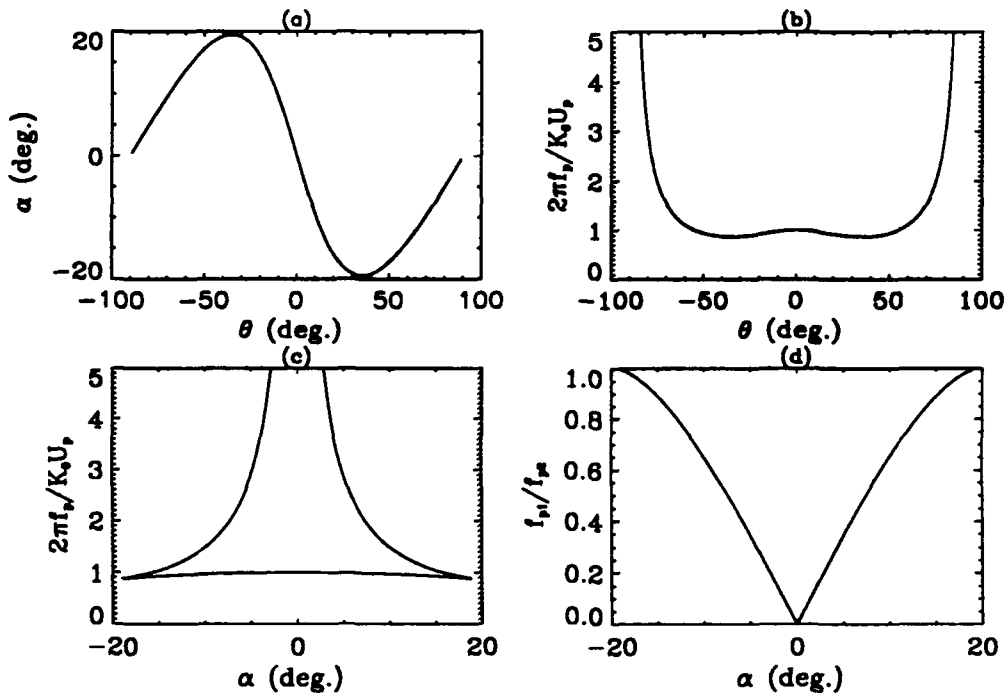

Figure 4.7: Relations between the wave angle θ, cut angle α and frequency f_p at peaks. (a) α versus θ; (b) $\frac{2\pi f_p}{K_0 U_p}$ versus θ; (b) $\frac{2\pi f_p}{K_0 U_p}$ versus α; (b) $\frac{f_{p1}}{f_{p2}}$ versus α.

With the above relation of θ and α, the special frequency points f_p are obtained from $f - |\Phi(\theta)| = 0$ in the form

$$\frac{2\pi f_p}{K_0 U_p} = \frac{1}{\cos\theta\sqrt{4 - 3\cos^2\theta}} \quad . \tag{4.22}$$

The frequencies also can be directly expressed in a function of the wave cut angle α:

$$\frac{2\pi f_p}{K_0 U_p} = \sqrt{\frac{3}{4 - r_{1,2}^2(\alpha)}} \tag{4.23}$$

where $K_0 = \frac{g}{U^2}$, and U_p and U are the speeds of the sensor and ship, respectively,

and where

$$r_{1,2}(\alpha) = \frac{(1 - 8\tan^2\alpha) \pm 3\sqrt{1 - 8\tan^2\alpha}}{2(1 + \tan^2\alpha)} \tag{4.24}$$

represents the value r_1 with "+" or r_2 with "−" before the sign of square root. Since r_1 and r_2 are real, $1 - 8tan^2\alpha \geq 0$, which is equivalent to $\alpha \leq |sin^{-1}\frac{1}{3}|$ as asserted above. In terms of (4.23) and (4.24), there are one or two frequency points, corresponding to r_1 and r_2, where the peaks appear. When $\alpha = 0$, there is a finite frequency point f_{p1} and an infinite frequency point $f_{p2} = \infty$; when $0 < \alpha < |sin^{-1}\frac{1}{3}|$, there are two finite frequency points, f_{p1} and f_{p2}; when $\alpha = |sin^{-1}\frac{1}{3}|$ there is only one finite frequency point $f_{p1} = f_{p2}$.

From the above special frequency points, the ship's direction is estimated first and then the speed is calculated. When $0 < \alpha < |sin^{-1}\frac{1}{3}|$, the direction is estimated by calculating the ratio of the above special frequencies, i.e.,

$$\frac{f_{p1}}{f_{p2}} = \sqrt{\frac{4 - r_2^2(\alpha)}{4 - r_1^2(\alpha}} \quad . \tag{4.25}$$

The frequencies f_{p1} and f_{p2} are found from the wave cut spectrum, then the wave cut angle is obtained by solving (4.25), and finally the ship speed is calculated from (4.23) by noting the relation of K_0 with the speed, i.e., $K_0 = \frac{g}{U^2}$. Figure 4.7 (d) shows the curve of the ratio $\frac{f_{p1}}{f_{p2}}$ versus the wave cut angle α. When $\alpha = 0$, the ship speed is directly estimated from f_{p1} with the formula

$$\frac{2\pi f_{p1}}{K_0 U_p} = 1 \quad . \tag{4.26}$$

To demonstrate the above one-cut method, consider here an example in which the wave elevation cut, shown in Figure 4.8(a) is calculated using WAVEAMP. The ship model is the same as in the above two dimensional case. Each cut has 256 data points and a sampling interval of 0.001 seconds. It is assumed that the ship has a

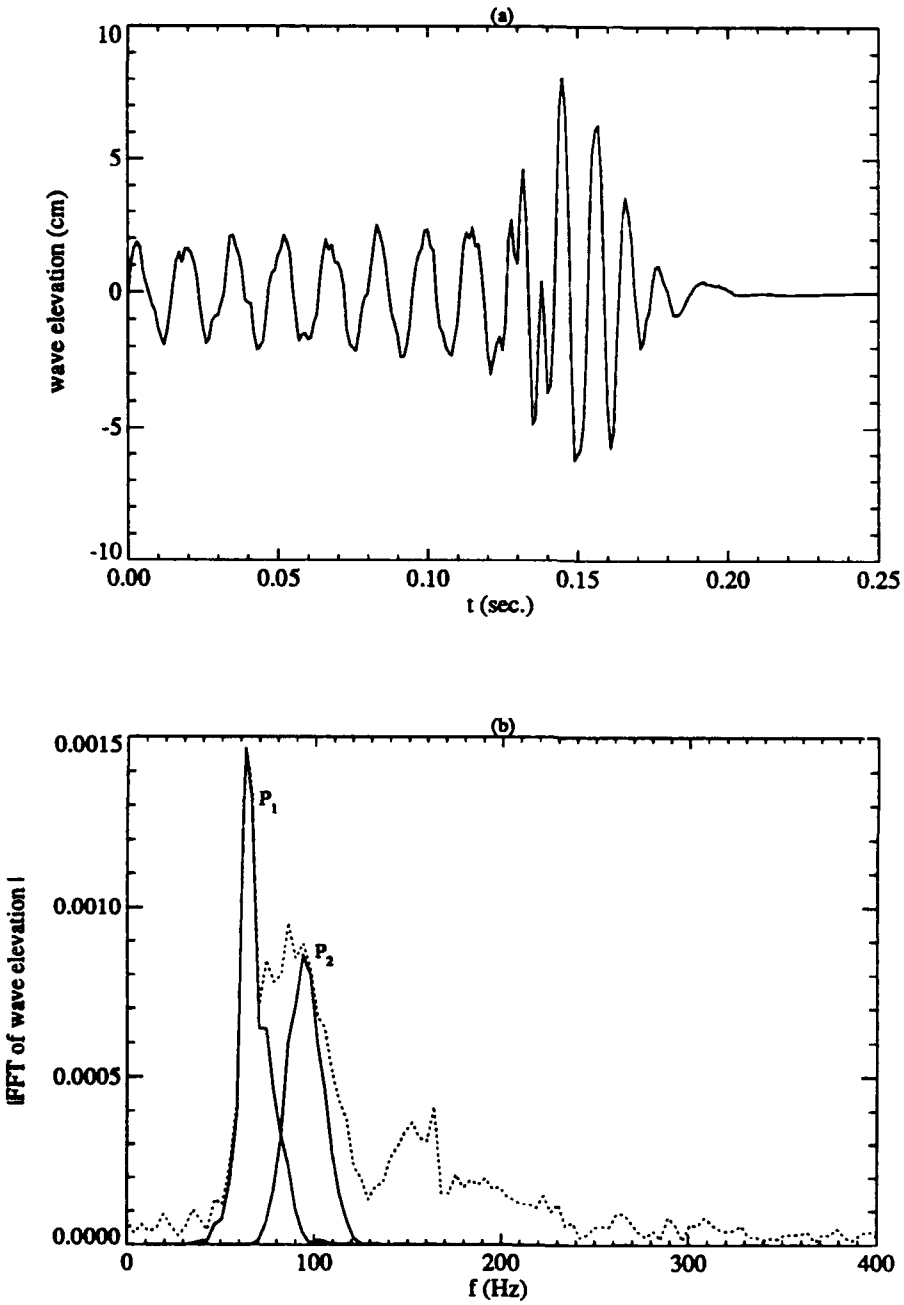

Figure 4.8: (a) Wave elevation cut calculated from WAVEAMP for the Quapaw model with wave cut angle $\alpha = 10°$, speed $U = 2.229$ m/s, and $(x_{m0}, y_{m0}) = (-48.5087, -20.5690)$; (b) Magnitude of the Fourier transform (dotted line) of the wave elevation from (a), and two peaks (solid lines) where $f - |\Phi(\theta)| = 0$.

direction of $\alpha = 10°$ relative to the sensor's direction, and that the sensor's speed is $U_p = 199.219$ meters/second. The frequency points at peaks are obtained from the spectrum, which is the dotted line in Figure 4.8(b). The two desired peaks have been detected and are shown in solid lines in the figure. Since the two peaks are located close together, the peak P_2 has a little left shift in the spectrum shown in the dotted line. Thus, the peak P_2 has to be determined after removing the peak P_1 from the spectrum using a bandpass filter with good selectivity. The filtering, position detection and all other calculation can be automatically completed using a computer program. According to the computer calculation, the detected position of the two peaks are $f_{p1} = 62.5\ H_z$ and $f_{P2} = 95.7\ H_z$; the estimated direction is $\hat{\alpha} = 10.019°$ with a relative error of 0.19%; the estimated speed is $\hat{U} = 2.195$ meters/second with a relative error of 1.51%.

4.3.2 Two-cut Method

When a wave cut is parallel to the ship's central line, the wave cut angle is equal to zero. For this case, an alternative method can be used, which is called here the two-cut method because two wave cuts parallel to the ship's central lines are used. In this method, the ship speed is estimated from the relative phase difference between the Fourier transforms of the two wave cuts. The derivation and example are now given below.

First, recall the relation between the wave amplitude function and the Fourier transform of a wave cut with $\alpha = 0$, which are given in (3.46) and (3.47):

$$A(\theta) = \tilde{H}(f)\frac{|K_y(\theta)|}{2\pi}e^{j(K_x(\theta)x_0 + K_y(\theta)y_0)} \tag{4.27}$$

$$f - \frac{g}{2\pi U \cos\theta} = 0 \ . \tag{4.28}$$

Now, consider two parallel wave cuts with cut angle $\alpha = 0$, distance $\Delta y = y_2 - y_1$ and the same starting point x_0 in the x-direction. The Fourier transforms of the two wave cuts are $\tilde{H}_1(f)$ and $\tilde{H}_2(f)$. Since the wave amplitude function $A(\theta)$ is supposed to be the same for the two wave cuts, using the above relation and dividing $\tilde{H}_2(f)$ by $\tilde{H}_1(f)$ leads the following relation

$$\frac{\tilde{H}_1(f)}{\tilde{H}_2(f)} = e^{jf\Delta y \frac{g}{U^2} \frac{\sin\theta(f)}{\cos^2\theta(f)}} \tag{4.29}$$

where the relation $K_y = \frac{g\sin\theta}{U^2\cos^2\theta}$ has been used. If the phase difference of $\tilde{H}_2(f)$ and $\tilde{H}_1(f)$ is represented by $\Delta\phi_H$, then the phase relation in (4.29) can be written in the form

$$\frac{g\sin\theta(f)}{U^2\cos^2\theta(f)} = \frac{\Delta\phi_H}{f\Delta y} \quad . \tag{4.30}$$

From (4.28), $\cos\theta(f) = \frac{g}{2\pi f U}$. Substituting this relation into (4.30) yields

$$\frac{(2\pi)^4 U^2}{g^2}[1 - (\frac{g}{2\pi f U})^2] = \frac{\Delta\phi_H}{f\Delta y} \quad . \tag{4.31}$$

Note that from the above expression, $\frac{g}{2\pi f U}$ approaches 1 as $\Delta\phi_H$ approaches 0. Thus, once we can find the frequency f_{min} corresponding to the minimum value of $|\Delta\phi_H|$, then the ship speed can be found from

$$\hat{U} = \frac{g}{2\pi f_{min}} \quad . \tag{4.32}$$

To demonstrate this two-cut method, consider an example in which the ship wave elevation cuts were measured by three capacitance wave probes when the Quapaw model was towed in a tow tank [1]. Three wave cuts were obtained for each run. The wave elevation of two runs, RUN3 and RUN5, are shown in Figure 4.9. As an example, Figure 4.10 shows the magnitude of the spectra of wave cuts RUN5-B

[1]The experiments were made by Ship Hydrodynamics Laboratory, Department of Naval Architecture and Marine Engineering, the University of Michigan in October, 1990.

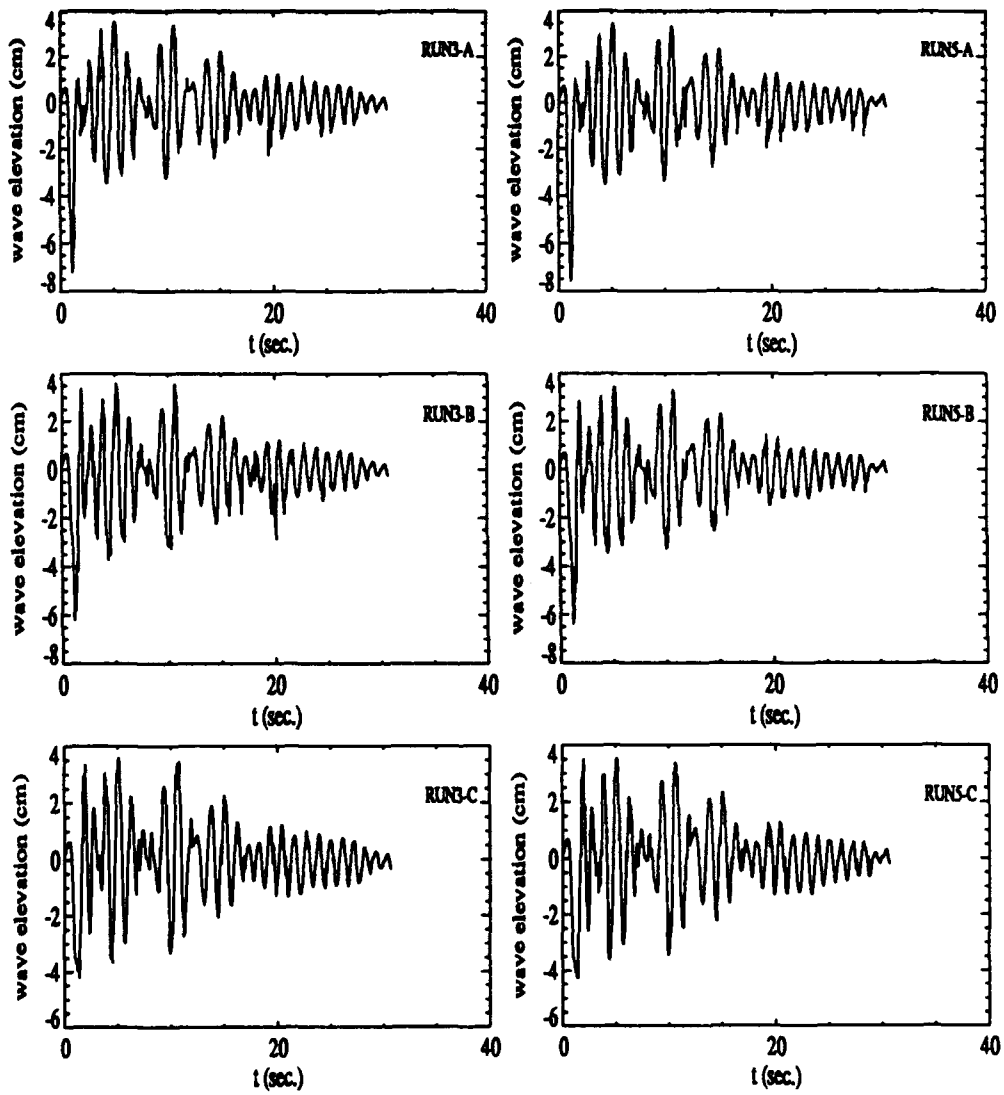

Figure 4.9: Wave elevation cuts from tow tank experiments for the Quapaw model.

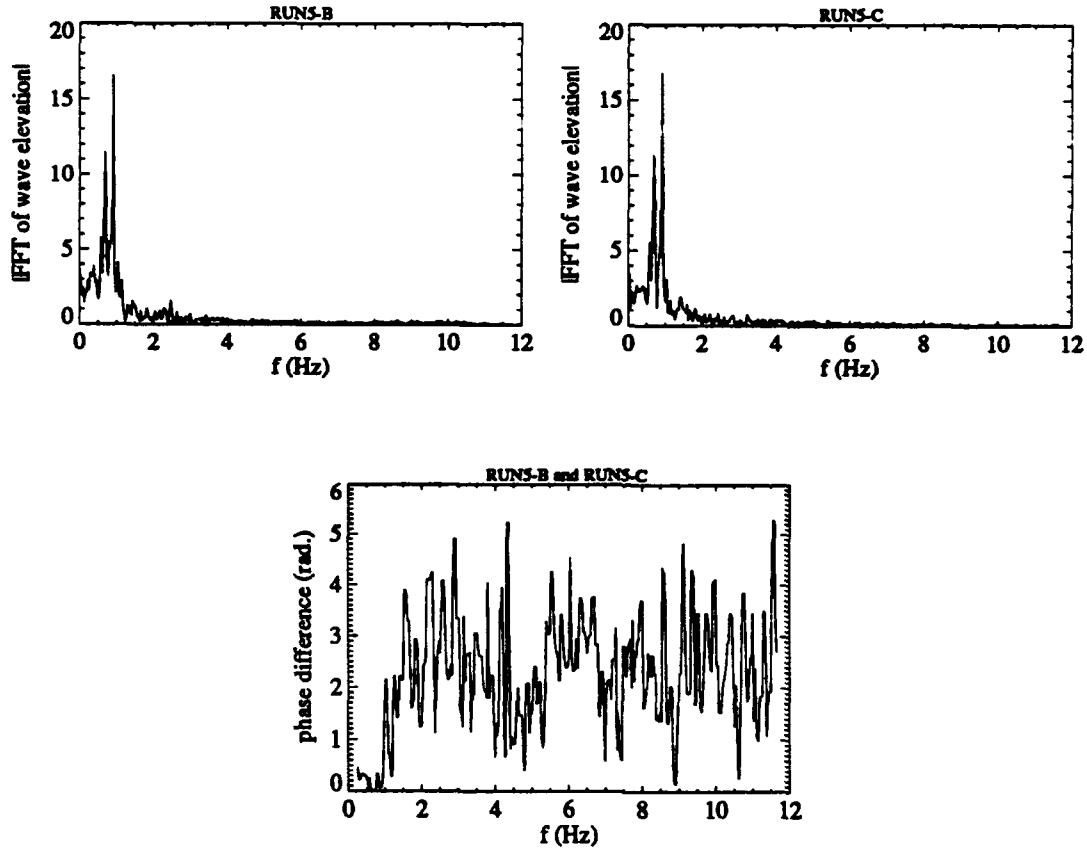

Figure 4.10: Magnitude of the FFT of wave cuts, RUN5-B and RUN5-C, and their phase difference $\Delta\phi_H$.

and RUN5-C and their phase difference. Here, $\Delta\phi_H$ has been processed using a median filter with a 3-point window size for detecting the minimum point of the phase difference. The estimation results are listed in Table 4.1.

So far, the methods for estimating a moving ship's direction and speed from one and two dimensional wave spectra have been discussed. Comparing these methods, the two dimensional method has three primary advantages. First, it has no limitation on the ship's moving direction, except for the 180° ambiguity that results if no further prior information is used. This is opposed to the one-cut method, which is suitable only for the cut angles, α, between $[-19.5°, 19.5°]$, but is unable to tell the positive

	RUN3		*RUN5*	
cuts	$\hat{U}$ *(m/s)*	*error (%)*	$\hat{U}$ *(m/s)*	*error (%)*
a & b	2.283	2.4	2.283	2.4
a & c	2.283	2.4	2.283	2.4
b & c	2.283	2.4	2.179	2.2

Table 4.1: Ship speed estimated from the Quapaw's wave cuts using the two-cut method.

or negative angle, and may result in false detection if obvious peaks also exists when $|\alpha| > 19.5°$. Second, the two dimensional method works well even in the presence of ambient waves and background noise because of the spectrum feature of ship generated waves. In the one-cut method, the ship wave signal can be easily corrupted by ambient waves and background noise, and thus it may result in false detection of the peak position. Third, the two dimensional method appears to achieve more accurate estimation results than the one dimensional methods. Because of these reasons, the two dimensional method should be always considered first when two dimensional spectra are available. It has recently become possible to obtain these data from air-borne or space-borne radar systems or other modern remote sensing techniques.

CHAPTER V

ESTIMATION OF SHIP LENGTH

This chapter gives a detailed discussion of the estimation of a ship's length from its amplitude function. The ship length is an important quantity to be estimated in remotely sensing ship characteristics, and it is also an important parameter in the further estimation of ship hull. In recovering a ship's hull shape from the wave amplitude function, an inversion problem is involved, that is, an integral equation must be solved, which will be discussed in the next chapters. The integral limits along the x-direction are specified by the ship length. Therefore, the accuracy of the recovered ship hull shape will depend, to a great extent, on the accuracy of the estimated ship length.

The principle of the estimation of ship length is that there is the relation between a ship's hull and its wave amplitude function, and that ship length information is contained in the observable periodic character of the wave amplitude function. This character can be found not only in the real and imaginary parts of the wave amplitude function, but also in the magnitude of the wave amplitude function.

In this chapter, a theoretical model of the wave amplitude function is developed, and three methods are designed for the estimation of a ship's length. The first section discusses the relationship between a ship's hull and its wave amplitude function; the

second section gives the theoretical proof and analysis about this periodic character for general ship hull shapes and the relation between a ship's length and its bow and stern's shapes; the final section gives a discussion of the estimation methods.

5.1 Relationship between a Ship's Hull and its Wave Amplitude Function

In the study of fluid motion, wave flows due to a moving body are imagined to be generated by a continuous volume distribution of singularities within the body, extending out to its surface [14]. In this section, the discussion starts directly from the relationship between the wave amplitude function and wave source densities or source singularities. The non-dimensional form of the relation has been described by Eggers et al. [20]. After some mathematical manipulations, the dimensional form of this relation is given by

$$A(\theta) = \frac{4g\sec^3\theta}{U^3}\int_D \sigma(x,y,z)\exp\{K(\theta)z + \mathrm{j}(K_x(\theta)x + K_y(\theta)y\}dD \tag{5.1}$$

where σ represents the source distribution, D is the source region, and K, K_x, and K_y are the wave numbers defined in Chapter 2. To estimate a ship's length and hull by using this formula, the following two assumptions are made about the source region and the relation between the singularity distribution and the ship hull.

To simplify the source region, it is now assumed that the ship hull is thin, that is, the beam is small compared to all other characteristic lengths of the problem [14]. Thus, the singularity distribution can be envisaged to be on the ship's centerplane, instead of on the ship's hull surface, and the source region is considered to be $-\frac{L}{2} \le x \le \frac{L}{2}$ and $-H \le z \le 0$, where L and H denote the ship length and draft, respectively. Under this assumption, (5.1) becomes

$$A(\theta) = \frac{4g\sec^3\theta}{U^3}\int_{-\frac{L}{2}}^{\frac{L}{2}}\int_{-H}^{0} \sigma(x,z)\exp\{K(\theta)z + \mathrm{j}K_x(\theta)x\}dxdz \ . \tag{5.2}$$

This formula will be used to analyze the periodic character of the wave amplitude function.

In the estimation of ship hull shape in the next chapter, the explicit relation between the wave amplitude function and the ship hull is useful, and thus is given below. To the first-order approximation, the relationship between a hull's geometry and its centerplane singularity distribution can be obtained:

$$\sigma(x,y) = \frac{U}{2\pi}\frac{\partial\zeta(x,z)}{\partial x} \tag{5.3}$$

where $\zeta(x,z)$ defines the local half-beam of the hull surface. Thus, combining (5.2) and (5.3) gives the explicit relation between the wave amplitude function and the ship's hull:

$$A(\theta) = \frac{2g\sec^3\theta}{\pi U^2}\int_{-\frac{L}{2}}^{\frac{L}{2}}\int_{-H}^{0}\frac{\partial\zeta(x,z)}{\partial x}\exp\{K(\theta)z + \mathrm{j}K_x(\theta)x\}dxdz \ . \tag{5.4}$$

For simplicity in discussion, the normalization of x and z with respect to the ship length L and draft H is considered. By letting

$$x = \frac{L}{2}x' \qquad x' \in [-1,1] \tag{5.5}$$

$$z = Hz' \qquad z' \in [-1,0] \tag{5.6}$$

equations (5.2) and (5.4) respectively become

$$A(\theta) = \frac{2}{g^2}LHU^3K_x^3(\theta)\int_{-1}^{1}\int_{-1}^{0}\sigma(x',z')e^{\mathrm{j}\nu(\theta)x'}\,e^{\mu(\theta)z'}dx'dz' \tag{5.7}$$

$$A(\theta) = \frac{2}{\pi g^2}HU^4K_x^3(\theta)\int_{-1}^{1}\int_{-1}^{0}\frac{\partial\zeta(x',z')}{\partial x'}e^{\mathrm{j}\nu(\theta)x'}\,e^{\mu(\theta)z'}dx'dz' \tag{5.8}$$

where

$$\nu(\theta) = \frac{L}{2}K_x(\theta) = \frac{gL}{2U^2\cos\theta} = \frac{1}{2F_n^2\cos\theta} \tag{5.9}$$

$$\mu(\theta) = \frac{HU^2}{g}K_x^2(\theta) = \frac{gH}{U^2\cos^2\theta} = \frac{H}{L}\frac{1}{F_n^2\cos^2\theta} \tag{5.10}$$

For ease of notation, the prime on x and z will be ignored in the following discussion.

5.2 Periodic Character of the Ship Wave Amplitude Function

The periodic character of the ship wave amplitude function can be observed when the wave amplitude function is described as a function of the longitudinal wave number K_x and plotted on a K_x-A diagram. This periodicity is proved mathematically in this section, and the inherent connection between the ship length and the periodic character will be discussed.

In the following derivation, the wave amplitude function with two dimensional integral form in (5.7) is rewritten into a marginal integral of only x. Its integrand is expressed in the form of a power series and the integral is then calculated. After mathematic manipulations, the real and imaginary parts of the wave amplitude function are expressed in the form of cosine functions and their periodic characters are then analyzed.

The wave amplitude function in (5.7) can be expressed as a marginal integral of x by defining a function $F(x)$, i.e.,

$$A(K_k) \triangleq A(\theta) = \int_{-1}^{1} F(x) e^{j\nu x} dx \tag{5.11}$$

where

$$F(x) \triangleq \frac{2}{g^2} LHU^3 K_x^3 \int_{-1}^{0} \sigma(x,z)\, e^{\mu z} dz \ . \tag{5.12}$$

Here, the wave amplitude function has also been written into a function of variable K_x instead of θ. The integrand function $F(x)$ is another weighted integral of the singularity distributions. With the assumption given in (5.3), $F(x)$ will directly relate to the ship hull shape, thus generally $F(x)$ is a smooth function. In the discussion here, it is assumed that $F(x)$ and its derivatives are continuous in the

region $-1 \leq x \leq 1$, so that $F(x)$ can be expressed in the form of a power series of x

$$F(x) = \sum_{j=0}^{\infty} a_j x^j = \sum_{i=0}^{\infty} a_{2i} x^{2i} + \sum_{i=0}^{\infty} a_{2i+1} x^{2i+1} \quad . \tag{5.13}$$

Now, substitute (5.13) into (5.11) and then integrate it. In the calculations, the following integral formulas are useful:

$$\int x^n \cos ax = p_{R_n}(a,x) \cos ax + q_{R_n}(a,x) \sin ax \tag{5.14}$$

$$\int x^n \sin ax = p_{I_n}(a,x) \cos ax + q_{I_n}(a,x) \sin ax \tag{5.15}$$

where n is an integer and

$$p_{R_n}(a,x) = \begin{cases} 0 & \text{for } n = 0 \\ \sum_{r=0}^{[\frac{n-1}{2}]} (-1)^r \frac{n!}{(n-2r-1)!} \cdot \frac{x^{n-2r-1}}{a^{2r+2}} & \text{for } n > 0 \end{cases} \tag{5.16}$$

$$q_{R_n}(a,x) = \sum_{r=0}^{[\frac{n}{2}]} (-1)^r \frac{n!}{(n-2r)!} \cdot \frac{x^{n-2r}}{a^{2r+1}} \tag{5.17}$$

$$p_{I_n}(a,x) = \sum_{r=0}^{[\frac{n}{2}]} (-1)^{r+1} \frac{n!}{(n-2r)!} \cdot \frac{x^{n-2r}}{a^{2r+1}} \tag{5.18}$$

$$q_{I_n}(a,x) = \begin{cases} 0 & \text{for } n = 0 \\ \sum_{r=0}^{[\frac{n-1}{2}]} (-1)^r \frac{n!}{(n-2r-1)!} \cdot \frac{x^{n-2r-1}}{a^{2r+2}} & \text{for } n > 0 \end{cases} \tag{5.19}$$

With the above integral formulas, the wave amplitude function in (5.11) becomes a form from which the periodic character can be observed much more easily:

$$\begin{aligned} A(K_x) &\triangleq A_R(K_x) + \mathrm{j} A_I(K_x) \\ &= Q_R(K_x) \cos \Theta_R(K_x) + \mathrm{j} Q_I(K_x) \cos \Theta_I(K_x) \end{aligned} \tag{5.20}$$

where $A_R(K_x) = Q_R(K_x) \cos \Theta_R(K_x)$ and $A_I(K_x) = Q_I(K_x) \cos \Theta_I(K_x)$ denote the real and imaginary parts of the wave amplitude function. When the function $F(x)$ is an even function of x, A_R will vanish. With the notation $\nu = \frac{L}{2} K_x$ as in (5.9),

$Q_R(K_x)$, $Q_I(K_x)$, $\Theta_R(K_x)$ and $\Theta_I(K_x)$ in (5.20) are defined by

$$Q_R(K_x) = 2[(\sum_{i=0}^{\infty} a_{2i}\, p_{R_{2i}}(\nu))^2 + (\sum_{i=0}^{\infty} a_{2i}\, q_{R_{2i}}(\nu))^2]^{\frac{1}{2}} \tag{5.21}$$

$$Q_I(K_x) = 2[(\sum_{i=0}^{\infty} a_{2i+1}\, p_{I_{2i+1}}(\nu))^2 + (\sum_{i=0}^{\infty} a_{2i+1}\, q_{I_{2i+1}}(\nu))^2]^{\frac{1}{2}} \tag{5.22}$$

$$\Theta_R(K_x) = \nu - \phi_R(\nu) \tag{5.23}$$

$$\Theta_I(K_x) = \nu - \phi_I(\nu) \tag{5.24}$$

where

$$\phi_R(\nu) = \tan^{-1}[\frac{\sum_{i=0}^{\infty} a_{2i} q_{R_{2i}}(\nu)}{\sum_{i=0}^{\infty} a_{2i} p_{R_{2i}}(\nu)}] \tag{5.25}$$

$$\phi_I(\nu) = \tan^{-1}[\frac{\sum_{i=0}^{\infty} a_{2i+1} q_{I_{2i+1}}(\nu)}{\sum_{i=0}^{\infty} a_{2i+1} p_{I_{2i+1}}(\nu)}] \tag{5.26}$$

$$p_{R_{2i}}(\nu) = \begin{cases} 0 & \text{for } i = 0 \\ \sum_{r=0}^{i-1}(-1)^r \frac{(2i)!}{(2i-2r-1)!} \cdot \frac{1}{\nu^{2r+2}} & \text{for } i = 1, 2, 3, \ldots \end{cases} \tag{5.27}$$

$$q_{R_{2i}}(v) = \sum_{r=0}^{i}(-1)^r \frac{(2i)!}{(2i-2r)!} \cdot \frac{1}{\nu^{2r+1}} \tag{5.28}$$

$$p_{I_{2i+1}}(\nu) = \sum_{r=0}^{i}(-1)^{r+1} \frac{(2i+1)!}{(2i-2r+1)!} \cdot \frac{1}{\nu^{2r+1}} \tag{5.29}$$

$$q_{I_{2i+1}}(\nu) = \sum_{r=0}^{i}(-1)^r \frac{(2i+1)!}{(2i-2r)!} \cdot \frac{1}{\nu^{2r+2}} \tag{5.30}$$

From (5.20), it is found that both the real and imaginary parts A_R and A_I of the wave amplitude function consist of signals with an K_x-varying magnitude and an K_x-varying "frequency". That is, both the magnitudes, $Q_R(K_x)$ and $Q_I(K_x)$, and the instantaneous "frequencies", $\frac{1}{2\pi}\frac{d\Theta_R}{dK_x}$ and $\frac{1}{2\pi}\frac{d\Theta_I}{dK_x}$, change with K_x. Here, the frequency concept for a time signal is used. By quoting the terminologies in telecommunications, the real and imaginary parts look like two signals, both amplitude and angle modulated with "carrier frequency" $\frac{L}{4\pi}$ if K_x is the analog of time t.

In the above discussion, it has been assumed that $F(x)$ and its derivatives are smooth and continuous in the hull surface region. Thus, there is one dominant fre-

quency component at frequency $\frac{L}{4\pi}$ in the above expressions of A_R and A_I. However, the real situation may not be so perfect. $F(x)$ may be a piecewise smooth function, that is, there are some discontinuous function and derivative points. In this case, harmonic frequency components will appear. For example, assume that there is one discontinuous point at $x = x_b \in (-1, 1)$, and $F(x)$ is expressed in the form

$$F(x) = \begin{cases} \sum_{j=0}^{\infty} a_j x^j & \text{for } -1 \leq x \leq x_b \\ \sum_{j=0}^{\infty} b_j x^j & \text{for } x_b \leq x \leq 1 \end{cases} \tag{5.31}$$

Substituting (5.31) into (5.11) yields the results

$$\begin{aligned} A_R(K_x) &= Q_{R_1}(K_x)\cos(\nu - \phi_{R_1}(v)) + \\ &\quad Q_{R_2}(K_x, x_b)\cos(x_b\nu - \phi_{R_2}(v, x_b)) \end{aligned} \tag{5.32}$$

$$\begin{aligned} A_I(K_x) &= Q_{I_1}(K_x)\cos(\nu - \phi_{I_1}(v)) + \\ &\quad Q_{I_2}(K_x, x_b)\cos(x_b\nu - \phi_{I_2}(v, x_b)) \end{aligned} \tag{5.33}$$

where the magnitudes Q_{R_1}, Q_{R_2}, Q_{I_1}, Q_{I_2} and the phases ϕ_{R_1}, ϕ_{R_2}, ϕ_{I_1}, ϕ_{I_2} are combined with the coefficients $p_{R_i}(v, x)$, $q_{R_i}(v, x)$, $p_{I_i}(v, x)$ and $q_{I_i}(v, x)$, defined in (5.16) $-$(5.19), at $x = -1, x_b$, or 1. The detailed expressions for these magnitudes and phases can be found in the appendix. In (5.32) and (5.33), $\cos(\nu - \phi_{R_1}(v))$ and $\cos(\nu - \phi_{I_1}(v))$ represent higher frequency components generated at the ship's bow and stern, i.e., $x = \pm 1$, and they are similar to those in (5.20) with frequency $\frac{L}{4\pi}$. The new frequency components $\cos(x_b\nu - \phi_{R_2}(v, x_b))$ and $\cos(x_b\nu - \phi_{I_1}(v, x_b))$ are generated by the discontinuous point at $x = x_b$, and their frequency $\frac{x_b L}{4\pi}$ is lower than $\frac{L}{4\pi}$ since $|x_b| < 1$. When $x_b = 0$, A_R and A_I may contain a direct current component.

Generally speaking, each discontinuous point in the function $F(x)$ may add a new frequency component to A_R and A_I, and the frequency is always lower than $\frac{L}{4\pi}$. As mentioned before, the function $F(x)$ is related to the shape of a ship hull.

Thus, the increase in the discontinuity of the hull surface or its derivatives will result in an increase in the discontinuity of $F(x)$ or its derivatives and, hence, in an increase in the frequency components in the wave amplitude function. According to the ship wave resistance theory, the resistance is proportional to the weighted integral of the square of the wave amplitude function [14]. Hence, this increase of the frequency components may result in an increase in the ship wave resistance. Therefore, ship hulls are usually designed to be smooth so that the resistance can be reduced. Additionally, note that the coefficients in (5.16) $-$(5.19) contain the factor x^{n-2r-1} or x^{n-2r} in each term, and are small for $x = x_b < 1$ compared to those for $x = \pm 1$. Thus, these lower frequency components generally will not be dominant as found in real examples. Therefore, the following discussion will still focus on the problems with the assumption of smooth hulls.

In the estimation of ship length from A_R or A_I, the phases $\Theta_R(K_x)$ and $\Theta_I(K_x)$ are more interesting than the magnitudes $Q_R(K_k)$ and $Q_I(K_k)$ because of the direct relation of the ship length with the phases. For this reason, the discussion about the estimation of ship length from A_R and A_I will mainly focus on phase. It is found from (5.23) and (5.24) that $\Theta_R(K_x) = \frac{L}{2}K_x$ and $\Theta_I(K_x) = \frac{L}{2}K_x$ when $\phi_R(\nu)$ $\phi_I(\nu)$ approaches zero. Thus, the curves $A_R(K_x)$ and $A_I(K_x)$ corresponding to the real or imaginary parts of the wave amplitude function have the period $\frac{4\pi}{L}$. If the period is measured, then the ship length can be estimated.

In general, however, neither $\phi_R(\nu)$ nor $\phi_I(\nu)$ approaches zero, thus the estimation of ship length becomes complicated. In terms of (5.25) and (5.26), the phases ϕ_R and ϕ_I depend not only on ν but also on the coefficients a_i which are related to a ship's hull shape. The relationship between the phases and the ship shape is usually not straightforward and obvious. If a reasonable approximation is made, however,

more insight on the relation can be still gained.

5.2.1 Approximation of $A(K_x)$ for larger ν

If a large value of ν is assumed, the expressions for Q_R, Q_I, ϕ_R and ϕ_I can be greatly simplified and it is found that they depend on the function values and the first derivatives of $F(x)$ at the ship's bow and stern. This subsection discusses the validity of the assumption and gives the approximate expressions.

With the assumption of large ν, the approximate expressions of the coefficients in (5.27) −(5.30) are given first. The sums of $p_{R_{2i}}$, $q_{R_{2i}}$, $q_{I_{2i+1}}$ and $q_{I_{2i+1}}$ in (5.27) −(5.30) consist of i or $i+1$ terms. For not too large i, these sums can be approximated by their first or second term when ν is large enough. With this approximation, (5.27) −(5.30) become

$$p_{R_{2i}}(\nu) \approx i\frac{2}{\nu^2} = ip_{R_2}(\nu) \tag{5.34}$$

$$q_{R_{2i}}(v) \approx \frac{1}{\nu} = q_{R_0}(\nu) \tag{5.35}$$

$$p_{I_{2i+1}}(\nu) \approx -\frac{1}{\nu} = p_{I_1}(\nu) \tag{5.36}$$

$$q_{I_{2i+1}}(\nu) \approx (2i+1)\frac{1}{\nu^2} = (2i+1)q_{I_1}(\nu) \tag{5.37}$$

$$\text{for } i = 0, 1, 2, 3, \ldots$$

The errors caused by the above approximation are dependent on variable ν and index i. The approximation errors for $i \leq 7$ are plotted in Figures 5.1 −5.4 together with the curves of $p_{R_2}(\nu)$,$q_{R_0}(\nu)$, $p_{I_1}(\nu)$ and $q_{I_1}(\nu)$. It is found from the figures that given i, there is a value such that the approximation errors will become very small when ν is larger than this value. For instance, the errors approach zero when ν is much larger than 3 for $i \leq 3$ and when ν is much larger than 7 for $i \leq 7$. Recalling expression (5.13), the largest power of x in (5.13) is $j = 7$, corresponding to $i = 3$,

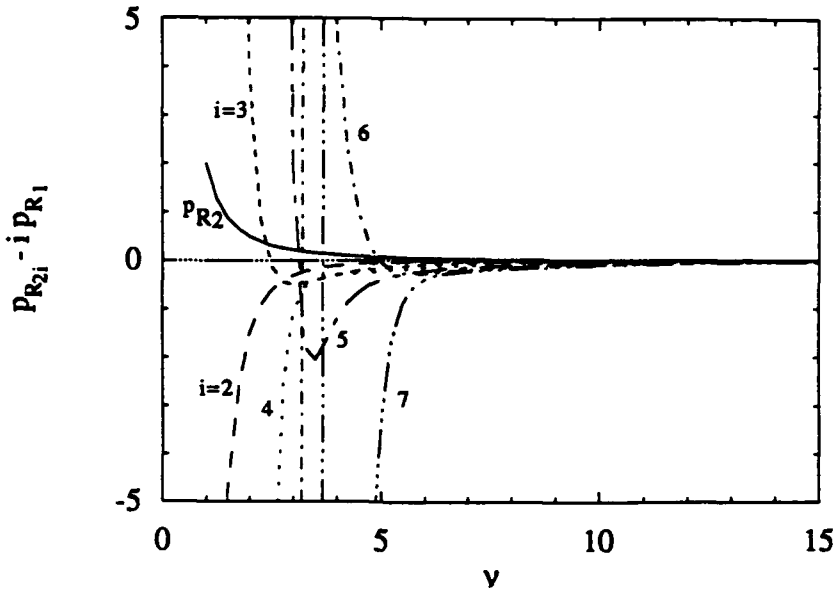

Figure 5.1: $p_{R_2}(\nu)$ and the approximation errors of $p_{R_{2i}}$.

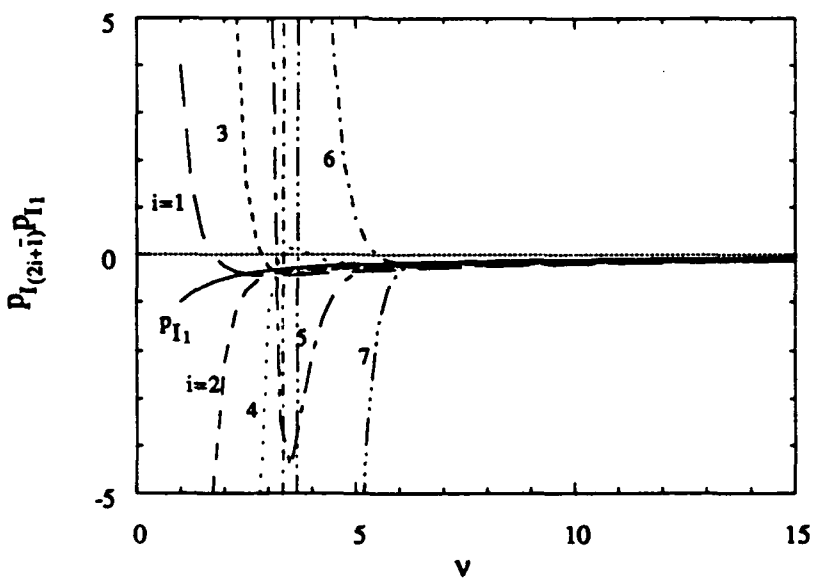

Figure 5.2: $p_{I_1}(\nu)$ and the approximation errors of $p_{I_{2i+1}}$.

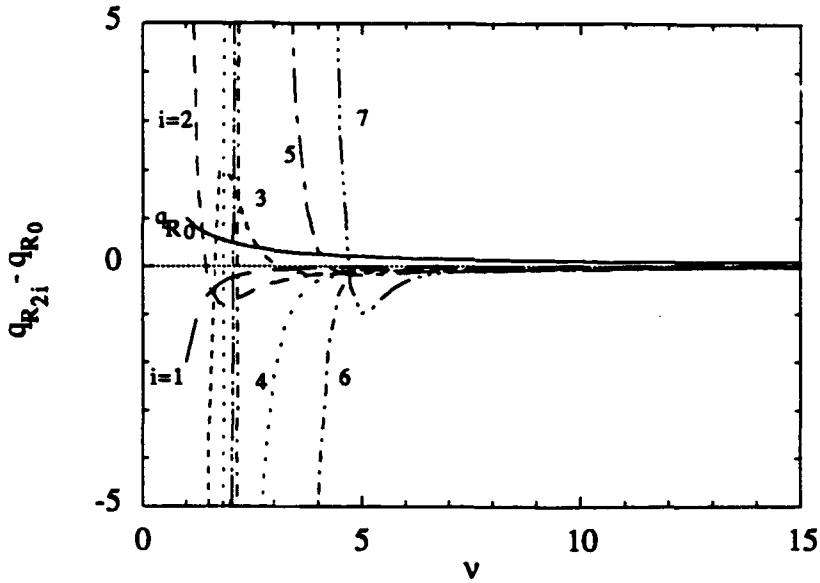

Figure 5.3: $q_{R_0}(\nu)$ and the approximation errors of $q_{R_{2i}}$.

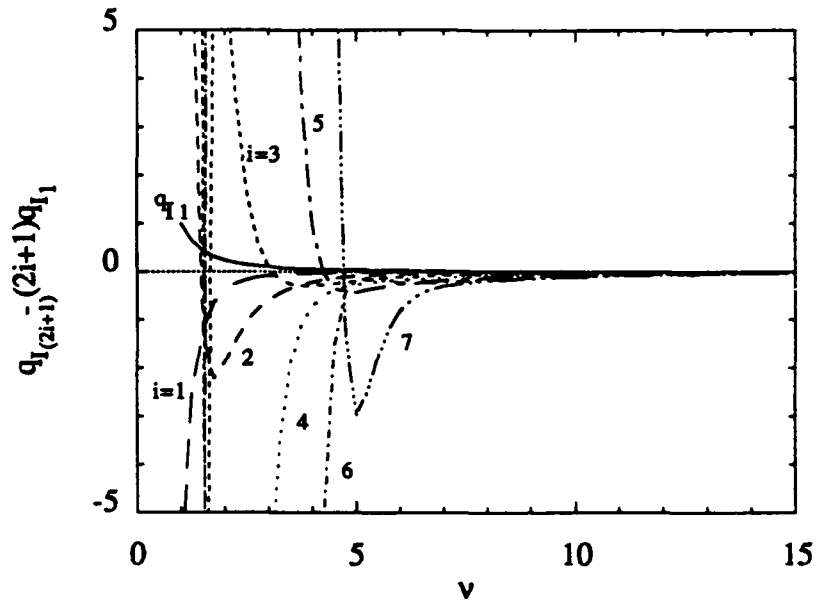

Figure 5.4: $q_{I_1}(\nu)$ and the approximation errors of $q_{I_{2i+1}}$.

and $j = 15$ to $i = 7$. Since a ship's hull shape is usually smooth, the series $F(x)$ will be convergent and the coefficient a_j in (5.13) will be very small or even can be neglected for large j. From the figures, $\nu \geq 3$ is a reasonable assumption for most real situations where $i \leq 3$.

In addition to index i, the range of ν needs to be verified to make sure that the approximation errors are small enough. To understand which value of ν is reasonable for an approximation, ν is here related to the Froude number since the scale of the Froude number is available in ship building references. By the definition of the Froude number given in Subsection 3.3.3, it follows that

$$\nu = \frac{L}{2}K_x = \frac{L}{2}\frac{g}{U^2\cos\theta} = \frac{1}{2F_n^2\cos\theta} \quad . \tag{5.38}$$

Usually $0.1 < F_n < 0.5$ for ships [16]; thus, ν ranges from $\frac{50}{\cos\theta}$ to $\frac{2}{\cos\theta}$ correspondingly and increases with the increase in the wave angle θ. From (5.38), the minimum ν is determined by $\nu_{min} = \frac{1}{2F_n^2}$. Thus, $\nu_{min} = 2$ corresponds to $F_n = 0.50$, $\nu_{min} = 3$ to $F_n = 0.41$, and $\nu_{min} = 50$ to $F_n = 0.10$. Therefore, the assumption that $\nu \geq 3$ is suitable for the cases where $F_n \leq 0.41$, in particular, for most merchant ships, for which $0.1 < F_n < 0.3$ [16].

To simplify the expression of the phases ϕ_R and ϕ_I, substituting the approximate expressions in (5.34)−(5.37) into (5.25) and (5.26), it follows that

$$\phi_R(\nu) \approx \tan^{-1}[\frac{\nu}{\beta_R}] \tag{5.39}$$

$$\phi_I(\nu) \approx -\tan^{-1}[\frac{\beta_I}{\nu}] \tag{5.40}$$

where β_R and β_I are given by

$$\beta_R = \frac{\sum_{i=0}^{\infty} 2ia_{2i}}{\sum_{i=0}^{\infty} a_{2i}} \tag{5.41}$$

$$\beta_I = \frac{\sum_{i=0}^{\infty}(2i+1)a_{2i+1}}{\sum_{i=0}^{\infty} a_{2i+1}} \quad . \tag{5.42}$$

By using the triangle relation that $tan^{-1}\xi = \pm\frac{\pi}{2} - tan^{-1}\frac{1}{\xi}$, where "+" is taken for positive ξ and "−" for negative ξ, $\phi_R(\nu)$ can be expressed in the form

$$\phi_R(\nu) = \pm\frac{\pi}{2} + \phi_{R0}(\nu) \tag{5.43}$$

where

$$\phi_{R0}(\nu) \triangleq -\tan^{-1}[\frac{\beta_R}{\nu}] \ . \tag{5.44}$$

Now, the phases Θ_R in the real part of the wave amplitude function can be given from (5.23) and (5.44) by

$$\Theta_R(K_x) \ = \ \nu - \phi_{R0}(\nu) - (\pm\frac{\pi}{2}) \tag{5.45}$$

In terms of the above relations, the real and imaginary parts of the wave amplitude function can be now rewritten as

$$A_R(K_x) \ = \ \pm Q_R(K_x)\sin(\nu - \phi_{R0}(v)) \tag{5.46}$$

$$A_I(K_x) \ = \ Q_I(K_x)\cos(\nu - \phi_I(v)) \ . \tag{5.47}$$

The signs before $\frac{\pi}{2}$ in (5.45) and before Q_R in (5.46) are taken as before, i.e., "+" is taken for positive β_R and "−" for negative β_R.

At this stage, it is now possible to relate the phase parameters, β_R and β_I, and the magnitude, $Q(K_x)$ and $Q_I(K_x)$, to the function $F(x)$. To obtain this relation, break up $F(x)$ and its derivative $F'(x)$ into their even and odd parts, i.e.,

$$F(x) \ = \ F_e(x) + F_o(x) = \sum_{i=0}^{\infty} a_{2i}x^{2i} + \sum_{i=0}^{\infty} a_{2i+1}x^{2i+1} \tag{5.48}$$

$$F'(x) \ = \ F'_e(x) + F'_o(x) = \sum_{i=0}^{\infty} 2ia_{2i}x^{2i-1} + \sum_{i=0}^{\infty}(2i+1)a_{2i+1}x^{2i} \ . \tag{5.49}$$

The values of $F(x)$ and $F'(x)$ at the end point $x = 1$ can be evaluated now, and they are given by

$$F_e(1) \ = \ \sum_{i=0}^{\infty} a_{2i} \tag{5.50}$$

$$F_o(1) = \sum_{i=0}^{\infty} a_{2i+1} \tag{5.51}$$

$$F_e'(1) = \sum_{i=0}^{\infty} 2i a_{2i} \tag{5.52}$$

$$F_o'(1) = \sum_{i=0}^{\infty} (2i+1) a_{2i+1} \ . \tag{5.53}$$

Comparing the above expressions with the definition of β_R and β_I in (5.41) and (5.42) leads to

$$\beta_R = \frac{F_e'(1)}{F_e(1)} \tag{5.54}$$

$$\beta_I = \frac{F_o'(1)}{F_o(1)} \ . \tag{5.55}$$

Note that the even and odd parts of a function can be expressed in the function itself, that is,

$$F_e(x) = \frac{1}{2}[F(x) + F(-x)] \tag{5.56}$$

$$F_o(x) = \frac{1}{2}[F(x) - F(-x)] \ . \tag{5.57}$$

Similarly, the derivative of $F(x)$ can be expressed by

$$F_e'(x) = \frac{1}{2}[F'(x) - F'(-x)] \tag{5.58}$$

$$F_o'(x) = \frac{1}{2}[F'(x) + F'(-x)] \ . \tag{5.59}$$

By substituting the above relations into (5.54) and (5.55), β_R and β_I can now be written as

$$\beta_R = \frac{F'(1) - F'(-1)}{F(1) + F(-1)} \tag{5.60}$$

$$\beta_I = \frac{F'(1) + F'(-1)}{F(1) - F(-1)} \tag{5.61}$$

Similarly, by substituting the relations in (5.50)–(5.53) and (5.56)–(5.59) into (5.21) and (5.22), the magnitudes of the real and imaginary parts of the wave am-

plitude function can be expressed in the form

$$Q_R(K_x) = \frac{1}{\nu^2}[(F'(1) - F'(-1))^2 + \nu^2(F(1) + F(-1))^2]^{\frac{1}{2}} \tag{5.62}$$

$$Q_I(K_x) = \frac{1}{\nu^2}[(F'(1) + F'(-1))^2 + \nu^2(F(1) - F(-1))^2]^{\frac{1}{2}} \ . \tag{5.63}$$

As discussed in the last subsection, the variation of the parameters β_R and β_I causes the frequency modulation of the wave amplitude function, and complicates the ship length estimation. With the assumption of large ν, these parameters are simplified and are related to only the values of the function $F(x)$ at the ship's bow and stern. Thus, it is possible to find their values by solving $F(1)$, $F(-1)$, $F'(1)$ and $F'(-1)$ from (5.62) and (5.63). Since many values of Q_R and Q_I at different K_x can be obtained, least square methods can be used.

So far, the wave amplitude function's real and imaginary parts, A_R and A_I, have been simplified under the assumption of large ν. From (5.60)–(5.63), it is found that both the magnitude and the phases of A_R and A_I depend on the variable $\nu = \frac{L}{2}K_x$ and the values of the function $F(x)$ at the ship's bow and stern. This result also explains the phenomena that the wave generated by the bow and stern are dominant in the ship's wake compared to those generated by other parts of the ship. Thus, the ship wave is sometimes considered to be generated by a moving dipole, or a pair of moving pressure points separated by a distance equal to the ship length. Based on the approximate expressions, the discussion of the estimation of ship length from A_R or A_I is further given in the following subsections.

5.2.2 Periodic Character and the Ship Length Estimation

As indicated in (5.46) and (5.47), A_R and A_I represent two signals that are both magnitude and angle modulated. Their instantaneous angle frequencies, $\frac{d\Theta_R}{dK_x}$ and

$\frac{d\Theta_I}{dK_x}$, are given from (5.24) and (5.45) as

$$\omega_R \triangleq \frac{d\Theta_R}{dK_x} = \frac{L}{2} - \frac{2L\beta_R}{L^2K_x^2 + 4\beta_R^2} \tag{5.64}$$

$$\omega_I \triangleq \frac{d\Theta_I}{dK_x} = \frac{L}{2} - \frac{2L\beta_I}{L^2K_x^2 + 4\beta_I^2} \ . \tag{5.65}$$

These two expressions show that the angle frequencies have a direct relation with the ship length and wave number K_x. In order to understand the variation of the angle frequencies with K_x and their effect on the ship length estimation, a brief analysis of the above two expressions is given here. Note that ω_R and ω_I have the same form except for the subscripts. Therefore, the discussion below will focus only on ω_I, and the results can be extended to ω_R.

For the extreme case where K_x approaches infinity, ω_I approaches a constant $\frac{L}{2}$. By determining ω_I or its corresponding period T_I, the ship length can be determined by

$$\hat{L}_\infty = 2\omega_I = \frac{4\pi}{T_I} \tag{5.66}$$

where $\hat{L}_\infty$ denotes an estimate of the ship length when K_x approaches infinity, and it depends only on ω_I or T_I.

For another extreme case where $K_x^2 \ll \frac{4\beta_I^2}{L^2}$, ω_I approaches another constant $\frac{L}{2}(1 - \frac{1}{\beta_I})$, and the ship length can be determined in a manner similar to the above case if ω_I and β_I are available. If β_I is not known and the estimate $\hat{L}_\infty$ is used to determine the ship length, then under- or over-estimation may occur depending on the value of β_I, i.e., positive or negative. It will be over-estimated if $\beta_I < 0$ and under-estimated if $\beta_I > 0$.

For general cases, the wave amplitude function is recovered from wave spectra; thus, the available K_x may neither approach infinity nor satisfy $K_x^2 \ll \frac{4\beta_I^2}{L^2}$. In these cases, the ship length is determined in terms of (5.65). If $\hat{L}_\infty$ is used to determine

the ship length, errors will be introduced. In order to know the error effect on the estimation, consider the first order derivative of ω_I. From (5.65),

$$\omega_I' = \frac{d\omega_I}{dK_x} = \frac{4L^3\beta_I K_x}{(L^2K_x^2 + 4\beta_I^2)^2} \quad . \tag{5.67}$$

Because $K_x > 0$, $\omega_I' > 0$ if $\beta_I > 0$, and $\omega_I' < 0$ if $\beta_I < 0$. Hence, the angle frequency ω_I increases monotonically with K_x when $\beta_I > 0$ and decreases monotonically with K_x when $\beta_I < 0$. That is, the period decreases monotonically with K_x when $\beta_I > 0$ and increases monotonically with K_x when $\beta_I < 0$. Thus, there are two cases for the distribution of the zero-crossing points, i.e., the intersection points of the curve A_I and the K_x-axis. For the first case, where $\beta_I > 0$, the zero-crossing points becomes denser as K_x increases; for the second case, where $\beta_I < 0$, the zero-crossing points becomes less dense as K_x increases.

According to the above analysis, there is a rule of thumb to know the trend of the estimation error when $\hat{L}_\infty$ is used to determine the ship length. There will be an over-estimation if the zero-crossing points become less dense ($\beta_I < 0$), and there will be a under-estimation if the cross-zero points become denser ($\beta_I > 0$). This rule is also suitable for the estimation from the curve of $A_R(K_x)$. The above estimation error will be reduced as K_x increases. Hence, it is suggested that the period T_I at larger K_x be taken to determine $\hat{L}_\infty$. In Section 5.3, several ideas will be proposed to reduce or avoid the estimation error.

So far, the periodic character and its effect on the ship length estimation have been discussed. The conclusions show that the sign of the value of β_R or β_I plays an important role in the estimation performance, and the sign of the value β_R or β_I can usually be determined from the distribution of the zero-crossing points. In some cases, however, it may not be easy to identify whether the zero-crossing points become more or less dense. For these cases, the phase difference between the curves

$A_R(K_x)$ and $A_I(K_x)$ may be used to determine the sign of β_R.

To determine the sign of β_R from the phase difference, calculate the phase difference from (5.24) and (5.45):

$$\Delta\Theta \triangleq \Theta_I - \Theta_R = \pm\frac{\pi}{2} + (\tan^{-1}\frac{2\beta_I}{LK_x} - \tan^{-1}\frac{2\beta_R}{LK_x}) \ . \tag{5.68}$$

Note here that before $\frac{\pi}{2}$, "+" is taken for positive β_R and "−" for negative β_R. In the extreme case where K_x approaches infinity, the value of $(\tan^{-1}\frac{2\beta_I}{LK_x} - \tan^{-1}\frac{2\beta_R}{LK_x})$ approaches zero, and the phase difference is given by $\Delta\Theta = \frac{\pi}{2}$ if $\beta_R > 0$ and $\Delta\Theta = -\frac{\pi}{2}$ if $\beta_R < 0$. Thus, the sign of β_R can be determined according to whether the phase difference is $\frac{\pi}{2}$ or $-\frac{\pi}{2}$.

In fact, the above extreme case can be generalized provided that the value $(\tan^{-1}\frac{2\beta_I}{LK_x} - \tan^{-1}\frac{2\beta_R}{LK_x})$ is in $[-\frac{\pi}{2}, \frac{\pi}{2}]$. If the phase difference is limited to the range $[-\pi, \pi]$, then the following rule of thumb to determine the sign of β_R is obtained: β_R is positive if Θ_I leads Θ_R ($\Delta\Theta > 0$), and β_R is negative if Θ_I lags behind Θ_R ($\Delta\Theta < 0$).

5.2.3 Periodic Character and the Shape of a Ship's Bow and Stern

This subsection reveals a relation between the periodic character and the shape of a thin ship's bow and stern under the assumption of separation of variables. This assumption allows the ship hull surface function to be written in the separated form

$$\zeta(x, z) = f(x)h(z) \ . \tag{5.69}$$

Note that here x and z are the normalized variables. The function $\zeta(x, z_0)$ represents a waterline curve of a ship at $z = z_0$. For the upper half waterline curve, $\zeta(x, z)$ is positive. Thus, positive $f(x)$ and $h(z)$ can be found. When $\zeta(x, z)$ is separated as in (5.69), the waterline curve depends mainly on the function $f(x)$. The shape of

the curve, particularly at the bow and stern of a ship, has an effect on the periodic character of the wave amplitude function.

With the above separation assumption, the phases and the magnitude of A_R and A_I given in Subsection 5.2.1 can be simplified and related to the hull's first and second order derivatives. For a thin ship, the function $F(x)$ defined in (5.12) can be written in the following form by substituting (5.3) and (5.69) into (5.12) :

$$F(x) \triangleq f'(x)\, c_0(K_x) \tag{5.70}$$

where

$$c_0(K_x) = \frac{2}{\pi g^2} H U^4 K_x^3 \int_{-1}^{0} h(z)\, e^{\mu x} dz \ . \tag{5.71}$$

Equation (5.70) is substituted into (5.60) −(5.63), yielding the following expressions for the phase parameter and magnitudes.

$$\beta_R = \frac{f''(1) - f''(-1)}{f'(1) + f'(-1)} \tag{5.72}$$

$$\beta_I = \frac{f''(1) + f''(-1)}{f'(1) - f'(-1)} \tag{5.73}$$

$$Q_R(K_x) = \frac{|c_0(K_x)|}{\nu^2} [(f''(1) - f''(-1))^2 + \nu^2 (f'(1) + f'(-1))^2]^{\frac{1}{2}} \tag{5.74}$$

$$Q_I(K_x) = \frac{|c_0(K_x)|}{\nu^2} [(f''(1) + f''(-1))^2 + \nu^2 (f'(1) - f'(-1))^2]^{\frac{1}{2}} \tag{5.75}$$

where $f'(1)$ and $f'(-1)$ denote the first order derivatives at the bow ($x = 1$) and stern ($x = -1$), and $f''(1)$ and $f''(-1)$ denote the second order derivatives at the bow and stern.

In terms of the function $f(x)$ and the above expressions, the relation between the parameters, β_R and β_I, and the geometric shape of a ship's bow and stern can be analyzed. According to the geometric meaning of the first and second derivatives of a function, the slopes $f'(1)$ and $f'(-1)$ are proportional to the bow and stern's half

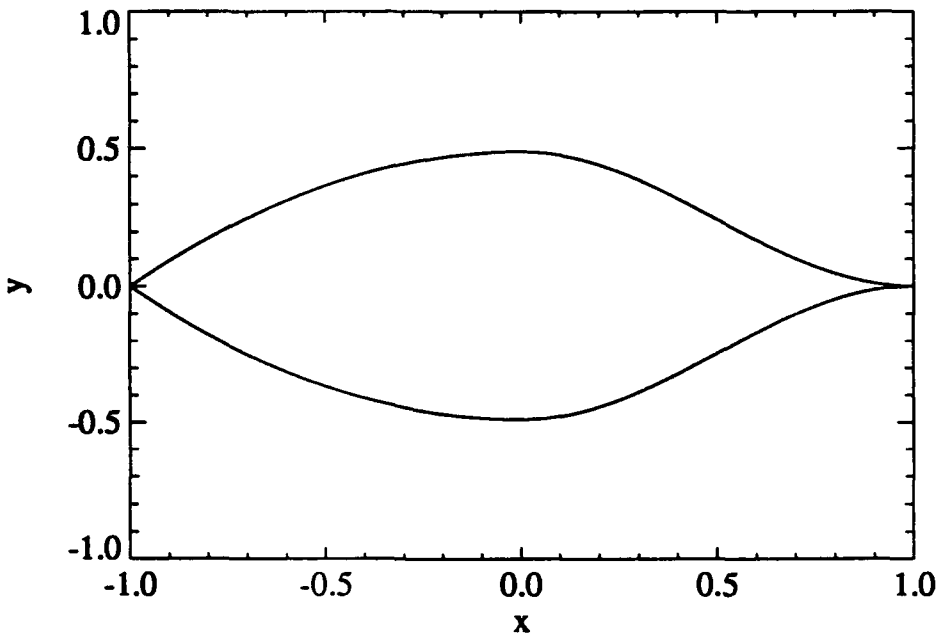

Figure 5.5: Hull waterline curve $y = \pm\zeta(x, z_0)$.

angles, and $f'(1) < 0$ and $f'(-1) > 0$ for the upper half waterline curve as shown in Figure 5.5. The second derivatives $f''(1)$ and $f''(-1)$ describe the concaveness and convexity of the bow and stern. When the second derivative at the bow or stern is positive, the shape of the waterline curve at the bow or stern is concave, and when the second derivative at bow or stern is negative, the shape is convex. Therefore, the parameters β_R and β_I depend on the the half angle and the concaveness or convexity of the bow and stern. In terms of (5.73), if both bow and stern are convex (or concave), then β_I will be positive (or negative); if one is convex and the other is concave the sign of β_I will be determined by whichever shape is dominant, i.e., whichever shape is more extreme. A similar conclusion can not easily be obtained for β_R from (5.72), because the values of $f''(1) - f''(-1)$ and $f'(1) + f'(-1)$ depend on the specific derivative values.

The above analysis tells us that the half angles and the concaveness or convexity of the bow and stern are related to the parameters β_R and β_I. Thus, the half angles and the concaveness or convexity of the bow and stern can be predicted if the parameters β_R and β_I are known. In fact, however, the sign of the parameters β_R and β_I can also be used to predict roughly the concaveness or convexity of the bow and stern. Obtaining the sign is usually much easier than obtaining the exact values of β_R and β_I. As discussed in Subsection 5.2.2, the sign of β_R and β_I may be found from the distribution of the zero-crossing points and the phase difference. The following is the main conclusion about the prediction of the concaveness or convexity of the bow and stern from the sign of β_R and β_I:

1) If $\beta_I > 0$, then the bow and/or stern have a convex shape. This is because $f''(1) + f''(-1) < 0$ when $\beta_I > 0$; thus, $f''(1)$ and/or $f''(-1)$ are negative.

2) If $\beta_I < 0$, then the bow and/or stern have a concave shape. This is because $f''(1) + f''(-1) > 0$ when $\beta_I < 0$; thus, $f''(1)$ and/or $f''(-1)$ (or both) are positive.

If the sign of the parameter β_R is also available and if it can be assumed that the half angle of the stern is larger than that of bow or vice versa, then additional information about the concaveness and convexity of the bow and stern can be obtained by analyzing (5.72) and (5.73) together.

5.2.4 Ship Length Estimation from the Magnitude of $A(K_x)$

In the above subsections, it has been assumed that both the real part $A_R(K_x)$ and the imaginary part $A_I(K_x)$ of the wave amplitude function $A(K_x)$ are available. In many practical situations, however, only the magnitude of the wave function $A(K_x)$ is available, and its phase is not known or ambiguous. Thus, $A_R(K_x)$ and $A_I(K_x)$ can not be obtained. This particularly happens when only the power spectrum is known

and the phase information is lost. This may also happen in the case where the ship center can not be exactly determined. This is because when the wave spectrum is calculated from the wave elevation, the origin of the wave data coordinate system has a translation with the ship center, i.e., the origin of the reference coordinate system; thus, an additional phase factor is produced. Since the wave amplitude function is recovered from the wave spectrum, the wave amplitude function has an additional phase factor, too.

This subsection discusses the estimation of ship length from the magnitude $|A(K_x)|$. The periodic character can also be found in $|A(K_x)|$, as in the real and imaginary parts of $A(K_x)$,. For simplicity in theoretical analysis, the square of the magnitude, denoted by $A_m(K_x)$, is considered in the following. From (5.46) and (5.47), it follows that

$$A_m(K_x) \triangleq |A(K_x)|^2 = \rho_0(K_x) + \rho(K_x)\cos(2\nu - \phi_m(\nu)) \tag{5.76}$$

where

$$\begin{aligned}
\rho_0(K_x) &= Q_R^2(K_x) + Q_I^2(K_x) && (5.77)\\
\rho(K_x) &= [Q_R^4(K_x) - 2Q_R^2(K_x)Q_I^2(K_x)\cos(\phi_I(\nu) - \phi_{R0}(\nu)) \\
&\quad + Q_I^4(K_x)]^{\frac{1}{2}} && (5.78)\\
\phi_m(\nu) &= tan^{-1}[\frac{Q_R^2(K_x)\sin(2\phi_{R0}(\nu)) - Q_I^2(K_x)\sin(2\phi_I(\nu))}{Q_R^2(K_x)\cos(2\phi_{R0}(\nu)) - Q_I^2(K_x)\cos(2\phi_I(\nu))} . && (5.79)
\end{aligned}$$

Since there is always a $\rho \leq \rho_0$, the right hand side of (5.76) is nonnegative for any K_x, and, thus, the absolute symbol is omitted. $A_m(K_x)$ looks also like a signal, both magnitude and angle modulated, but the "carrier frequency" $\frac{L}{2\pi}$ is double compared to that of $A_R(K_x)$ or $A_I(K_x)$, $\frac{L}{4\pi}$. The frequency again contains the information about the ship length L.

To analyze the periodic character of $A_m(K_x)$, the magnitude and phase are discussed further here. Comparing $\rho_0(K_x)$ with $\rho(K_x)\cos(2\nu - \phi_m(\nu))$, it follows that $\rho_0(K_x)$ is a slowly varying component. The estimation of ship length is based on the periodic character in $\cos(2\nu - \phi_m(\nu))$. Hence, we need to make sure that $\rho(K_x)$ is also a slowly varying, non-zero component compared to $\cos(LK_x - \phi_m(\nu))$. To do this, the phase difference $(\phi_I - \phi_{R0})$ in (5.78)) is first simplified below. In terms of (5.40) and (5.44), $(\phi_I - \phi_{R0})$ is rewritten as

$$\phi_I(\nu) - \phi_{R0}(\nu) = tan^{-1}[\frac{\nu(\beta_I - \beta_R)}{\nu^2 - \beta_I\beta_R}] \approx (\beta_I - \beta_R)\frac{1}{\nu} \tag{5.80}$$

where the assumption that $\nu^2 \gg \beta_I^2$ and $\nu^2 \gg \beta_P^2$ has been made in the last step. Now, consider the behavior of $\rho(K_x)$ as $\nu \to \infty$. In terms of (5.80), $\cos 2(\phi_I - \phi_{R0})$ approach 1 when ν becomes very large, and thus the oscillation magnitude of $\rho(K_x)$ approaches $|(Q_R^2(K_x) - Q_I^2(K_x))^2|$. By using the results in Subsection 5.2.1, $\rho(K_x)$ can be expressed for large ν from (5.62) and (5.63) as

$$\begin{aligned} \rho(K_x) &\approx |Q_R^2(K_x) - Q_I^2(K_x)| \\ &= \frac{4}{\nu^4}|-F'(1)F'(-1) + \nu^2 F(1)F(-1)| \end{aligned} \tag{5.81}$$

Thus, $\rho(K_x)$ changes slowly with K_x compared to $\cos(LK_x - \phi_m(\nu))$. If $\nu \gg |\frac{F'(1)F'(-1)}{F(1)F(-1)}|$, then $\rho(K_x)$ is approximately equal to $\frac{4}{\nu^2}|F(1)F(-1)|$.

Now, consider the phase ϕ_m for large ν. By substituting (5.40) and (5.44) into (5.79), ϕ_m is given approximately by

$$\phi_m(\nu) \approx tan^{-1}[2\nu\frac{Q_I^2\beta_I(\nu^2 + \beta_{R0}^2) - Q_R^2\beta_{R0}(\nu^2 + \beta_I^2)}{Q_I^2(\nu^2 - \beta_I^2)(\nu^2 + \beta_{R0}^2) - Q_R^2(\nu^2 - \beta_{R0}^2)(\nu^2 + \beta_I^2)}] \tag{5.82}$$

If it is further assumed that $\nu^2 \gg \beta_I^2$ and $\nu^2 \gg \beta_R^2$, then ϕ_m can be approximated by

$$\phi_m \approx -tan^{-1}\frac{\beta_m}{\nu} \tag{5.83}$$

where

$$\beta_m = -2\frac{Q_I^2\beta_I - Q_R^2\beta_{R0}}{Q_I^2 - Q_R^2} \quad . \tag{5.84}$$

Substituting (5.60) −(5.63) in (5.84) yields

$$\lim_{\nu\to\infty} \beta_m = \frac{F'(1)}{F(1)} - \frac{F'(-1)}{F(-1)} \quad . \tag{5.85}$$

According to the above analysis, the phase ϕ_m will be small when ν is large, thus LK_x in the phase plays a dominant role and the periodic character can be observed in the curve $A_m(K_x)$. Methods for estimating ship length from $A_m(K_x)$ will be introduced in Section 5.3. One practical example, estimating the length of a real ship hull model from $A_m(K_x)$, will be given in Section 5.4, and the results show that good estimation can be obtained from $A_m(K_x)$.

5.2.5 Examples of Ship Hulls

This subsection gives some examples of ship hulls to demonstrate their wave amplitude function and evaluate the parameter β from the theoretical calculation and the approximation formulas given in the above subsections.

The first example is Wigley's Hull, which is frequently used in theoretical analysis. The normalized expression of Wigley's hull is describe by

$$\zeta(x,z) = \frac{B}{2}(1-x^2)(1-z^2) \qquad x \in [-1,1], z \in [-1,0] \tag{5.86}$$

where x and z are the variables normalized by the half ship length and draft, respectively, as defined in (5.5) and (5.6). The primes have been omitted for ease of notation. Substituting (5.86) into (5.8), the wave amplitude function is given by

$$A(K_x) = \mathrm{j}Q_I(K_x)\cos(\frac{L}{2}K_x + tan^{-1}\frac{2}{K_xL}) \tag{5.87}$$

where

$$Q_I(K_x) = c_1(K_x)\frac{8}{L^2K_x^2}\sqrt{4+L^2K_x^2} \tag{5.88}$$

$$c_1(K_x) = \frac{B}{\pi H K_x \mu(K_x)}[\mu(K_x)^2 - 2 + 2(1+\mu(K_x))e^{-\mu(K_x)}] \tag{5.89}$$

$$\mu(K_x) = \frac{U^2H}{g}K_x^2 \quad . \tag{5.90}$$

Indeed, the wave amplitude function in (5.87) has the form we expect, and its phase consists two terms. The second term in the phase, $-tan^{-1}\frac{2}{LK_x}$, is recognized as ϕ_I as discussed before, and it becomes very small as K_x increase. Thus, the first term $\frac{L}{2}K_x$ will be dominant.

Now, let us evaluate the parameter β_I from the theoretical result and from the approximation method directly based on the shape of hull. Comparing the phase in (5.87) with that in (5.24) and (5.40) yields $\beta_I = 1$. To obtain β_I directly from the hull shape, consider the hull shape function $\zeta(x,z)$. Since it is separable, β_I can be directly estimated from $f(x) = 1 - x^2$ in terms of (5.73), and has the same value as above. Here, β_I is larger than zero, thus the zero-crossing points of the curve $A_I(K_x)$ become denser as K_x increases and under-estimation may occur.

The second example is the Cosine-Sine Hull with the normalized hull expression

$$\zeta(x,z) = \frac{B}{2}[1+\cos(\pi x)][1-\sin(\frac{\pi}{2}z)] \qquad x \in [-1,1], z \in [-1,0] \tag{5.91}$$

Similar to Wigley's hull, its wave amplitude function can be found and is given by

$$A(K_x) = \mathrm{j}Q_I(K_x)\sin(\frac{L}{2}K_x) \tag{5.92}$$

where

$$\begin{aligned} Q_I(K_x) = & \frac{8\pi BU^2K_x\mu(K_x)}{g(4\pi^2 - L^2K_x^2)}[\frac{1}{\mu(K_x)} + \frac{\frac{\pi}{2}}{\mu(K_x)^2 + (\frac{\pi}{2})^2} \\ & -(\frac{1}{\mu(K_x)} + \frac{\mu(K_x)}{\mu(K_x)^2 + (\frac{\pi}{2})^2})e^{\mu(K_x)}] \quad . \end{aligned} \tag{5.93}$$

This theoretical result can be further verified from the analysis of the ship hull function. For this hull, $f(x) = 1 - x^2$ and β_I approaches infinity when it is evaluated in terms of (5.73). Thus, ϕ_I is $\frac{\pi}{2}$ from (5.40) and $\cos(\frac{L}{2}K_x - \phi_I) = \sin(\frac{L}{2}K_x)$. This is the same as the above theoretical result in (5.93). Note that the angle frequency is a constant equal to $\frac{L}{2}$, meaning that theoretically, there will be no over- or underestimation of ship length from the wave amplitude function.

The third example is the Wigley-Cosine Hull. Its normalized hull expression is described by

$$\zeta(x,z) = \frac{B}{2} f(x) \cdot (1 - z^2) \qquad x \in [-1,1], z \in [-1,0] \tag{5.94}$$

where

$$f(x) = \begin{cases} \frac{1}{2}[1 + \cos(\pi x)] & 0 \le x \le 1 \\ 1 - x^2 & -1 \le x < 0 \end{cases} \tag{5.95}$$

This hull has a discontinuity at $x = 0$, i.e., the derivatives $f''(0), f^{(4)}(0), \ldots$ are not continuous. Additionally, it is not symmetric in the x-direction, thus the wave amplitude function will contain both real and imaginary parts, which are given by

$$A_R(K_x) = Q_{R0}(K_x) + Q_R(K_x)\cos(\frac{L}{2}K_x - \phi_R(\nu)) \tag{5.96}$$

$$A_I(K_x) = Q_I(K_x)\cos(\frac{L}{2}K_x - \phi_I(\nu)) \tag{5.97}$$

where

$$Q_{R0}(K_x) = c_1(K_x)[\frac{\pi^2}{2(\nu^2 - \pi^2)} - \frac{2}{\nu^2}] \tag{5.98}$$

$$Q_R(K_x) = -c_1(K_x)[\frac{4}{\nu^2} + (\frac{\pi^2}{2(\nu^2 - \pi^2)} + \frac{2}{\nu^2})^2]^{\frac{1}{2}} \tag{5.99}$$

$$Q_I(K_x) = c_1(K_x)[\frac{4}{\nu^2} + (\frac{2}{\nu^2} - \frac{\pi^2}{2(\nu^2 - \pi^2)})^2]^{\frac{1}{2}} \tag{5.100}$$

$$\phi_R(\nu) = \tan^{-1}\{\nu[\frac{4(\nu^2 - \pi^2)}{(4 + \pi^2)\nu^2 - 4\pi^2}]\} \tag{5.101}$$

$$\phi_I(\nu) = -\tan^{-1}\{\frac{1}{\nu}[1 - \frac{\pi^2\nu^2}{4(\nu^2 - \pi^2)}]\} \ . \tag{5.102}$$

Here, $c_1(K_x)$ is the same as in (5.89) and $\nu = \frac{L}{2}K_x$. To compare the above result to that from the approximation method, we substitute $f(x) = 1 - x^2$ into (5.72) and (5.73), and obtain the parameters β_R and β_I in (5.39) and (5.40), i.e., $\beta_R = \frac{4+\pi^2}{4}$ and $\beta_I = \frac{4-\pi^2}{4}$, which are the same as the limits of the factors in the square brackets in (5.101) and (5.102) as $\nu \to \infty$. Since $\beta_R > 0$, the estimation from A_R will be under-estimated, and since $\beta_I < 0$ the estimation from A_I will be over-estimated if no compensation is made.

5.3 Methods of Determination of Ship Length

As discussed in previous sections, the wave amplitude function has a periodic character and the ship length can be predicted from the periodicity. The simplest method to predict the ship length is to evaluate the period when K_x approaches infinity and then calculate $\hat{L}_\infty$ as described in Subsection 5.2.2. Since K_x depends on the wave angle θ, i.e., $K_x = \frac{g}{U^2 \cos\theta}$, a large K_x requires a large resolvable wave angle. In real situations, however, the maximum available wave angle is limited by the data sampling interval and ship speed, which has been discussed in Section 3.3.

In general, the more periods available in the data of $A(K_x)$, the better for obtaining a good estimation of ship length. However, the number of the periods or the available zero-crossing points depends on the maximum available wave angle. The relation between the wave angle and the number of zero-crossing points can be understood through a simplified model of $A(K_x)$. As seen in the above discussion, the real or imaginary part of $A(K_x)$ has a pattern like $cos(\frac{L}{2}K_x - \phi)$, the zero-crossing points appear at

$$\frac{L}{2}K_x - \phi = \frac{\pi}{2}(2m+1) \quad \text{for } m = m_0, m_0+1, m_0+2, \cdots \tag{5.103}$$

and, thus, the wave angles at the zero-crossing points can be expressed from (5.9)

and (5.103) in the form

$$\theta = \cos^{-1}[\frac{1}{((2m+1)\pi+\phi)F_n^2}] \tag{5.104}$$

where $F_n = \frac{U}{\sqrt{gL}}$ is the Froude number and m_0 is the smallest integer such that $\frac{1}{((2m+1)\pi+\phi)F_n^2} \leq 1$. Thus, the large number of zero-crossing points needs the large maximum available wave angles available.

Because of these reasons, K_x can not be very large in practical situations. Hence, the effect of the phase factors ϕ_R, ϕ_I, or ϕ_m on the period estimation may not be negligible. In addition, in order to obtain results quickly and accurately, data processing and automatic detection are necessary. In this section, several algorithms to determine ship length are introduced. Although the discussion about these algorithms focuses mainly on the software realization, it is also possible to use them in hardware realizations for real time estimations.

These algorithms include the spectrum method, zero-crossing method, and frequency demodulation method. In the spectrum method, the period is estimated by calculating the power spectrum of A_R, A_I or A_m. In the zero-crossing method, the zero-crossing points of the curve A_R, A_I or A_m are detected, and then used to find the period variation with K_x for further ship length estimation. In the frequency demodulation method, the frequency of A_R, A_I or A_m is demodulated, and then the frequency variation with K_x is used to estimate ship length . In the following, these methods are demonstrated through an example of a Wigley-Cosine hull, since its wave amplitude function contains both real and imaginary parts and thus is a typical example.

Generally speaking, the behavior of the curves A_R and A_I is better than A_m, thus the estimation of ship length from A_R or A_I is easier than from A_m. However, in practical situations, the estimation from A_m may be more useful since A_m is easier

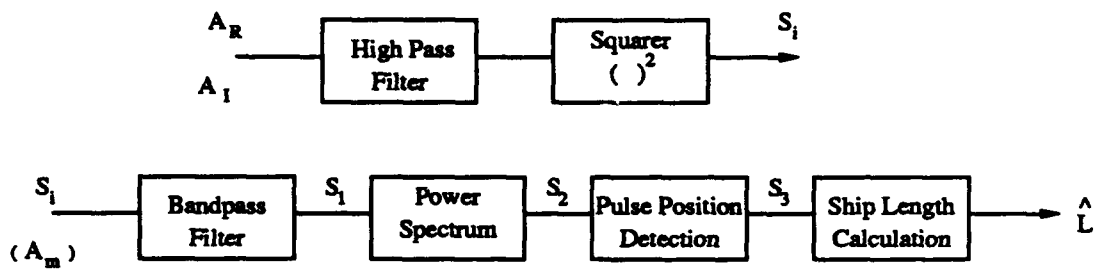

Figure 5.6: Spectrum method for the estimation of ship length

to determine than A_R or A_I.

5.3.1 Spectrum Method

A scheme for the estimation of ship length using the spectrum method is shown Figure 5.6. In general, the signal A_R, A_I or A_m can be directly inputted to the system for processing. In many real situations, however, the available data record are short, only a couple of periods of signal in length, in particular, for A_R and A_I. Thus, it is preferred to use A_R^2 and A_I^2 as the input signals, so that the frequency of the signals is doubled, and the number of zero-crossing points increases. This will be helpful to detect the signal periods. Before the square operation is taken, it is suggested that the signal A_R or A_I be filtered using a high pass filter to remove the direct current component and the component lower than $\frac{L}{4\pi}$, as shown in Figure 5.6. For example, consider $A_R(K_x) = Q_{R0}(K_x) + Q_R(K_x)\cos(\frac{L}{2}K_x - \phi_R(\nu))$. After the high pass filter, the lower frequency component $Q_{R0}(K_x)$ is filtered out and the signal becomes $Q_R(K_x)\cos(\frac{L}{2}K_x - \phi_R(\nu))$. After the square operation, the signal is $\frac{1}{2}Q_R^2(K_x)\,[1 - 2\cos(LK_x + 2\phi_R)]$, where $\cos(LK_x + 2\phi_R)$ is the desired component and has frequency $\frac{L}{2\pi}$. If the high pass filter is not used, there will additionally exist the components of $Q_{R0}(K_x)\,Q_R(K_x)\cos(\frac{1}{L}K_x - \phi_R)$ which is not desired now. After this, the squared signal will undergo further processing for estimating ship length.

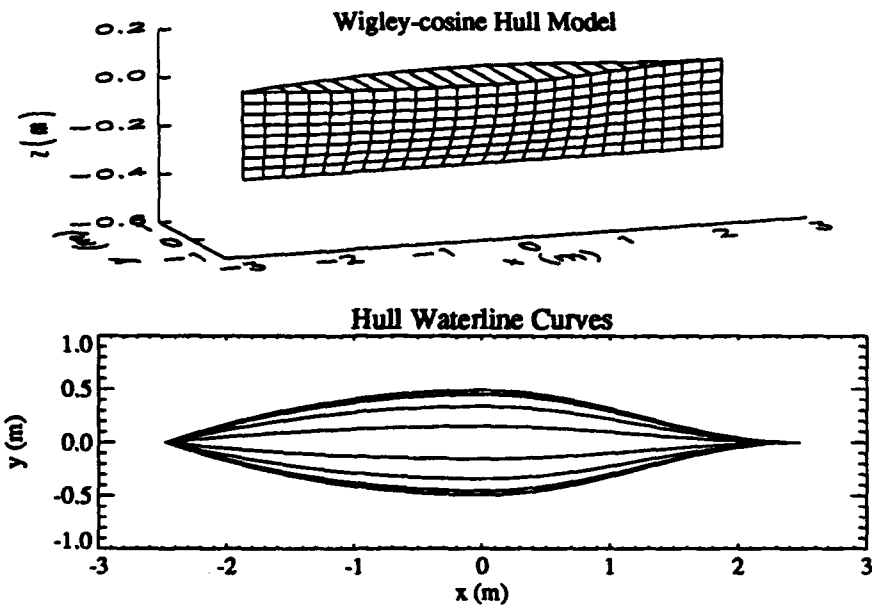

Figure 5.7: A Wigley-Cosine hull model and its waterline curves $y = \pm\zeta(x,z)$ at $z = -0.3, -0.2, -0.1, 0.0$ meters.

In the bottom digram in Figure 5.6, a bandpass filter centered at $f_{K_x} = \frac{L}{2\pi}$ is used to remove noise and undesired lower or higher frequency components. For example, the component $Q_R^2(K_x)$ in the squared signal is filtered out. The cutoff frequency of the filter can be roughly determined by measuring the period of the input signal s_i. Then, the output signal $s_1(K_x)$ of the filter is used to calculate the power spectrum. At this stage, the spectrum diagram shows a pulse at around $f_{K_x} = \frac{L}{2\pi}$. If the transverse axis is labeled as $\hat{L} = 2\pi f_{K_x}$, then the ship length can be directly read from the pulse position. In order to determine the pulse's frequency position automatically and accurately, however, a method called the pulse position detection can be used. In this method, the pulse is cut by a threshold. The average frequency position, denoted by $\bar{f}_{K_{x0}}$, of the data points larger than the threshold is then calculated and is used to obtain the ship length, $\hat{L}_{sp} = 2\pi\bar{f}_{K_{x0}}$.

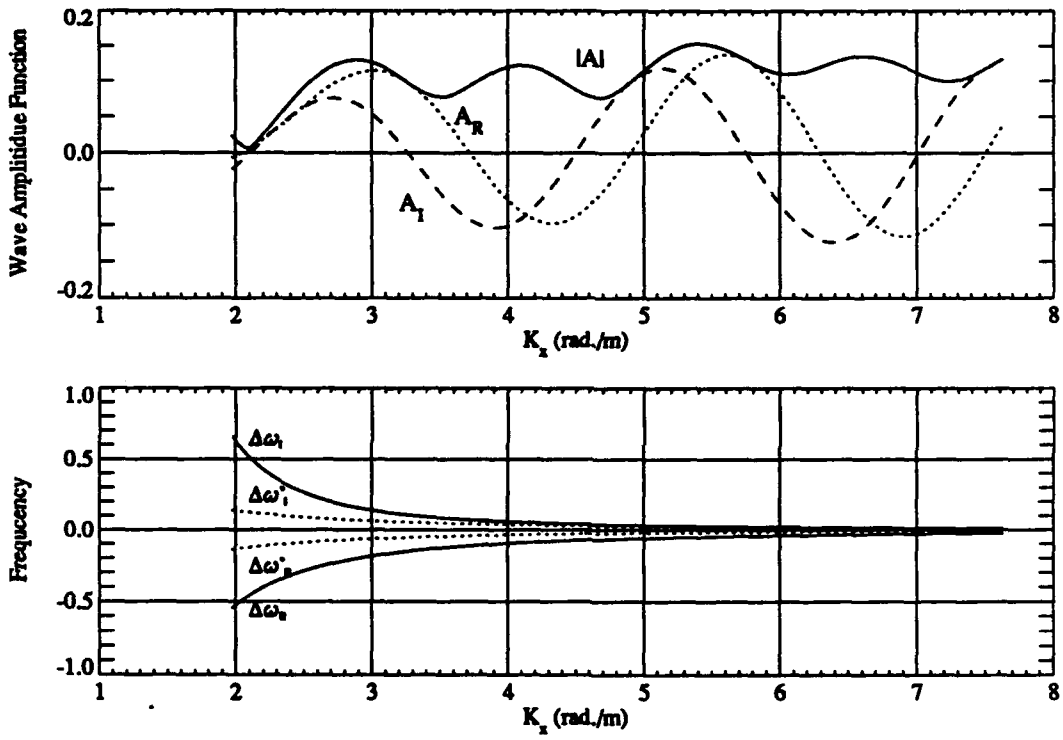

Figure 5.8: (a) Wave amplitude function of the Wigley-Cosine hull model; (b) Frequency variation of A_R and A_I and their approximation.

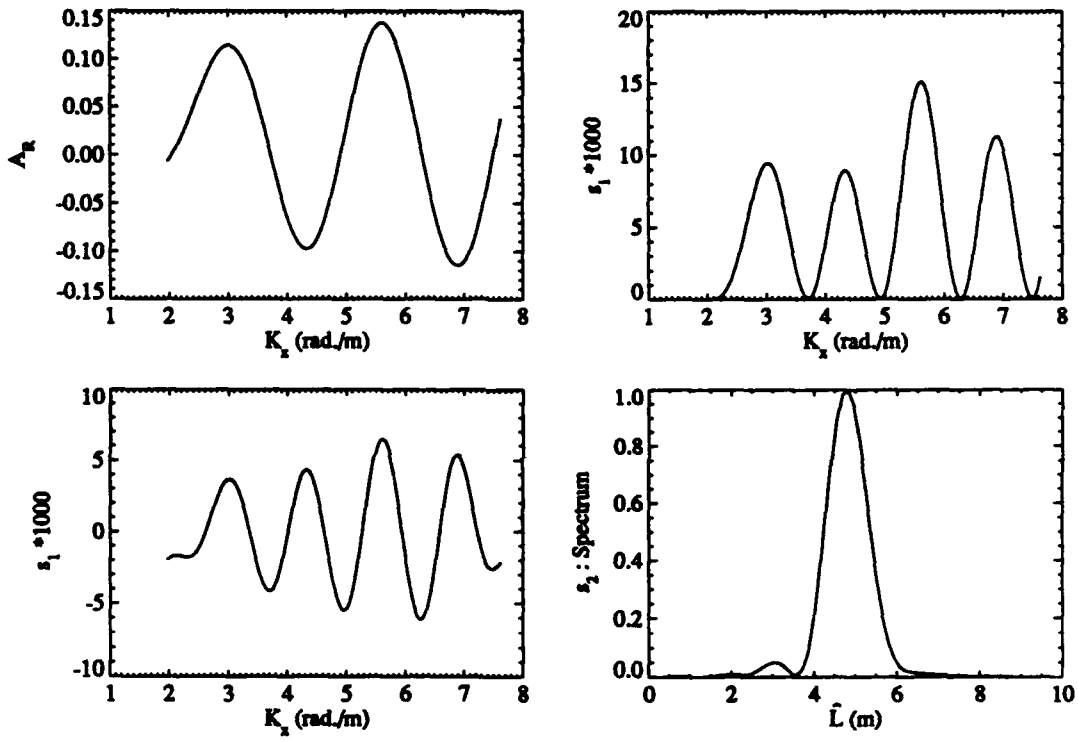

Figure 5.9: Signal waveforms in the ship length estimation from A_R for the Wigley-Cosine hull model using the spectrum method. The estimated ship length is $\hat{L} = 4.825\ m$ with a relative error of 2.6%.

As a example, consider a Wigley-Cosine hull model with length $L = 4.953$ meters, width $B = 0.978$ meters and draft $H = 0.362$ meters. The ship's speed is given as $U = 2.229$ meters/second. The hull surface and the waterline contour plot are given in Figure 5.7. The real part A_R, the imaginary part A_I and the magnitude $|A|$ of the wave amplitude function and the frequency variation of A_R and A_I are shown in Figure 5.8. A_R, A_I and $|A|$ are calculated from (5.96) and (5.97). In Figure 5.8, $\Delta\omega_R = \frac{d\Theta_R(K_x)}{dK_x} - \frac{L}{2} = -\frac{d\phi_R(\nu)}{dK_x}$ and $\Delta\omega_I = \frac{d\Theta_I(K_x)}{dK_x} - \frac{L}{2} = -\frac{d\phi_I(\nu)}{dK_x}$; $\Delta^*\omega_R$ and $\Delta^*\omega_I$ are the approximations of $\Delta\omega_R$ and $\Delta\omega_I$, and are calculated from (5.64) and (5.65) with $\beta_R = \frac{4+\pi^2}{4}$ and $\beta_I = \frac{4-\pi^2}{4}$.

The signals at each stage in Figure 5.6 are given in Figure 5.9. The input signal s_i is the squared A_R, the real part of the wave amplitude function. There are 128 data points, each separated by an interval of 0.0445 rad./meter. K_x ranges from 1.974 to 7.626 rad./meter, corresponding to the wave angle from 0° to 75°. The cut-off frequency of the high pass filter is 0.1 Hz, and the cut-off frequencies of the bandpass filter are 0.5 and 1.5 Hz. The spectrum is directly calculated according to the definition given in [11] using the FFT algorithm. The spectrum, s_2, has been normalized by the value at the peak, and the abscissa has labeled directly the length scale instead of $2\pi f_{K_x}$ for easy observation of the length estimation. Cyclic spectral analysis methods and other advanced spectral analysis methods may be used for high performance [35] - [38]. Here, however, a simple method is used to increase the spectrum resolution, that is, the data length is increased to 1024 points by padding zeros. The computer calculation gives the ship length estimation as $\hat{L} = 4.825$ meters. It is under-estimated as predicted from theoretical analysis, with a relative error of 2.6%.

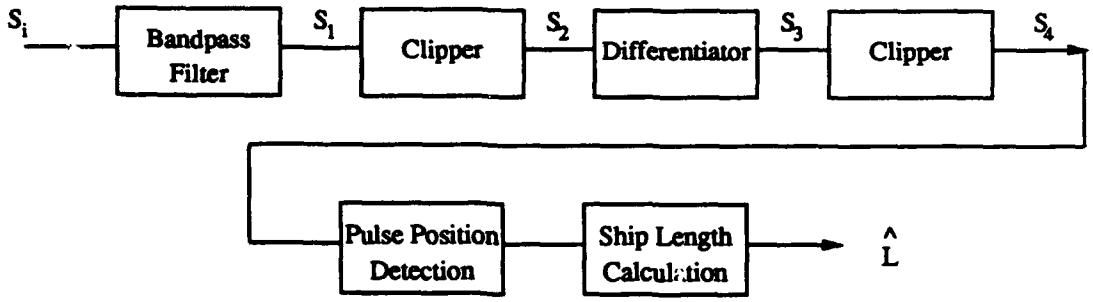

Figure 5.10: Zero-crossing method for the estimation of ship length.

5.3.2 Zero-Crossing Method

A scheme for the estimation of ship length using the zero-crossing method is shown in Figure 5.10. Similar to the spectrum method, the input signal is considered to be $A_m(K_x)$ or the filtered and squared signal $A_R(K_x)$ or $A_I(K_x)$. The difference is that following the bandpass filter, the signal is clipped instead of being used to calculated the power spectrum. The clipper is set to have a threshold such that the signal $s_2(K_x)$ is a square wave signal with a magnitude close to zero. Then, the clipped signal is differentiated, giving $s_3 = \frac{ds_2}{dK_x}$. The differentiation is realized by using the three point Lagrangian interpolation method [34]. The differentiated signal is combined with the pulses located at zero-crossing points. To obtain the periods, the positive pulses are taken using another clipper. The positive pulse signal $s_4(K_x)$ is then used to calculate the periods at different K_x. Similarly, the pulse position detection method is used here for fast and accurate calculation. The interval between two pulses is the period at the corresponding K_x. The first and last pulses may not be counted to avoid false periods at the beginning and end of the input signal. Finally, these periods are used to calculated the ship length.

In the calculation of ship length from the periods, different strategies can be considered. If the periods $\{T_{K_{xi}}, i = 1, ..., l\}$ do not form a monotonic sequence

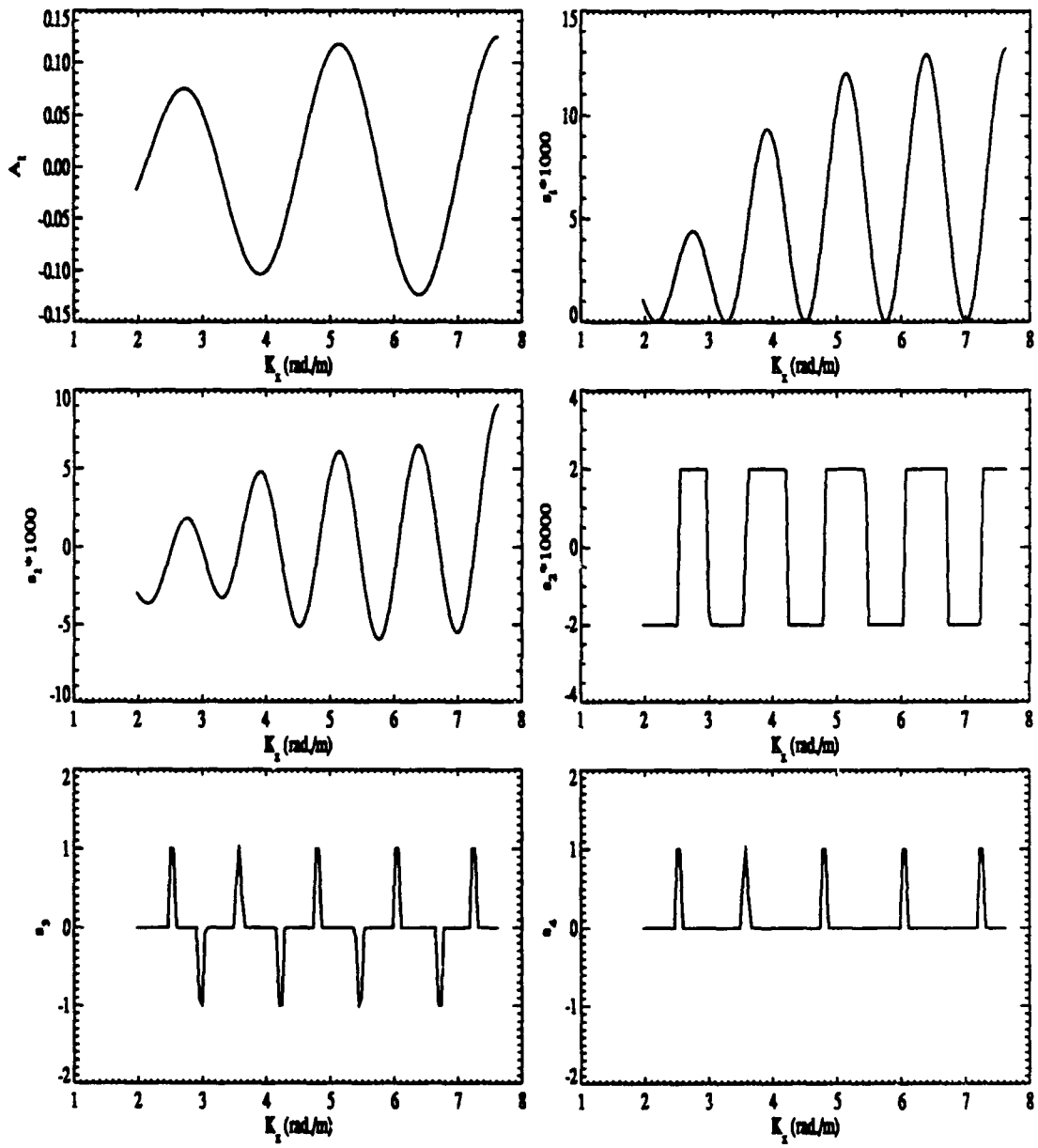

Figure 5.11: Signal waveforms in the ship length estimation from A_I for the Wigley-Cosine hull model using the zero-crossing method. The estimated ship length is $\hat{L}_{zc} = 5.042\ m$ with a relative error of 1.8%.

and their lengths appears to be random, then the ship length is calculated from the average of the period length, that is, $\hat{L}_{xc} = \frac{2\pi}{l}\sum_{i=1}^{l} T_{K_{xi}}$. This case may happen in the estimation from $A_m(K_x)$, or the magnitude of the wave amplitude function. If the obtained periods $\{T_{K_{xi}}, i = 1, ..., l\}$ do form a monotonic sequence, then the ship length is calculated from the last period, i.e., $\hat{L}_{xc} = 2\pi T_{K_{xl}}$. In this case, the estimation error trends can be predicted in terms of whether the sequence is monotonically increasing or decreasing. If the variation in periods is small near $T_{K_{xl}}$, then the error will not be large. To achieve high accuracy in the estimation, the following method may be used if at least three zero-crossing positions are available. For the signal A_m, squared A_R or A_I, the phase is given by $\Theta \approx LK_x + \frac{4\beta}{LK_x}$, where β denotes β_m, β_R or β_I. Since the cosine function has a phase period $2n\pi$, Θ can be written in the form

$$LK_{xi} + \frac{4\beta}{LK_{xi}} = \frac{\pi}{2} + 2(i-1)\pi \quad i = 1, ..., l \tag{5.105}$$

where l is the number of zero-crossing points K_{xi} to be considered. If three or more K_{xi} are available, then the ship length and β can be found by solving this set of equations. Least square methods can be used if more than three points can be available. As an example, a three-point formula is given in the following. Assume that there are three points K_{x1}, K_{x2} and K_{x3}. The ship length and β are estimated from

$$\hat{L} = \frac{2\pi}{K_{x3} - K_{x1}}\left(\frac{K_{x3}}{K_{x3} - K_{x2}} - \frac{K_{x1}}{K_{x2} - K_{x1}}\right) \tag{5.106}$$

$$\beta = -\frac{L^2}{4}\frac{K_{x3} - 2K_{x2} + K_{x1}}{\frac{1}{K_{x3}} - \frac{2}{K_{x2}} + \frac{1}{K_{x1}}} \quad . \tag{5.107}$$

The above discussion considers the signal $s_4(K_x)$ with only the positive pulses. If the negative pulses are considered too, then (5.105) can be modified as follows.

$$LK_{xi} + \frac{4\beta}{LK_{xi}} = (2i-1)\frac{\pi}{2} \quad i = 1, ..., l' \tag{5.108}$$

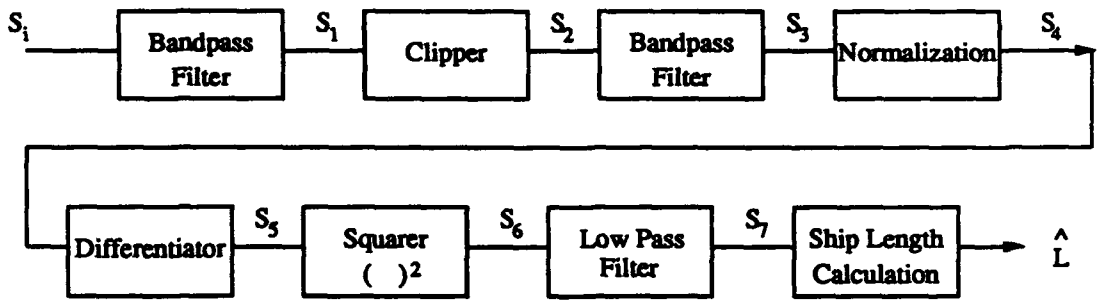

Figure 5.12: Frequency demodulation method for the estimation of ship length.

where l' is the number of zero-crossing points K_{xi} to be considered. $\hat{L}$ and β can be derived in the same way.

As an example, consider the same Wigley-Cosine hull model. Here, the input is A_I. The signals at each stage in Figure 5.10 are given in Figure 5.11. The cut-off frequencies of the bandpass filter are 0.4 Hz and 11.2 Hz (Nyquist frequency). According to the calculated results, the zero-crossing point position is 3.55372, 4.79989, 6.04606, without considering the first and last points. The periods are 1.24617 and 1.24617. Thus, the estimated ship length is $\hat{L} = 5.042$ meters. It is over-estimated as predicted from theoretical analysis with a relative error of 1.80%.

5.3.3 Frequency Demodulation Method

In the above zero-crossing method, the periods, which vary with K_x, are estimated by locating the position of the zero-crossing points, and the ship length is then calculated. In the frequency demodulation method, the instantaneous frequency is detected, and then the ship length is estimated. The scheme for the frequency demodulation method is shown in Figure 5.12. The first four operations in the diagram transform the input signal s_i, an unequal-amplitude angle modulated signal, into an equal-amplitude angle modulated signal; the last four operations detect the

"carrier frequency" $\frac{L}{2\pi}$, and then the ship length is calculated.

In order to obtain an equal-amplitude signal, a clipper is used following the bandpass filter. Instead of determining the position of the zero-crossing points as in the zero-crossing method, the purpose for clipping $s_1(K_x)$ here is to obtain an equal-magnitude square signal. Thus, the threshold of the clipper is large, compared to that in the zero-crossing method. Following the clipper, a bandpass filter is then used to obtain an equal-amplitude angle modulated signal. After the amplitude is normalized, the unit-amplitude angle demodulated signal s_4 has the form

$$s_4(K_x) = cos(LK_x - 2\phi) \tag{5.109}$$

where $\phi = -tan^{-1}\frac{2\beta}{LK_x}$ and β denotes β_m, β_R or β_I. The "carrier frequency" $\frac{L}{2\pi}$ is desired and will be recovered.

In order to detect the frequency information, the differentiation, square operation and filtering are further used. The output of the differentiator is the signal

$$s_5(K_x) = -(L - \frac{4L\beta}{L^2K_x^2 + 4\beta^2})sin(LK_x - 2\phi) \quad . \tag{5.110}$$

The magnitude of s_5 contains the desired frequency information. The above differentiation can be realized by the Fourier transform method. The method is based on the property of the Fourier transform. That is, for an arbitrary function $f(x)$, its derivative is equal to the inverse Fourier transform of $jw\mathcal{F}\{f(x)\}$. A discussion of the design of an optimal FIR differentiator can be found in [33]. To obtain the frequency information from the magnitude, a squarer is used and the result is

$$s_6(K_x) = s_5^2 = \frac{1}{2}(L - \frac{4L\beta}{L^2K_x^2 + 4\beta^2})^2(1 - cos(2LK_x - 4\phi) \quad . \tag{5.111}$$

Then, a low pass filter is used to filter out the high frequency component $cos(2LK_x -$

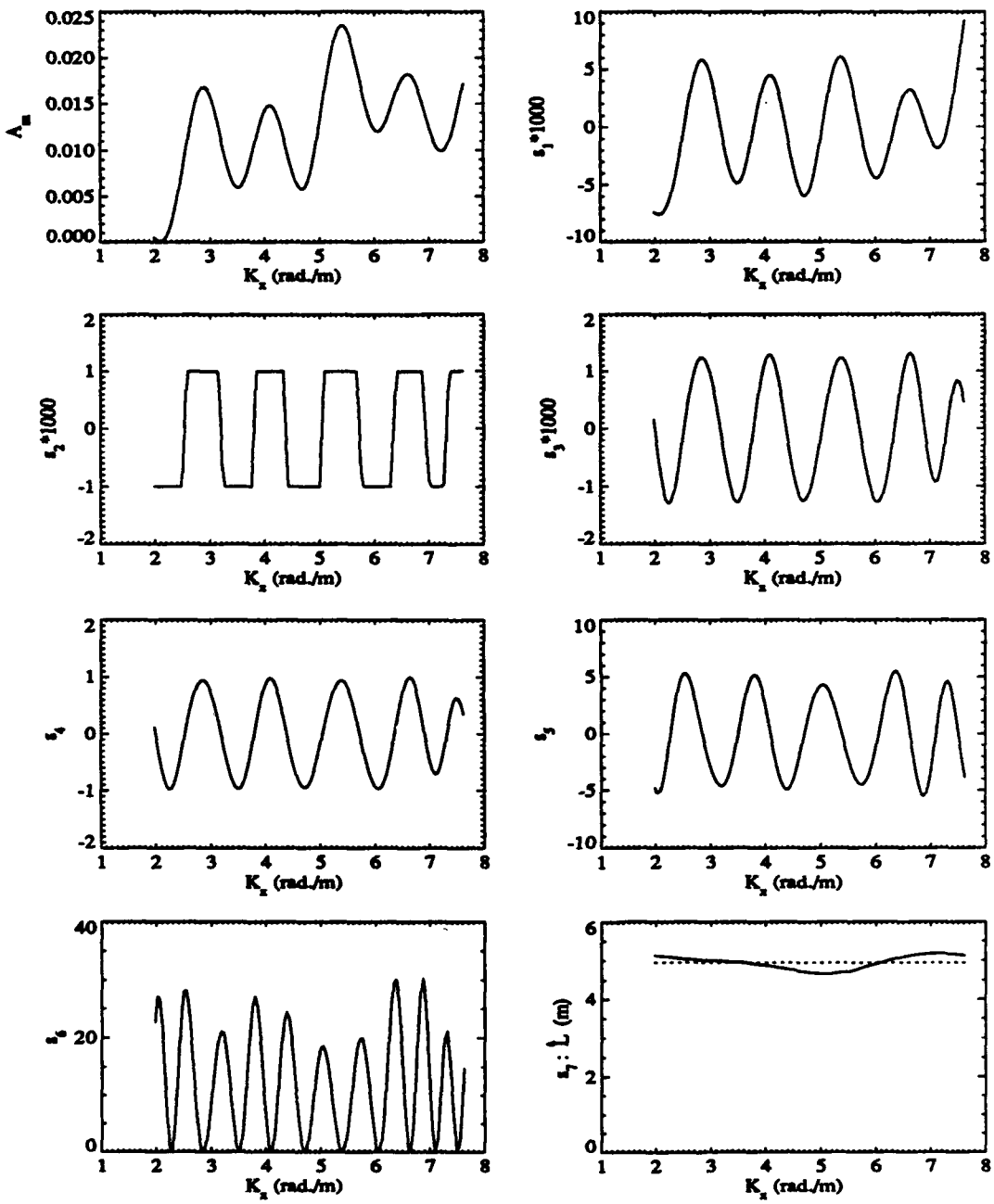

Figure 5.13: Signal waveforms in the ship length estimation from A_m for the Wigley-Cosine hull model using the frequency demodulation method. The estimated ship length is $\hat{L}_{fd} = 4.949$ meters with a relative error of 0.08%.

4ϕ). The output of the filter is

$$s_7(K_x) = \frac{1}{2}(L - \frac{4L\beta}{L^2K_x^2 + 4\beta^2})^2 \quad . \tag{5.112}$$

This is the desired frequency information containing the ship length. Similar to the zero-crossing method, several strategies can be used to estimate the ship length. If $s_7(K_x)$ is not a monotonic function, then β is not a constant and the average value of $s_7(K_x)$ can be considered. Since usually $L^2K_x^2 \gg 4|\beta - \beta^2|$, the estimate of ship length is given as

$$\hat{L} \approx \sqrt{2\bar{s}_7} \tag{5.113}$$

where $\bar{s}_7$ is the average of the signal $s_7(K_x)$. If $s_7(K_x)$ is a monotonic or almost monotonic function, then β can be considered as a constant and the ship length can be obtained by solving (5.112). Since there are two unknowns, L and β, in (5.112) and many function values of $s_7(K_x)$ are available, least square methods can be used here.

As an example, consider the Wigley-Cosine hull model again. Here, the input is A_m. The signals at each stage in Figure 5.12 are given in Figure 5.13. The cut-off frequencies of the filters are 0.4 Hz and 1.5 Hz for the first bandpass filter, and 0.5 Hz and 1.5 Hz for the second bandpass filter. The cut-off frequency for the low pass filter is 0.03 Hz. The signal s_7 in the diagram represents the frequency of A_m, the ordinate has been directly labeled with the length scale $\hat{L} = 2\pi f_{K_x}$ instead of f_{K_x} for easy observation of the estimated length. The dotted line is the average of the frequency, which gives the estimation of ship length. The estimated ship length is $\hat{L}_{fm} = 4.949$ meters with a relative error of 0.08%. The standard deviation of the variation of $2\pi f_{K_x}$ is 0.166 meters.

So far, three methods for the estimation of ship length have been introduced. In general, the spectrum method is a fundamental and powerful method, in particular for signals with noise or other undesired frequency components. The zero-crossing method and frequency demodulation method may be used to achieve more accurate results. In real situations, the methods can be combined in use. For example, the spectrum method may be used first to obtain a rough estimation, then the result can be refined using the zero-crossing method or the frequency demodulation method.

5.4 Estimation of the Quapaw Hull Length

This section applies the above theoretical analysis and methodology to a practical problem, the estimation of the Quapaw's length. This ship model has length $L = 4.953$ meters, width $B = 0.978$ meters and draft $H = 0.362$ meters. Here, the assumptions that $B/L \ll 1$ and B/H is small are not valid; thus, this is not a thin ship, that is, the hull is not narrow and deep. The hull surface and the waterline contour plot are given in Figure 5.14. The hull was towed in a tow tank with a constant speed $U = 2.229$ meters/second (7.31 feet/second). Three wave elevation cuts were measured with three independent sensors fixed in the tow tank as the ship hull passed. These wave cuts, shown in Figure 4.9 in Chapter 4, are parallel to the ship centerline and at the distance of $y_1 = 1.219$, $y_2 = 1.524$ and $y_3 = 1.8288$ meters from the centerline, respectively. The wave data have been preprocessed to remove the pulse-type noise caused by instrumentation and the stationary waves caused by the finite length of the tow tank.

Generally, four steps can be taken for estimating the ship length, that is, 1) calculate the FFT of the wave elevation $\eta(x, y_i)$; 2) calculate the wave amplitude function $A(K_x)$; 3) roughly guess the ship length from the curve $A(K_x)$; 4) estimate

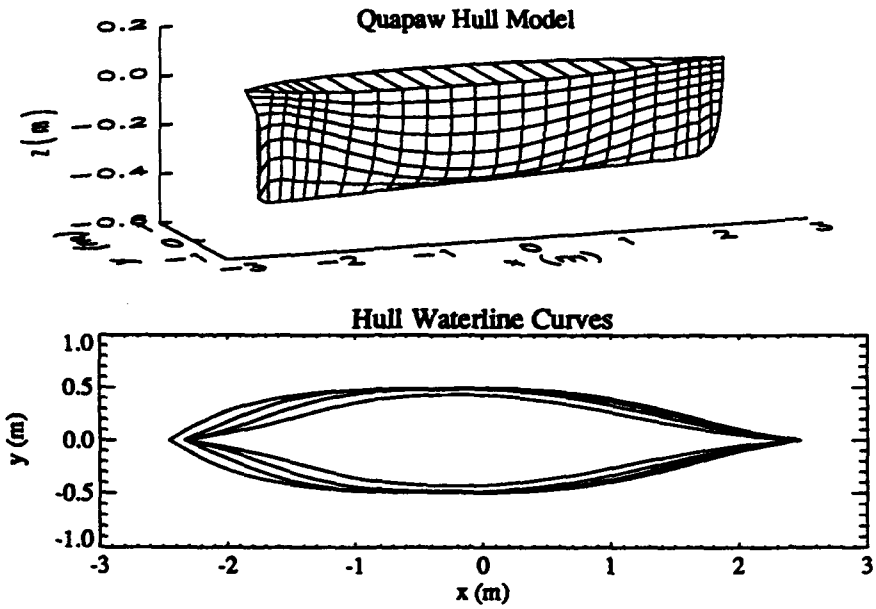

Figure 5.14: Quapaw hull model and its waterline curves $y = \pm\zeta(x, z)$ at $z = -0.3$, -0.2, -0.1, -0.001 meters.

the ship length using the methods introduced above. Figure 5.15 gives the FFT of $\eta(x, y_3)$, $|A(K_x)|$ and the spectrum of detrended $|A(K_x)|$ for the data RUN3.

Analysis of the plots in Figure 5.15 is given now. In the figure, (a) plots the magnitude of the FFT of the wave amplitude function; (b) plots the part of (a) to see the detail for lower spatial frequency components, and the abscissa has been relabeled as the wave number K_x, which is equal to $2\pi u$ here. It is found from (b) that there are two peaks which are much larger than others. The first peak in Figure 5.15(b), at $K_x = 1.974$ rad./meter, corresponds to the transverse waves; the second peak, at $K_x \approx 2.5$ rad./meter, corresponds to the diverging waves. This second peak and is larger, and, thus, the wave component it represents is dominant in the wave cut. The dominant wavelength can be estimated to be $\lambda = \frac{2\pi}{2.5} = 2.5$ meters. According to the theoretical analysis in Chapter 3, the wave number in the x-direction

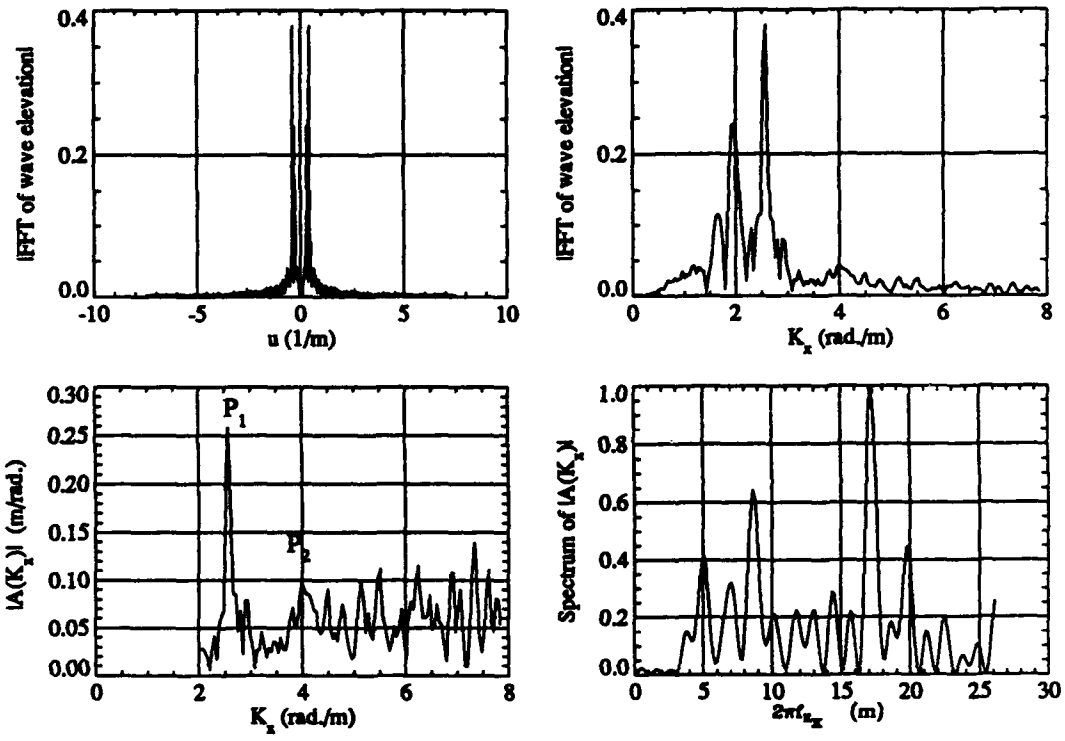

Figure 5.15: (a) Magnitude of the FFT of the wave elevation for data RUN3-C; (b) magnification of plot (a); (c) the magnitude of the wave amplitude function $|A(K_x)|$ calculated from (a); (d) the spectrum of detrended $|A(K_x)|$.

is $K_x = \frac{K_0}{cos\theta} = \frac{g}{U^2 cos\theta}$. The transverse wave crests are almost perpendicular to the ship centerline, i.e., $\theta \approx 0$; the transverse wave number is $K_0 = 1.974$ rad./meter. Since the wave cut is parallel to the the ship centerline, the apparent transverse wavelength in the wave cut is the same as K_0. However, the apparent diverging wavelength in the wave cut is larger than the diverging wavelength itself because the wave cut is not perpendicular to the diverging wave crests.

An empirical formula to guess the apparent diverging wavelength in wave cuts or to guess ship length may be obtained from a simplified model of the wave amplitude function. To do this, the relation between the wave amplitude function and the FFT of the wave elevation cut given in (3.50) is rewritten by changing variable θ into K_x in the form

$$A(K_x) \;=\; H(\frac{K_x}{2\pi})\frac{K_x}{\pi g}\sqrt{U^4K_x^2 - g^2}\, e^{\frac{K_x y_0}{g}\sqrt{U^4K_x^2-g^2}} \tag{5.114}$$

where $H(\frac{K_x}{2\pi})$ is the Fourier transform of the wave cut $\eta(x, y_0)$. When $U^4K_x^2 \gg g^2$, the magnitude of $A(K_x)$ is approximated as

$$|A(K_x)| \;\approx\; \frac{1}{\pi K_0}K_x^2\,|H(\frac{K_x}{2\pi})| \tag{5.115}$$

or the magnitude of $H(\frac{K_x}{2\pi})$ is written as

$$|H(\frac{K_x}{2\pi})| \;\approx\; \pi K_0\frac{|A(K_x)|}{K_x^2} \quad . \tag{5.116}$$

Now, consider a hull symmetrical in length. Its wave amplitude function can be described as a very simple form, $A(K_x) = \mathrm{j}Q\, cos[\frac{L}{2}(K_x - K_0) + \phi_{K_0}]$, where ϕ_{K_0} is the phase at $K_x = K_0$ and Q is a constant. $A(K_x)$ approaches zero when $K_x < K_0$ since the minimum wave number is K_0. Although $A(K_x)$ has a cosine form, $|H(\frac{K_x}{2\pi})|$ decays very fast as K_x increases because of the factor $\frac{1}{K_x^2}$. Thus, the first maximum

as $K_x > K_0$ is important, and it is approximately given as

$$K_{x_{max}} \approx K_0 + \kappa \frac{\pi}{L} \tag{5.117}$$

where κ can be between 0.5 and 1.0, depending on the phase ϕ_{K_0}. For example, κ can be taken as 1.0 for $\phi_{K_0} \approx (2n+1)\frac{\pi}{2}$ and 0.5 for $\phi_{K_0} \approx (2n+1)\frac{\pi}{4}$. From this empirical formula, the apparent wavelength in a wave cut can be roughly estimated, if the ship length is known, using

$$\lambda_a = \frac{2\pi}{K_{x_{max}}} \approx \frac{2\pi}{K_0 + \kappa\frac{\pi}{L}} \tag{5.118}$$

$$= \frac{2\pi F_n^2 L}{1 + \kappa\pi F_n^2} \tag{5.119}$$

where F_n is the Froude number. The ship length can be roughly estimated using

$$\hat{L} \approx \kappa \frac{\pi}{K_{x_{max}} - K_0} \quad . \tag{5.120}$$

From the FFT of the wave elevation cut in Figure 5.15, for example, $K_{x_{max}} \approx 2.5$, thus the ship length is roughly estimated as 3.14 to 6.28 meters.

Figure 5.16 (c) is the magnitude $|A(K_x)|$ of the wave amplitude function. It is not so smooth as the one in the above example of the Wigley-Cosine hull model. However, the peaks labeled with P_1 and P_2 still can be recognized as a period, which is approximately equal to 1.5 rad./meter. Thus, the ship length can be roughly estimated as $L \approx \frac{2\pi}{1.5} = 4.2$ meters.

To analyze the frequency components of $|A(K_x)|$ in detail, the data $|A_(K_x)|$ is detrended and then its power spectrum is calculated. In order to be consistent with the ship length scale, the abscissa has been labeled as $2\pi f_{K_x}$ instead of f_{K_x}, the frequency corresponding to K_x, in the spectrum diagrams given below. According to the theoretical analysis in the above sections, $A_R(K_x)$ or $A_I(K_x)$ contains the component $cos(\frac{L}{2}K_x - \phi)$, and, thus, has a dominant peak at $\frac{L}{2}$ in its spectrum;

$|A(K_x)|$ contains the component $cos(LK_x - \phi)$, and, thus, has a dominant peak at L in its spectrum. All the analysis is based on the linearized free-surface condition and the thin ship assumption. In the spectra of $|A(K_x)|$ calculated from real ship wave data, however, there may exist many peaks presenting different frequency components, as seen in Figure 5.15 (d). In this diagram, the peak at around 5 meters is the second harmonic component L, representing the ship length. The basic component at $\frac{L}{2}$ is a small peak here since this spectrum is of $|A(K_x)|$. In addition to these two components, there are several higher order harmonic components and other frequency components. These additional components may result from the nonlinear effects of ship waves, which have been neglected in the above theoretical analysis. These nonlinear effects on the wave elevation are very small, and wave components caused by the nonlinear effects have a very small energy. However, they locate at the end of higher frequencies in the wave elevation spectrum; thus, these components are greatly enhanced in $|A(K_x)|$ because of the factor K_x^2 in $|A(K_x)| \approx \frac{1}{\pi K_0} K_x^2 |H(\frac{K_x}{2\pi})|$. This is the situation found in Figure 5.15 (d), in which a couple of frequency components are larger than the component at $2\pi f_{K_x} = 5$. Thus, we need to guess the ship length first using the first two important peaks in the diagram of $|A(K_x)|$ and using the empirical formula (5.120) to know which component is our desired one in the spectrum of $|A(K_x)|$.

The results of ship length estimated form the three wave cuts of the data RUN3 are shown in Figures 5.16, 5.17, and 5.18. The magnitude $|A(K_x)|$ of the wave amplitude function is first calculated from the FFT of the wave cut, and then it is detrended. The detrended signal, denoted as $A_d(K_x)$, is filtered by a bandpass filter with bandwidth 0.4 Hz and central frequency 0.8 Hz. Finally, the filtered signal, denoted as $A_f(K_x)$, is used to estimate the ship length. The three methods

methods	*wave cut A*	*wave cut B*	*wave cut C*	*9-cut average*	*rms error*
$\hat{L}_{sp}$ (ϵ_L)	4.746(4.2%)	4.812(2.8%)	5.347(8.0%)	4.968(0.3%)	0.330(6.7%)
$\hat{L}_{zc}$ (ϵ_L)	5.240(5.8%)	5.190(4.8%)	5.290(6.8%)	5.240(5.8%)	0.291(5.9%)
$\hat{L}_{fd}$ (ϵ_L)	4.959(0.1%)	4.946(0.1%)	5.078(2.5%)	4.994(0.8%)	0.084(1.7%)

Table 5.1: Quapaw hull length estimated from the three wave cuts of RUN3 using the spectrum method, zero-crossing method and frequency demodulation method. The unit of the ship length in the table is *meters*, and the true hull length is 4.953 meters.

introduced in the last section are used here. The spectrum of A_f has been normalized in the figures. The results of the ship length estimation is listed in Table 5.1, where $\hat{L}_{sp}$, $\hat{L}_{zc}$ and $\hat{L}_{fd}$ denote the estimated lengths using the spectrum method, zero-crossing method and frequency demodulation method, respectively, and ϵ_L denotes their relative error. According to the statistical analysis of the nine lengths estimated from the three wave cuts using the three methods, the mean of the estimated ship length is 5.068 meters with a relative error of 2.3%. The root mean square (rms) is 0.243 meters with a relative rms error of 4.9%. This example shows that although the theoretical analysis and the methodology are based on the linearized free-surface condition and the thin-ship assumption, they can be used for estimating a non-thin ship's length from real wave data, and good estimation results can be obtained.

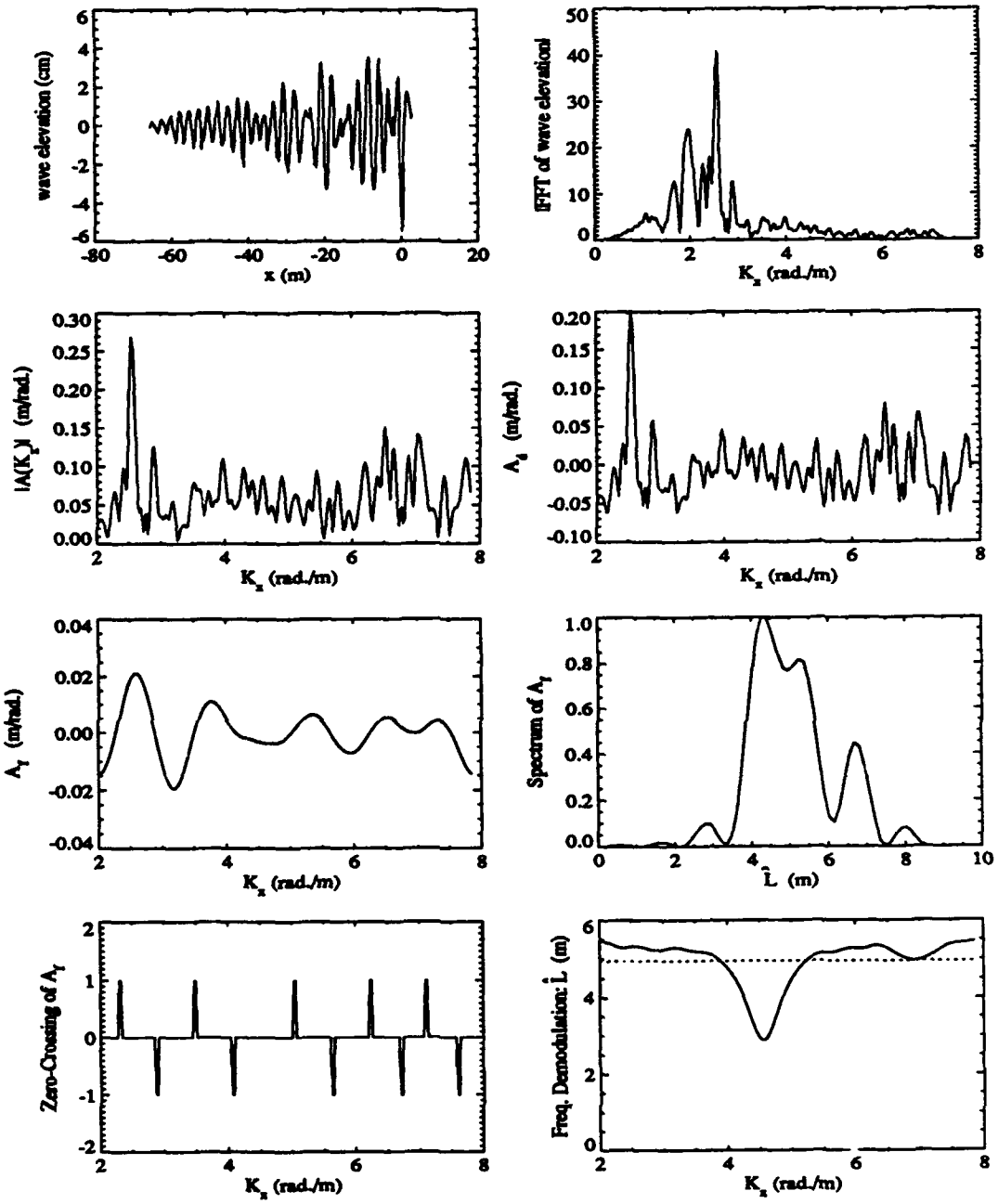

Figure 5.16: Quapaw hull length estimation from the tow tank wave cut RUN3-A at $y = 1.219\ m$ using three methods. The estimated ship length is $\hat{L}_{sp} = 4.746\ m$ ($\epsilon_L = 4.2\%$) for the spectrum method, $\hat{L}_{zc} = 5.240\ m$ ($\epsilon_L = 5.8\%$) for the zero-crossing method, and $\hat{L}_{fd} = 4.959\ m$ ($\epsilon_L = 0.1\%$) for the frequency demodulation method.

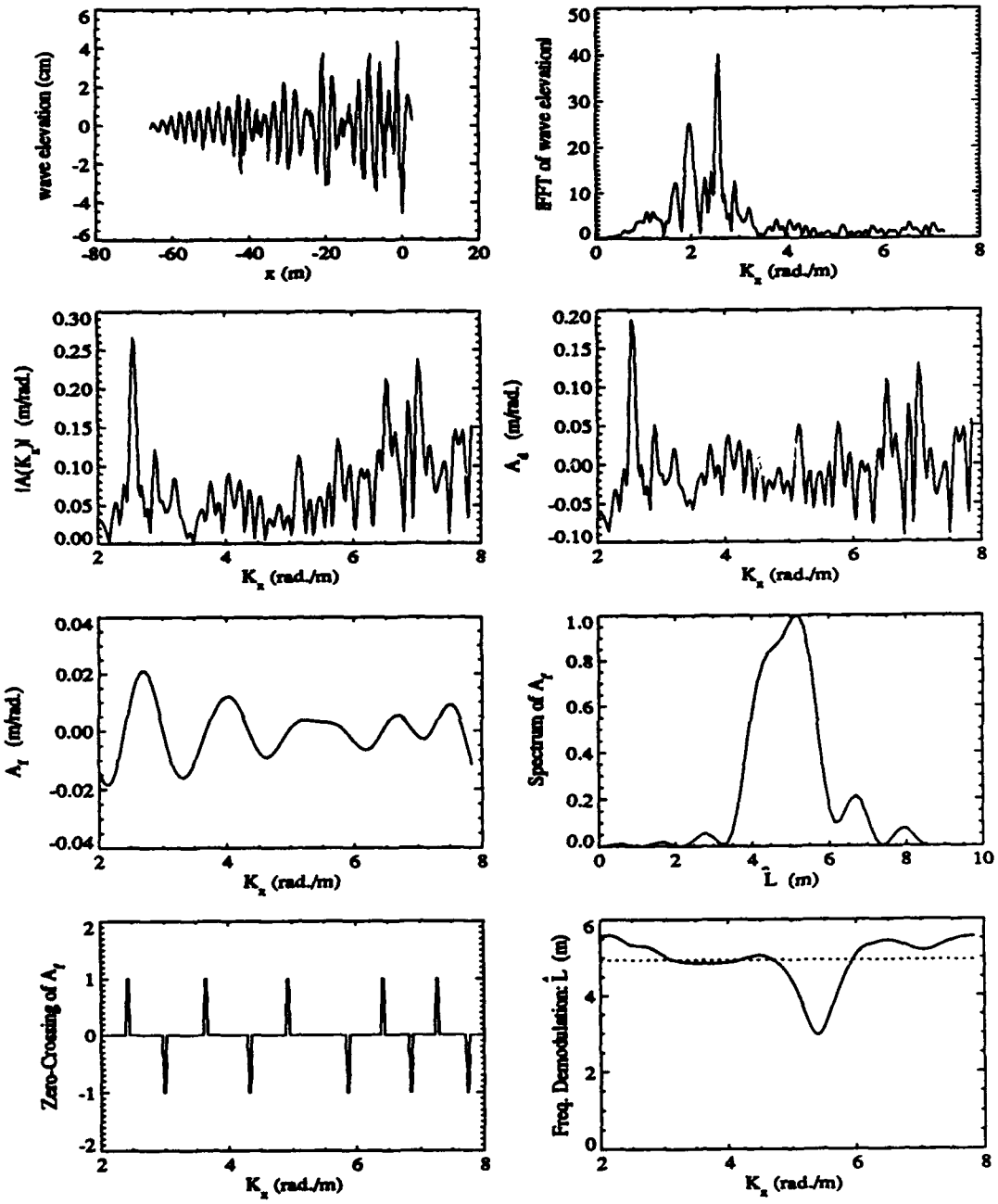

Figure 5.17: Quapaw hull length estimation from the tow tank wave cut RUN3-B at $y = 1.524\ m$ using three methods. The estimated ship length is $\hat{L}_{sp} = 4.812\ m$ ($\epsilon_L = 2.8\%$) for the spectrum method, $\hat{L}_{zc} = 5.190\ m$ ($\epsilon_L = 4.8\%$) for the zero-crossing method, and $\hat{L}_{fd} = 4.946\ m$ ($\epsilon_L = 0.1\%$) for the frequency demodulation method.

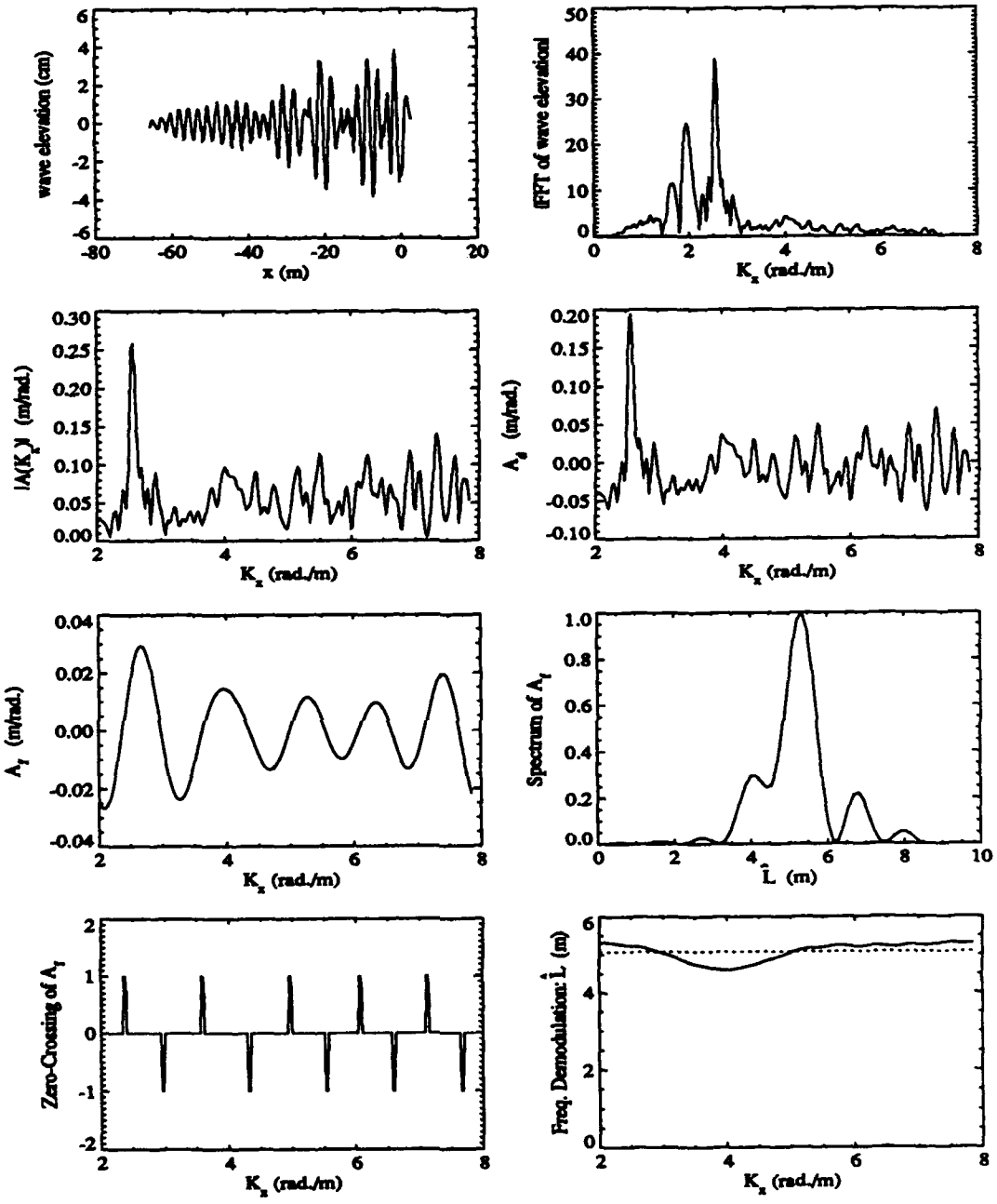

Figure 5.18: Quapaw hull length estimation from the tow tank wave cut RUN3-C at $y = 1.8288\ m$ using three methods. The estimated ship length is $\hat{L}_{sp} = 5.347\ m$ ($\epsilon_L = 8.0\%$) for the spectrum method, $\hat{L}_{zc} = 5.290\ m$ ($\epsilon_L = 6.8\%$) for the zero-crossing method, and $\hat{L}_{fd} = 5.078\ m$ ($\epsilon_L = 2.5\%$) for the frequency demodulation method.

CHAPTER VI

EXTRACTION OF SHIP HULL GEOMETRY INFORMATION

The prediction of a ship's hull geometry from the ship generated wave pattern can be considered as an inverse Kelvin wake problem. Solutions to this problem are becoming more practical with advances in remote sensing technology.

The idea used here to extract a ship's hull shape is based on the relation of the ship hull shape and the wave amplitude function under the thin-ship assumption, and the relation of the wave amplitude function and the ship wave spectrum. These relations have been discussed in the previous chapters, thus, this chapter focuses on the technique to extract a ship's hull geometry shape from the wave amplitude function. Mathematically, the problem is to find the function of hull surface $\zeta(x,z)$, given the wave amplitude function $A(\theta)$ and the integral

$$A'(\theta) = H \int_{-1}^{1} \int_{-1}^{0} \frac{\partial \zeta(x,z)}{\partial x} e^{j\nu(\theta)x} e^{\mu(\theta)z} dx dz \tag{6.1}$$

where ν and μ have been given in (5.9) and (5.10), and $A'(\theta)$ is defined as

$$A'(\theta) \triangleq \frac{\pi U^2}{2g} \cos^3(\theta) A(\theta) \ . \tag{6.2}$$

In the above, (6.1) is obtained from (5.8) under the thin-ship assumption. x and z are the variables normalized by the ship length and draft, and $e^{j\nu(\theta)x} e^{\mu(\theta)z}$ is a kernel function with parameter θ.

To solve this continuous inversion problem, we prefer to convert it to a discrete inversion problem first, and then solve it using discrete inversion techniques. The reasons for this are that it is difficult, in general, to solve a continuous inversion problem analytically and that the values of the wave amplitude function are usually available in discrete form. To obtain the discrete form, the integral may be approximated as a summation using the trapezoidal rule or some other quadrature formula. In this hull inversion problem, however, the spectral method is adopted instead of the above quadrature methods. In the spectral method, the unknown function is approximated as a weighted summation of some basis functions. Because the basis functions are known and the integrals associated with them can be computed, solving the continuous inversion problem becomes a matter of solving a set of discrete equations to determine the weights or coefficients. The advantage of the spectral method is that the number of unknowns to be determined can be reduced greatly. This is especially important for two dimensional inverse problems.

When both the magnitude and phase of the wave amplitude function are well known, the ship hull inverse problem becomes a linear inverse problem. The singularity of the kernel matrix in the linear problem and noise of the observed data may have severe effects on the inversion results, and thus special techniques may have to be considered. In particular, the methods of constrained linear inversion and the maximum likelihood estimation with constraints will be considered in solving the ship hull inversion.

However, if only the magnitude of the wave amplitude function is available, then a complicated non-linear inverse problem must be handled. For the hull inverse problem, the non-linear inversion is solved based on the criterion of the maximum likelihood estimation with constraints using optimization techniques. Examples of

linear inversion and non-linear inversion will be demonstrated for both mathematically well-defined ship hulls and the model of the real ship Quapaw.

In the following, bold lowercase letters denote vectors, and bold uppercase letters denote matrices.

6.1 Spectral method

In this section, the spectral method is used to convert the continuous inverse problem to a discrete inverse problem. In the following, the solution of the inverse problem, $\zeta(x,z)$, is approximated by a weighted summation of basis functions. Inserting the summation into the integral equation (6.1) yields a set of algebraic equations for different values of the parameter θ. The solution of the algebraic equations gives the weights, or coefficients, of the summation, and any value of $\zeta(x,z)$ in the specified region can be evaluated from the summation of basis functions.

For this goal, let the basis functions in the $x-$ and $z-$directions be $\phi_i(x), i = 1,2,\cdots,M$ and $\beta_j(z), j = 1,2,\cdots,N$, respectively. $\zeta(x,z)$ is now expressed in the form

$$\zeta(x,z) = \sum_{i=1}^{M}\sum_{j=1}^{N} a_{ij}\phi_i(x)\beta_j(z) \quad . \tag{6.3}$$

and its partial derivative with respect to x is given as

$$\frac{\partial\zeta(x,z)}{\partial x} = \sum_{i=1}^{M}\sum_{j=1}^{N} a_{ij}\dot{\phi}_i(x)\beta_j(z) \tag{6.4}$$

where $\dot{\phi}_i(x)$ denotes the derivative of $\phi_i(x)$. Substitution of (6.4) into (6.1) gives the following linear equation with the coefficients a_{ij} to be determined:

$$A'(\theta) = \sum_{i=1}^{M}\sum_{j=1}^{N} a_{ij}[\,W_{Rij}(\theta) + \mathrm{j}W_{Iij}(\theta)\,] \ , \tag{6.5}$$

where

$$W_{Rij}(\theta) \triangleq W_{XRi}(\theta)\, W_{Zj}(\theta) \tag{6.6}$$

$$W_{Iij}(\theta) \triangleq W_{XIi}(\theta)\, W_{Zj}(\theta) \tag{6.7}$$

$$W_{XRi}(\theta) \triangleq \int_{-1}^{1} \dot{\phi}_i(x) \cos\left[\nu(\theta)x\right] dx \tag{6.8}$$

$$W_{XIi}(\theta) \triangleq \int_{-1}^{1} \dot{\phi}_i(x) \sin\left[\nu(\theta)x\right] dx \tag{6.9}$$

$$W_{Zj}(\theta) \triangleq H \int_{-1}^{0} \beta_j(z) e^{\mu(\theta)z} dz \tag{6.10}$$

In general, the amplitude function $A(\theta)$ is complex, and, thus, $A'(\theta)$ is too. If $A'_R(\theta) \triangleq Re\{A'(\theta)\}$ and $A'_I(\theta) \triangleq Im\{A'(\theta)\}$ denote the real and imaginary parts, respectively, then (6.5) gives

$$\begin{aligned} A'_R(\theta) &= \sum_{i=1}^{M}\sum_{j=1}^{N} a_{ij}\, W_{Rij}(\theta) \\ A'_I(\theta) &= \sum_{i=1}^{M}\sum_{j=1}^{N} a_{ij}\, W_{Iij}(\theta) \ . \end{aligned} \tag{6.11}$$

Given K values of θ, there is a set of equations

$$\begin{aligned} A'_R(\theta_k) &= \sum_{i=1}^{M}\sum_{j=1}^{N} a_{ij}\, W_{Rij}(\theta_k) \\ A'_I(\theta_k) &= \sum_{i=1}^{M}\sum_{j=1}^{N} a_{ij}\, W_{Iij}(\theta_k) \\ & k = 1, 2, \cdots, K \ . \end{aligned} \tag{6.12}$$

In order to get a unique solution of the $M \times N$ coefficients, a_{ij}, there must be at least $M \times N$ equations. Thus, the number of parameters θ_k. should satisfy $K \geq \frac{1}{2} M \times N$.

The above equations can be written in a vector and matrix form by rearranging the subscripts. According to the rule that the subscripts $((\{ij\}, j = 1, 2, \cdots, N), i = 1, 2, \cdots, M)$ are mapped to $(\{l\}, l = 1, 2, \cdots, MN)$, and the coefficients $\{(a_{ij}, j = 1, 2, \cdots, N), i = 1, 2, \cdots, M\}$ are mapped into $\{b_l, l = 1, 2, \cdots, MN\}$, (6.12) can be

written in the form

$$\mathbf{a} = \mathbf{W}\mathbf{b} \tag{6.13}$$

where $\mathbf{a} = [A'_R(\theta_1), A'_R(\theta_2), \cdots, A'_R(\theta_K), A'_I(\theta_1), A'_I(\theta_2), \cdots, A'_I(\theta_K)]^T$ with dimension $2K \times 1$, $\mathbf{b} = [b_1, b_2, \cdots, b_{MN}]^T$ with dimension $MN \times 1$, and T signifies transpose. The matrix $\mathbf{W}$ may be called the kernel matrix as it is related to the kernel function. It has dimension $2K \times MN$ and is given as

$$\mathbf{W} = \begin{bmatrix} W_{R111} & W_{R121} & \cdots & W_{R1N1} & W_{R211} & \cdots & W_{R(M-1)N1} & W_{RM11} & \cdots & W_{RMN1} \\ W_{R112} & W_{R122} & \cdots & W_{R1N2} & W_{R212} & \cdots & W_{R(M-1)N2} & W_{RM12} & \cdots & W_{RMN2} \\ \vdots & & & & & & & & & \\ W_{R11K} & W_{R12K} & \cdots & W_{R1NK} & W_{R21K} & \cdots & W_{R(M-1)NK} & W_{RM1K} & \cdots & W_{RMNK} \\ W_{I111} & W_{I121} & \cdots & W_{I1N1} & W_{I211} & \cdots & W_{I(M-1)N1} & W_{IM11} & \cdots & W_{IMN1} \\ W_{I112} & W_{I122} & \cdots & W_{I1N2} & W_{I212} & \cdots & W_{I(M-1)N2} & W_{IM12} & \cdots & W_{IMN2} \\ \vdots & & & & & & & & & \\ W_{I11K} & W_{I12K} & \cdots & W_{I1NK} & W_{I21K} & \cdots & W_{I(M-1)NK} & W_{IM1K} & \cdots & W_{IMNK} \end{bmatrix} \tag{6.14}$$

where W_{Rijk} and W_{Iijk} denote $W_{Rij}(\theta_k)$ $W_{Iij}(\theta_k)$, respectively.

Now, the continuous inverse problem has been converted to an algebraic inverse problem. In (6.13), $\mathbf{a}$ is usually obtained from measurements, $\mathbf{W}$ is known from construction, and $\mathbf{b}$ is to be solved for. The kernel matrix $\mathbf{W}$ depends on the wave angle, ship's length, draft and speed, and the choice of the basis functions. Thus, the next step is to select a set of appropriate basis functions.

6.2 Selection of Basis Functions

The most preferable basis functions should have the properties of easy computation, completeness and rapid convergence [40]. The property of easy computation means not only that the basis functions themselves should be easily calculated, but also that they should make the integrals in the elements of the above matrix,$W_{XRi}(\theta)$,$W_{XRi}(\theta)$ and $W_{Zj}(\theta)$, be analytically integrable. Thus, costly numerical computation time can be avoided. The completeness of the basis functions

make it possible for the solution to be represented to an arbitrarily high degree of accuracy by increasing the number of basis functions. The property of rapid convergence allows the number of basis functions used to be as small as possible. In addition, the geometry of the problem is another fact that needs to be considered when the basis functions are selected. Study on spectral methods indicates that the best choice for 95% of all applications is an ordinary Fourier series or a set of Chebyshev polynomials. For the non-periodic problem, the Chebyshev polynomials are extremely robust and give good results in almost all situations [40].

Based on the above principles, the Chebyshev polynomials $T_n(\xi)$ are chosen in both the $x-$ and $z-$directions. The explicit expressions of the Chebyshev polynomials $T_n(\xi)$ are given as

$$\begin{aligned} T_0(\xi) &= 1 \\ T_1(\xi) &= \xi \\ T_2(\xi) &= 2\xi^2 - 1 \\ &\cdots \\ T_{n+1}(\xi) &= 2\xi T_n(\xi) - T_{n-1}(\xi) \end{aligned} \tag{6.15}$$

$$\xi \in [-1, 1] \ ; \quad n \geq 1 \ .$$

They have two main properties: 1) $T_n(\xi)$ is even for even n, and odd for odd n; 2) $T_n(\pm 1) = 1$ for even n, and $T_n(\pm 1) = \pm 1$ for odd n.

The basis functions $\phi_i(x)$ and $\beta_j(z)$ are constituted by the Chebyshev polynomials. One strategy to select the basis functions is to set

$$\phi_i(x) = T_i(x) \ , \ i = 1, 2, \cdots, M \tag{6.16}$$

$$\beta_j(z) = T_{j-1}(z) \ , \ j = 1, 2, \cdots, N \, . \tag{6.17}$$

The reason not to include the lowest order of the Chebyshev polynomials, $T_0(x)$, in the basis functions of the $x-$direction is that the derivative of $T_0(x) = 1$ is equal to zero, and thus whether $T_0(x)$ is included or not has no effect on $\frac{\partial \zeta(x,z)}{\partial x}$ in the integral (6.1). Even if $T_0(x)$ is included, its coefficient can not be determined by solving (6.13). Thus, a constant must be finally determined according to the boundary condition of $\zeta(x,z)$ after the coefficients a_{ij} are found.

In fact, the function representing the ship hull shape, $\zeta(x,z)$, is zero on the ship hull boundary or outside of the boundary on the $x-z$ plane, that is, in the normalized coordinate system,

$$\zeta(\pm 1, z) = 0 , \tag{6.18}$$

$$\zeta(x, -1) = 0 . \tag{6.19}$$

These conditions can be imposed on the basis functions with the advantage that no constant needs to be determined. According to this idea, the basis functions in the $x-$direction are set to be

$$\phi_i(x) = \begin{cases} T_{i+1}(x) - 1 & \text{if } i \text{ is odd} \ ; \\ T_{i+1}(x) - x & \text{if } i \text{ is even} \ , \end{cases} \qquad i = 1, 2, \cdots, M, \tag{6.20}$$

If it is desired that the boundary condition in the $z-$direction given in (6.17) be imposed on the basis functions, then they should be set to be

$$\beta_j(z) = \begin{cases} T_j(z) + 1 & \text{if } j \text{ is odd} \ ; \\ T_j(z) - 1 & \text{if } j \text{ is even} \ , \end{cases} \qquad j = 1, 2, \cdots, N. \tag{6.21}$$

The proper choice of basis functions may not only make the elements of the kernel matrix $\mathbf{W}$ easier to compute, but also make the discrete inverse problem simpler. In

solving the inverse problem given in (6.1), the basis functions will be chosen from (6.17) and (6.20). The basis functions given in (6.20) have the property that $\phi_i(x)$ is even for odd i, and odd for even i according to the even and odd property of the Chebyshev polynomials. Thus, $\dot{\phi}_i(x)$ is even for even i, and odd for odd i. This fact further results in that $W_{XRi}(\theta) = 0$ for odd i and $W_{XIi}(\theta) = 0$ for even i since the integrands in the symmetric integrals (6.8) and (6.9) are odd. These properties of $W_{Rij}(\theta)$ and $W_{Iij}(\theta)$ can be used to simplify the kernel matrix $\mathbf{W}$ in (6.14). To show this, consider an example with $M = 4$, $N = 2$ and $K = 4$. In this case, the matrix $\mathbf{W}$ is given as

$$\mathbf{W} = \begin{bmatrix} 0 & 0 & W_{R211} & W_{R221} & 0 & 0 & W_{R411} & W_{R421} \\ 0 & 0 & W_{R212} & W_{R222} & 0 & 0 & W_{R412} & W_{R422} \\ 0 & 0 & W_{R213} & W_{R223} & 0 & 0 & W_{R413} & W_{R423} \\ 0 & 0 & W_{R214} & W_{R224} & 0 & 0 & W_{R414} & W_{R424} \\ W_{I111} & W_{I121} & 0 & 0 & W_{I311} & W_{I321} & 0 & 0 \\ W_{I112} & W_{I122} & 0 & 0 & W_{I312} & W_{I322} & 0 & 0 \\ W_{I113} & W_{I123} & 0 & 0 & W_{I313} & W_{I323} & 0 & 0 \\ W_{I114} & W_{I124} & 0 & 0 & W_{I314} & W_{I324} & 0 & 0 \end{bmatrix} . \tag{6.22}$$

Observing the pattern of the above matrix, we can find that if the columns of the matrix are rearranged, then the matrix can be written in the form

$$\mathbf{W}' = \begin{bmatrix} W_{R211} & W_{R221} & W_{R411} & W_{R421} & 0 & 0 & 0 & 0 \\ W_{R212} & W_{R222} & W_{R412} & W_{R422} & 0 & 0 & 0 & 0 \\ W_{R213} & W_{R223} & W_{R413} & W_{R423} & 0 & 0 & 0 & 0 \\ W_{R214} & W_{R224} & W_{R414} & W_{R424} & 0 & 0 & 0 & 0 \\ 0 & 0 & 0 & 0 & W_{I111} & W_{I121} & W_{I311} & W_{I321} \\ 0 & 0 & 0 & 0 & W_{I112} & W_{I122} & W_{I312} & W_{I322} \\ 0 & 0 & 0 & 0 & W_{I113} & W_{I123} & W_{I313} & W_{I323} \\ 0 & 0 & 0 & 0 & W_{I114} & W_{I124} & W_{I314} & W_{I324} \end{bmatrix} . \tag{6.23}$$

The new pattern of the matrix shows that the linear equation given in (6.13) can be split into two independent sets of linear equations with smaller dimensions if the matrix elements are rearranged according to the rules that for W_{Rijk}, the subscripts $\{(\{ij\}, j = 1, 2, \cdots, N), i = 2, 4, \cdots, M'\}$ are mapped into $(\{l_1\}, l_1 = 1, 2, \cdots, L_1)$, where $M' = M$ if M is even, and $M' = M - 1$ if M odd, and where $L_1 = \frac{M'}{2}N$; that for W_{Iijk}, the subscripts $\{(\{ij\}, j = 1, 2, \cdots, N), i = 1, 3, \cdots, M''\}$ are mapped into $(\{l_2\}, l_2 = 1, 2, \cdots, L_2)$, where $M'' = M - 1$ if M is even, and $M'' = M$ if M odd, and where $L_2 = \frac{M''}{2}N$. In addition, the coefficients $\{(a_{ij}, j = 1, 2, \cdots, N), i =$

$2, 4, \cdots, M'\}$ are represented by $\{c_l, l = 1, 2, \cdots, L_1\}$, and the coefficients $\{(a_{ij}, j = 1, 2, \cdots, N), i = 1, 3, \cdots, M''\}$ are represented by $\{d_l, l = 1, 2, \cdots, L_2\}$. After the subscripts are rearranged, the two independent sets of linear equations can be expressed in the matrix forms

$$\mathbf{a}_R = \mathbf{W}_R\,\mathbf{c} \tag{6.24}$$

$$\mathbf{a}_I = \mathbf{W}_I\,\mathbf{d} \tag{6.25}$$

where

$$\mathbf{a}_R = [A'_R(\theta_1), A'_R(\theta_2), \cdots, A'_R(\theta_K)]^T \tag{6.26}$$

$$\mathbf{a}_I = [A'_I(\theta_1), A'_I(\theta_2), \cdots, A'_I(\theta_K)]^T \tag{6.27}$$

$$\mathbf{c} = [c_1, c_2, \cdots, c_{L_1}]^T \tag{6.28}$$

$$\mathbf{d} = [d_1, d_2, \cdots, d_{L_2}]^T\ . \tag{6.29}$$

The matrix $\mathbf{W}_R$ with dimension $K \times L_1$ and $\mathbf{W}_I$ with dimension $K \times L_2$ are given by

$$\mathbf{W}_R = \begin{bmatrix} W_{R211} & W_{R221} & \cdots & W_{R2N1} & W_{R411} & \cdots & W_{R(M'-2)N1} & W_{RM'11} & \cdots & W_{RM'N1} \\ W_{R212} & W_{R222} & \cdots & W_{R2N2} & W_{R412} & \cdots & W_{R(M'-2)N2} & W_{RM'12} & \cdots & W_{RM'N2} \\ \vdots & & & & & & & & & \\ W_{R21K} & W_{R22K} & \cdots & W_{R2NK} & W_{R41K} & \cdots & W_{R(M'-2)NK} & W_{RM'1K} & \cdots & W_{RM'NK} \end{bmatrix} \tag{6.30}$$

and

$$\mathbf{W}_I = \begin{bmatrix} W_{I111} & W_{I121} & \cdots & W_{I1N1} & W_{I311} & \cdots & W_{I(M''-2)N1} & W_{IM''11} & \cdots & W_{IM''N1} \\ W_{I112} & W_{I122} & \cdots & W_{I1N2} & W_{I312} & \cdots & W_{I(M''-2)N2} & W_{IM''12} & \cdots & W_{IM''N2} \\ \vdots & & & & & & & & & \\ W_{I11K} & W_{I12K} & \cdots & W_{I1NK} & W_{I31K} & \cdots & W_{I(M''-2)NK} & W_{IM''1K} & \cdots & W_{IM''NK} \end{bmatrix} \tag{6.31}$$

Using the above mapping rule of the coefficients a_{ij}, the hull surface function can be expressed in a concise form

$$\zeta(x, z) = \mathbf{h}_o^T(x, z)\mathbf{c} + \mathbf{h}_e^T(x, z)\mathbf{d} \tag{6.32}$$

where vectors $\mathbf{h}_e(x,z)$ and $\mathbf{h}_o(x,z)$ are defined as

$$\begin{aligned}\mathbf{h}_o^T(x,z) &= [\phi_2(x)\beta_1(z),\ \phi_2(x)\beta_2(z),\ \ldots\ \phi_2(x)\beta_N(z),\\ &\quad \phi_4(x)\beta_1(z),\ \ldots\ \phi_{M'}(x)\beta_1(z),\ \ldots\ \phi_{M'}(x)\beta_N(z)] \qquad (6.33)\\ \mathbf{h}_e^T(x,z) &= [\phi_1(x)\beta_1(z),\ \phi_1(x)\beta_2(z),\ \ldots\ \phi_1(x)\beta_N(z),\\ &\quad \phi_3(x)\beta_1(z),\ \ldots\ \phi_{M''}(x)\beta_1(z),\ \ldots\ \phi_{M''}(x)\beta_N(z)]\ . \qquad (6.34)\end{aligned}$$

In (6.32), $\mathbf{h}_o^T(x,z)\mathbf{c}$ represents the odd part and $\mathbf{h}_e^T(x,z)\mathbf{d}$ the even part with respect to x if the basis functions $\phi_i(x)$ are selected to be even for odd i and odd for even i as in (6.20).

So far, two sets of linear equations have been established for determining the vectors $\mathbf{c}$ and $\mathbf{d}$, and thus the coefficients a_{ij}. If a ship hull is assumed to be bow-to-stern symmetric in its longitudinal distribution of volume, then $\zeta(x,z) = \zeta(-x,z)$, and thus $\mathbf{c} = \mathbf{0}$, and $\mathbf{a}_R = \mathbf{0}$ since the real part of the wave amplitude function is equal to zero. In this special case, only (6.25) needs to be solved.

For the basis functions composed of the Chebyshev polynomials, both $\dot{\phi}_i(x)$ and $\beta_j(z)$ are polynomials of x or z, thus W_{XRi}, W_{XIi} and W_{Zj} in (6.8)-(6.10) are combinations of integrals like

$$\begin{aligned}C_n &\triangleq \int_{-1}^{1} x^n \cos[\nu(\theta)x)]\,dx \qquad (6.35)\\ S_n &\triangleq \int_{-1}^{1} x^n \sin[\nu(\theta)x)]\,dx \qquad (6.36)\\ E_n &\triangleq \int_{-1}^{0} z^n e^{\mu(\theta)z} dz\ . \qquad (6.37)\end{aligned}$$

All of these are explicitly integrable, and $C_n = 0$ for odd n and $S_n = 0$ for even n.

6.3 Effects of Singularity and Data Error on Linear Inversion

Theoretically, once the measurement data $\mathbf{a}_R$ and $\mathbf{a}_I$ are given, and the elements of the matrices $\mathbf{W}_R$ and $\mathbf{W}_I$ are calculated for each given value of parameter θ, the unknown vectors $\mathbf{c}$ and $\mathbf{d}$ can be found by solving (6.24) and (6.25). To obtain a correct or reasonably accurate solution, however, we may have to take account of the ill-condition of the matrices, the noise involved in measurement data or the both. In the situations of ill-conditioned matrices, the solution may be unstable when there is a very small noise, or even no noise, just for a computer's finite floating point precision. Therefore, some special measures must be taken to solve linear inverse problems.

6.3.1 Effects of the Ill-condition of Matrices

The singularity or ill-condition of a matrix can be formally defined. According to the linear algebra theorem [42], any $\mathtt{M} \times \mathtt{N}$ matrix $\mathbf{A}$, whose number of rows $\mathtt{M}$ is greater than or equal to its number of columns $\mathtt{N}$, can be written as the product of an $\mathtt{M} \times \mathtt{N}$ column-orthogonal matrix $\mathbf{U}$, an $\mathtt{N} \times \mathtt{N}$ diagonal matrix $\mathbf{\Lambda} = [\mathrm{diag}(\lambda_i)]$ with non-negative elements, and the transpose of an $\mathtt{N} \times \mathtt{N}$ orthogonal matrix $\mathbf{V}$, that is,

$$\mathbf{A} = \mathbf{U}\,[\mathtt{diag}(\lambda_\mathtt{i})]\,\mathbf{V}^\mathtt{T} \ . \tag{6.38}$$

If the matrix $\mathbf{A}$ is square, $\mathtt{N} \times \mathtt{N}$ say, then the inverse of $\mathbf{A}$ is given by

$$\mathbf{A}^{-1} = \mathbf{V}\,[\mathtt{diag}(\frac{1}{\lambda_\mathtt{i}})]\,\mathbf{U}^\mathtt{T} \ . \tag{6.39}$$

The condition number of a matrix is defined as the ratio of the largest of the $\lambda_\mathtt{j}$'s to the smallest of the $\lambda_\mathtt{j}$'s. A matrix is singular if its condition number is infinite,

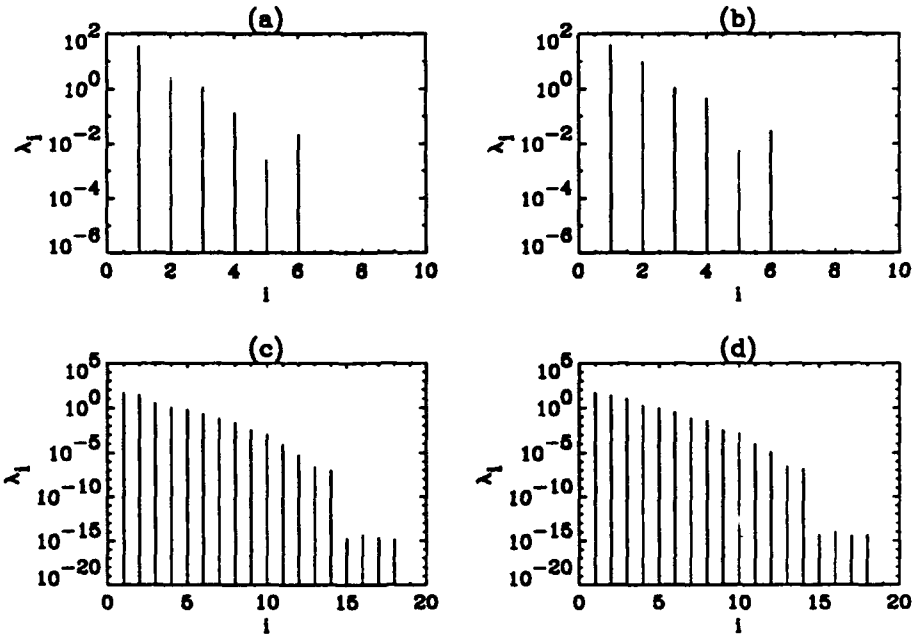

Figure 6.1: Elements λ_i of the diagonal matrices decomposed from (a) $\mathbf{W}_R$ and (b) $\mathbf{W}_I$ with $K = 135$ and $L_1 = 6$ associated with $M = 4$ and $N = 3$; (c) $\mathbf{W}_R$ and (d) $\mathbf{W}_I$ with $K = 135$ and $L_1 = 18$ associated with $M = 6$ and $N = 6$.

and it is ill-conditioned if its condition number is too large, that is, if its reciprocal approaches the computer machine's floating point precision.

Using this definition to examine the matrices $\mathbf{W}_R$ and $\mathbf{W}_I$ in the above ship hull inverse problem described by (6.24) and (6.25), we unfortunately find that even if there are no errors, the matrices may become ill-conditioned even for not very large M and N. As an example, consider the matrices $\mathbf{W}_R$ and $\mathbf{W}_I$ with the basis functions given in (6.17) and (6.20) and with parameters $L = 100$ meters, $H = 10$ meters and $U = 10$ m/s (equivalently, the Froude number $F_n = 0.32$). Figure 6.1 illustrates the elements λ_i of the diagonal matrices decomposed from $\mathbf{W}_R$ and $\mathbf{W}_I$ with parameters $K = 135$ and $L_1 = 6$ associated with $M = 4$ and $N = 3$, and with parameters $K = 135$ and $L_1 = 18$ associated with $M = 6$ and $N = 6$, respectively. From the

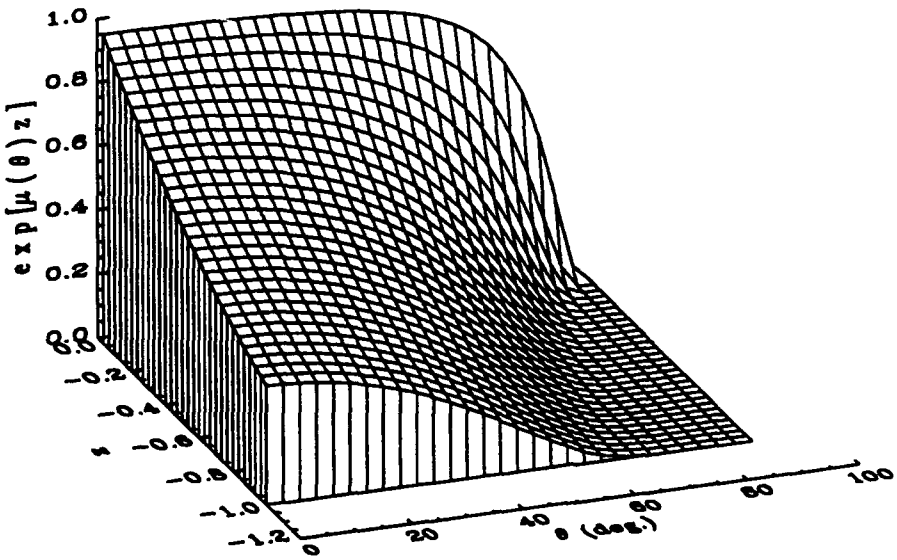

Figure 6.2: Kernel function $e^{s(\theta)z}$ with $F_n = 0.32$ and $\frac{H}{L} = 0.10$.

figure, it can be seen that the last elements of the diagonal matrices are close to zero and their reciprocal approaches a very large number, especially for the matrices with larger dimensions. The condition numbers are calculated as 7.642×10^4 and 6.333×10^4 corresponding to $\mathbf{W}_R$ and $\mathbf{W}_I$, respectively, for $M = 4$ and $N = 3$, and 1.018×10^{16} and 3.084×10^{17} corresponding to $\mathbf{W}_R$ and $\mathbf{W}_I$, respectively, for $M = 6$ and $N = 6$. Thus, the matrices in the latter case are considered to be ill-conditioned. The reason that the matrices become ill-conditioned for the large number of basis functions is that the number of rows K in the matrices $\mathbf{W}_R$ and $\mathbf{W}_I$ increase as M and N increase since there must be $K \geq \frac{M}{2}N$ for even M or $K \geq \frac{M+1}{2}N$ for odd M to avoid an underdetermined solution, but one row's elements are not very different from another row's as the number of rows increases. For example, let us examine the elements of matrix $\mathbf{W}_I$ in (6.31). From (6.7), (6.9) and (6.10), the elements can

be written as

$$W_{Iijk} \triangleq W_{Iij}(\theta_k) = (-\int_{-1}^{1} \dot{\phi}_i(x) \sin[\nu(\theta_k)x]dx) \cdot (H \int_{-1}^{0} \beta_j(z) e^{\mu(\theta_k)z} dz) \qquad (6.40)$$

Note that the kernel $e^{\mu(\theta_k)z}$ in the second integral varies little with the wave angle θ, especially when θ is in $0° - 40°$, as shown in Figure 6.2. It is the smoothness of the kernel that makes the rows of the matrix (6.31) become almost linear dependent. From the viewpoint of matrix theory, the rank of the matrix is decreased. Therefore, an increase in the number basis functions does not improve, but may worsen the ill-condition of the inverse problem. To avoid an ill-conditioned problem, the number of basis functions should be reasonable, although a good approximation for the function of the solution may be achieved for a large number of basis functions.

The condition numbers N_c of the kernel matrices $\mathbf{W}_R$ and $\mathbf{W}_I$ depend on the ratio H/L and the Froude number F_n since their elements depend on ν and μ, which are related to H/L and the Froude number F_n, as seen above. Figure 6.3 shows the relations between N_c and H/L and between N_c and F_n for the given numbers of basis functions $M = 4$ and $N = 3$. The values of θ are evenly-spaced in the range $[5°, 80°]$, and $K = 135$. From the figure, the curves of N_c versus H/L are flat; N_c's have smaller values when H/L is larger than 0.08 or when F_n ranges from 0.2 to 0.5. These areas with lower condition numbers are typical in real situations.

6.3.2 Effects of Data Noise

In practical problems, the amplitude function $A(\theta) = A_R(\theta) + \mathrm{j}A_R(\theta)$ is obtained from direct or indirect measurements; thus there must be some systematic or random noise or errors associated with them and these errors further cause errors in the solution $\mathbf{c}$ and $\mathbf{d}$ of (6.24) and (6.25). The solution $\mathbf{c}$ and $\mathbf{d}$ will be considered unstable if the errors in them are unacceptably large. In addition, note that all the

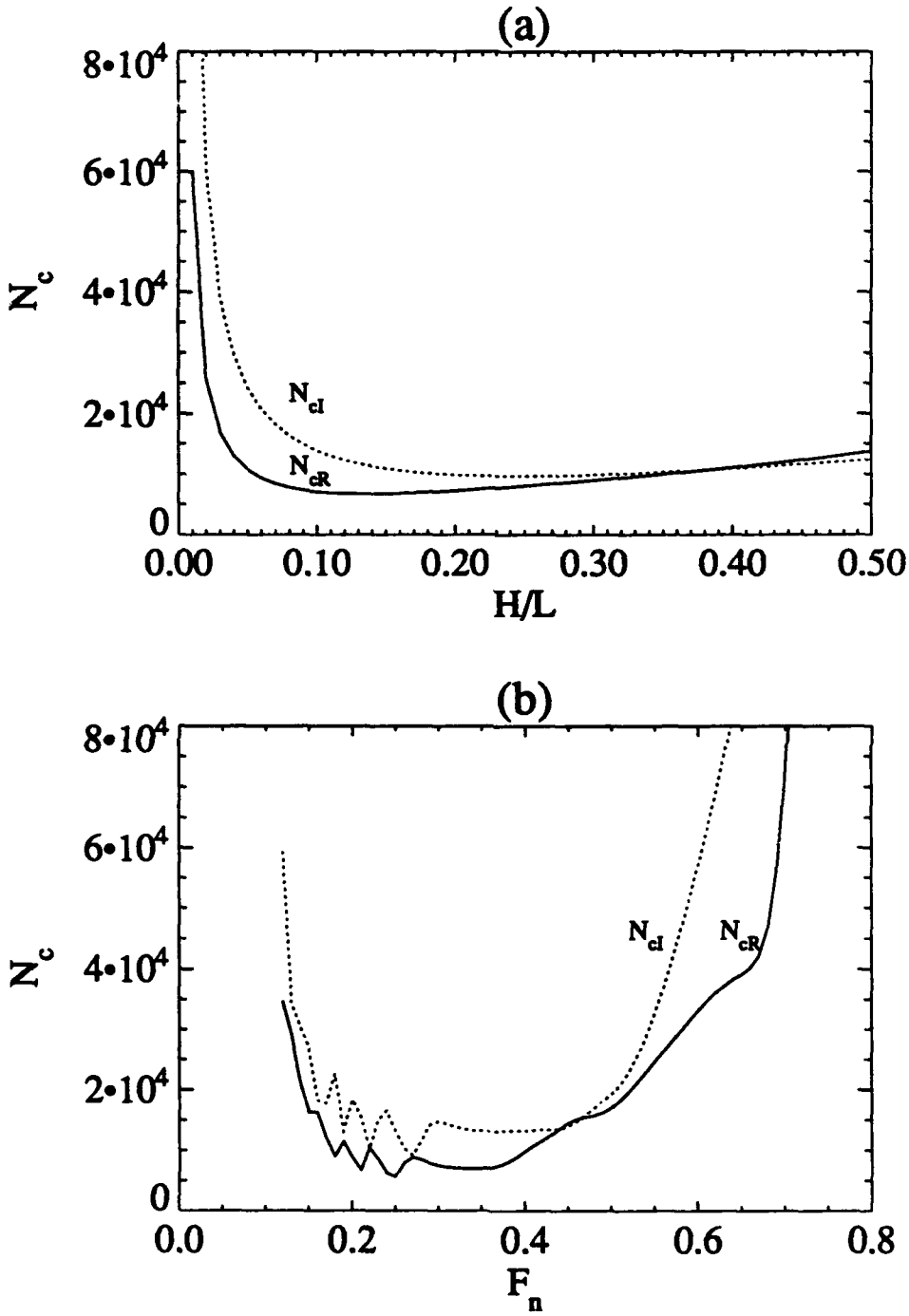

Figure 6.3: Relations (a) between N_c and H/L and (b) between N_c and F_n with $M = 4$, $N = 3$ and $K = 135$.

elements of the matrices $\mathbf{W}_R$ and $\mathbf{W}_I$ are calculated from the integrals (6.8)-(6.10) which contain the parameters of the ship's length L and draft H. The errors of these two parameters will cause errors in the matrices, and finally increase the errors in the solution. This subsection will focus on the error analysis of the solution $\mathbf{c}$ and $\mathbf{d}$.

First, measured or observed data are expressed into their true values plus noise. It is assumed that the noise on the measured data $A_R(\theta_k)$ and $A_I(\theta_k)$ is additive noise, thus, $A_R(\theta_k)$ and $A_I(\theta_k)$ with noise, denoted as $\hat{A}_R(\theta_k)$ and $\hat{A}_I(\theta_k)$, can be expressed as sums of the true values, $A_R(\theta_k)$ and $A_I(\theta_k)$, and noise $\Delta A_R(\theta_k)$ and $\Delta A_I(\theta_k)$:

$$\begin{aligned} \hat{A}_R(\theta_k) &= A_R(\theta_k) + \Delta A_R(\theta_k) \\ \hat{A}_I(\theta_k) &= A_I(\theta_k) + \Delta A_I(\theta_k) \quad . \end{aligned}$$

When noise is present, the vector forms of (6.26) and (6.27) become

$$\hat{\mathbf{a}}_R = \mathbf{a}_R + \Delta \mathbf{a}_R \tag{6.41}$$

$$\hat{\mathbf{a}}_I = \mathbf{a}_I + \Delta \mathbf{a}_I \quad . \tag{6.42}$$

Let ΔL and ΔH be the errors in the estimation of the ship's length L and draft H. It can be proved that ΔL and ΔH will cause errors $\Delta \mathbf{W}_R$ and $\Delta \mathbf{W}_I$ in the matrices $\mathbf{W}_R$ and $\mathbf{W}_I$, and the matrices with errors can be expressed as

$$\hat{\mathbf{W}}_R = \mathbf{W}_R + \Delta \mathbf{W}_R \tag{6.43}$$

$$\hat{\mathbf{W}}_I = \mathbf{W}_I + \Delta \mathbf{W}_I \quad . \tag{6.44}$$

For the case where noise or errors are present, (6.24) and (6.25) now become

$$\hat{\mathbf{a}}_R = \hat{\mathbf{W}}_R \hat{\mathbf{c}} \tag{6.45}$$

$$\hat{\mathbf{a}}_I = \hat{\mathbf{W}}_I \hat{\mathbf{d}} \quad . \tag{6.46}$$

where the unknowns $\hat{\mathbf{c}}$ and $\hat{\mathbf{d}}$ are also written into two parts, their true values and errors, i.e., $\hat{\mathbf{c}} = \mathbf{c} + \Delta\mathbf{c}$, and $\hat{\mathbf{d}} = \mathbf{d} + \Delta\mathbf{d}$. Substitution of (6.41) $\sim$ (6.44) into (6.45) and (6.46) yields two expressions

$$\Delta\mathbf{c} = \hat{\mathbf{W}}_R^{-1}\left[\Delta\mathbf{a}_R - \Delta\mathbf{W}_R\,\mathbf{c}\right] \tag{6.47}$$

$$\Delta\mathbf{d} = \hat{\mathbf{W}}_I^{-1}\left[\Delta\mathbf{a}_I - \Delta\mathbf{W}_I\,\mathbf{d}\right] \ . \tag{6.48}$$

Equations (6.47) and (6.48) show that the errors of the solution of (6.45) and (6.46), $\Delta\mathbf{c}$ and $\Delta\mathbf{d}$, depend not only directly on the errors of $\mathbf{a}_R$, $\mathbf{a}_I$, $\mathbf{W}_R$ and $\mathbf{W}_I$, but also on the properties of the inverse of the matrices $\mathbf{W}_R$ and $\mathbf{W}_I$. When the matrices are singular or ill-conditioned, the error in the solution will be very large even for a very very small error in the data $\mathbf{a}_R$, $\mathbf{a}_I$, L and H.

6.4 Constrained Linear Inversion

For ill-conditioned linear problems, neither the direct inversion nor the conventional least square methods work well [46]. A more powerful method to treat this kind of problem is the method of constrained linear inversion (CLI), as presented in [46]. Before discussing how to apply this method to the ship hull inversion problem, the concept of CLI is briefly stated below.

For a general one dimensional continuous inverse problem,

$$y(\theta) = \int_a^b K_e(\theta,\alpha)x(\alpha)d\alpha \tag{6.49}$$

its discrete form is written as

$$\mathbf{y} = \mathbf{K}_e\mathbf{x} \tag{6.50}$$

where $\mathbf{K}_e$ is the kernel matrix with dimensions $m \times n$, $\mathbf{y} = [y_1, y_2, ...y_m]$ is m measurements of $y(\theta)$, and $\mathbf{x} = [x_1, x_2, ...x_n]$ is the n discrete values of the desired function $x(\alpha)$.

To solve the problem, a non-negative scalar measure, $q(\mathbf{x})$, of the deviations from smoothness in $\mathbf{x}$ is introduced. If $\mathbf{x}$ is varied until $q(\mathbf{x})$ becomes minimal, the resulting $\mathbf{x}$ may be completely smooth in the sense that $q(\mathbf{x})$ will be zero. Most measures of non-smoothness are simple quadratic combinations of x_i. For example, $q = \sum_{i=1}^{n-1}(x_{i+1} - x_i)^2$ is the sum of the squares of the first differences, $q = \sum_{i=1}^{n-2}(-x_{i+2} + 2x_{i+1} - x_i)^2$ is the sum of the squares of the second differences, and $q = \sum_{i=1}^{n-3}(x_{i+3} - 3x_{i+2} + 3x_{i+1} - x_i)^2$ is the sum of the squares of the third differences. These summations can be written as a form $\mathbf{x}^T\mathbf{H}\mathbf{x}$, and their corresponding matrices $\mathbf{H}$ are given in [46] (pp. 124-127). According to the simulations in hull inverse problems, the measures of smoothness based on third differences are very effective in reducing the effects of singularities and noise.

The constrained linear inversion solution is obtained by minimizing $(\mathbf{K}_e\mathbf{x} - \mathbf{y})^T(\mathbf{K}_e\mathbf{x} - \mathbf{y})$ with a constraint of $q = \mathbf{x}^T\mathbf{H}\mathbf{x}$, and it can be written as

$$\mathbf{x} = (\mathbf{K}_e^T\mathbf{K}_e + \gamma\mathbf{H})^{-1}\mathbf{K}_e^T\mathbf{y} \tag{6.51}$$

where γ is a constraining parameter. Obviously, $\gamma = 0$ leads to a conventional least square solution. In a broad sense, thus, CLI can be counted as a least square method using constraints. The most appropriate value of γ can be determined by computing the residual $|\mathbf{K}_e\mathbf{x} - \mathbf{y}|$. If the residual is appreciably larger than the overall error in $\mathbf{y}$, then γ is too large, and the solution has been over constrained; if the residual is smaller than the estimated error in $\mathbf{y}$, the solution has been underconstrained.

Returning to the ship hull problem described in (6.24) and (6.25), we note that the vectors to be determined, $\mathbf{c}$ and $\mathbf{d}$, are the coefficients of the summation of basis functions instead of the hull surface itself. Thus, one possible method is to select the constraints directly based on $\mathbf{c}$ and $\mathbf{d}$. In many situations, however, these constraints may not be easy to select for lack of a priori information about the vectors $\mathbf{c}$ and

d. Usually, few properties of the coefficients are known in advance unlike the hull surface function they represent. For this reason, the smoothness measure can be selected based on the hull surface function $\zeta(x, z)$, which is usually smooth. To tell these two kinds of smoothness constraints apart, the constraints based on coefficient vectors are called the coefficient constraints and their quantity is expressed as q_c; the constraints based on hull surfaces are called the surface constraints and their quantity is expressed as q_s.

For the surface constraints, the constrained quantity q_s can be constituted from each area element of a hull surface or from each cut line on the hull surface. In the following, suppose for simplicity that q is constituted from the measure of smoothness of N_x cut lines on a hull surface along the x-direction, and that each line has N_x points. By letting $\zeta_{ij} \triangleq \zeta(x_i, z_j)$, $\mathbf{h}_{eij} \triangleq \mathbf{h}_e(x_i, y_j)$ and $\mathbf{h}_{oij} \triangleq \mathbf{h}_o(x_i, y_j)$, the discrete form of (6.32) becomes

$$\zeta_{ij} = \mathbf{h}_{eij}^T \mathbf{c} + \mathbf{h}_{oij}^T \mathbf{d} \tag{6.52}$$

and the values on the j th line of the hull surface can be expressed as a vector

$$\begin{aligned} \mathbf{z}_j &\triangleq [\zeta_{1j}\ \zeta_{2j} \dots \zeta_{N_x j}]^T \\ &= \mathbf{\Psi}_{ej}\mathbf{c} + \mathbf{\Psi}_{oj}\mathbf{d} \end{aligned} \tag{6.53}$$

where matrices $\mathbf{\Psi}_{ej}$ and $\mathbf{\Psi}_{oj}$ have dimension $N_x \times L_1$ and $N_x \times L_2$, respectively, and are defined as

$$\mathbf{\Psi}_{ej} \triangleq [\mathbf{h}_{e1j}\ \mathbf{h}_{e2j} \dots \mathbf{h}_{eN_x j}]^T \tag{6.54}$$

$$\mathbf{\Psi}_{ej} \triangleq [\mathbf{h}_{e1j}\ \mathbf{h}_{e2j} \dots \mathbf{h}_{eN_x j}]^T \ . \tag{6.55}$$

With these definitions, the smoothness measure for the j th line is

$$q_{sj}(\mathbf{c}, \mathbf{d}) = \mathbf{z}_j^T \mathbf{H} \mathbf{z}_j$$

$$= \mathbf{c}^T\mathbf{H}_{aj}\mathbf{d} + \mathbf{d}^T\mathbf{H}_{bj}\mathbf{c} + \mathbf{c}^T\mathbf{H}_{cj}\mathbf{c} + \mathbf{d}^T\mathbf{H}_{dj}\mathbf{d} \tag{6.56}$$

where

$$\begin{aligned}
\mathbf{H}_{aj} &\triangleq \mathbf{\Psi}_{ej}^T\mathbf{H}\mathbf{\Psi}_{oj} \\
\mathbf{H}_{bj} &\triangleq \mathbf{\Psi}_{oj}^T\mathbf{H}\mathbf{\Psi}_{ej} \\
\mathbf{H}_{cj} &\triangleq \mathbf{\Psi}_{ej}^T\mathbf{H}\mathbf{\Psi}_{ej} \\
\mathbf{H}_{dj} &\triangleq \mathbf{\Psi}_{oj}^T\mathbf{H}\mathbf{\Psi}_{oj} \ .
\end{aligned}$$

Thus, the total smoothness measure is given as

$$\begin{aligned}
q_s(\mathbf{c},\mathbf{d}) &= \sum_{j=1}^{N_s} q_{sj}(\mathbf{c},\mathbf{d}) \\
&= \mathbf{c}^T\mathbf{H}_a\mathbf{d} + \mathbf{d}^T\mathbf{H}_b\mathbf{c} + \mathbf{c}^T\mathbf{H}_c\mathbf{c} + \mathbf{d}^T\mathbf{H}_d\mathbf{d}
\end{aligned} \tag{6.57}$$

where

$$\begin{aligned}
\mathbf{H}_a &= \sum_{j=1}^{N_s}\mathbf{H}_{aj} \\
\mathbf{H}_b &= \sum_{j=1}^{N_s}\mathbf{H}_{bj} \\
\mathbf{H}_c &= \sum_{j=1}^{N_s}\mathbf{H}_{cj} \\
\mathbf{H}_d &= \sum_{j=1}^{N_s}\mathbf{H}_{dj} \ .
\end{aligned}$$

In general, $\mathbf{H} = \mathbf{H}^T$, thus $\mathbf{H}_{aj} = \mathbf{H}_{bj}^T$ and $\mathbf{H}_a = \mathbf{H}_b^T$. Therefore, if $\mathbf{H} = \mathbf{H}^T$, then

$$q_s(\mathbf{c},\mathbf{d}) = 2\mathbf{c}^T\mathbf{H}_a\mathbf{d} + \mathbf{c}^T\mathbf{H}_c\mathbf{c} + \mathbf{d}^T\mathbf{H}_d\mathbf{d} \ . \tag{6.58}$$

Having arrived at an expression for q_s, the constrained linear inverse problem of the ship hull can be described as

$$\begin{aligned}
&\textit{minimize}: && (\mathbf{W}_R\mathbf{c} - \mathbf{a}_R)^T(\mathbf{W}_R\mathbf{c} - \mathbf{a}_R) + (\mathbf{W}_R\mathbf{d} - \mathbf{a}_I)^T(\mathbf{W}_R\mathbf{d} - \mathbf{a}_I) \\
&\textit{holding constant}: && q_s(\mathbf{c},\mathbf{d})
\end{aligned}$$

The solution can be obtained using the Lagrangian multiplier method from

$$\begin{aligned} Q(\mathbf{c},\mathbf{d}) &= (\mathbf{W}_R\mathbf{c}-\mathbf{a}_R)^T(\mathbf{W}_R\mathbf{c}-\mathbf{a}_R)+(\mathbf{W}_R\mathbf{d}-\mathbf{a}_I)^T(\mathbf{W}_R\mathbf{d}-\mathbf{a}_I) \\ &\quad +\gamma q_s(\mathbf{c},\mathbf{d})\,. \end{aligned} \tag{6.59}$$

By the rules of matrix calculus, taking $\frac{\partial Q(\mathbf{c},\mathbf{d})}{\partial \mathbf{c}}=\mathbf{0}$ and $\frac{\partial Q(\mathbf{c},\mathbf{d})}{\partial \mathbf{d}}=\mathbf{0}$ yields

$$\begin{bmatrix} \mathbf{W}_R^T\mathbf{W}_R+\gamma\mathbf{H}_c & \gamma\mathbf{H}_a \\ \gamma\mathbf{H}_a & \mathbf{W}_I^T\mathbf{W}_I+\gamma\mathbf{H}_d \end{bmatrix}\begin{bmatrix} \mathbf{c} \\ \mathbf{d} \end{bmatrix}=\begin{bmatrix} \mathbf{W}_R^T\mathbf{a}_R \\ \mathbf{W}_I^T\mathbf{a}_I \end{bmatrix}\,. \tag{6.60}$$

For a ship hull symmetric in its longitudinal distribution of volume, $\mathbf{c}=\mathbf{0}$ and $\mathbf{a}_R=\mathbf{0}$, and thus (6.60) becomes

$$(\mathbf{W}_I^T\mathbf{W}_I+\gamma\mathbf{H}_d)\,\mathbf{d}=\mathbf{W}_I^T\mathbf{a}_I\,. \tag{6.61}$$

In many real situations, the surface constraint method may be used together with the coefficient constraint method to solve the linear inverse problem. For example, the coefficient constraint method is used to solve (6.60) or (6.61) instead of using the direct inverse method.

6.5 Application of Bayes Theorem to Inverse Problems

In inverse problems, the observation data contain random noise because they come from direct or indirect measurements, and thus it is reasonable to consider the data as random variables. In some cases, the parameters to be predicted from the observation data are also random variables. Hence, we wish to apply the statistic estimation theory to inverse problems to obtain an optimum estimation with regard to some criterion.

Now, consider a general problem

$$\mathbf{y}=\mathbf{f}(\mathbf{x}) \tag{6.62}$$

where $\mathbf{y}$ is a vector representing the observed or measured data, and $\mathbf{f}(\mathbf{x})$ is a vector depending on the vector $\mathbf{x}$, which is to be estimated from $\mathbf{y}$. It is assumed that the functional relation $\mathbf{f}$ is known and that $\mathbf{y}$ and $\mathbf{x}$ are random vectors. If $\hat{\mathbf{x}}$ denotes an estimate of $\mathbf{x}$ based on the observation vector $\mathbf{y}$, then the estimation error is defined as

$$\epsilon(\mathbf{y}) = \hat{\mathbf{x}}(\mathbf{y}) - \mathbf{x} \tag{6.63}$$

In the Bayes estimation theory, a scale function of $\mathbf{x}$ and $\hat{\mathbf{x}}$, called the cost function, is defined, and in many cases it is assumed to depend only on the error of estimate ϵ. For example, one cost function which is used frequently represents the sum of the square of each error component and is written as

$$C_t[\epsilon(\mathbf{y})] = \epsilon^T(\mathbf{y})\epsilon(\mathbf{y}) \tag{6.64}$$

Another cost function assigns zero cost to all errors less than $\pm\frac{\Delta}{2}$ and assigns a uniform value to all errors larger than $\pm\frac{\Delta}{2}$, that is,

$$C_t[\epsilon(\mathbf{y})] = \begin{cases} 1 & |\epsilon(\mathbf{y})| > \frac{\Delta}{2} \\ 0 & |\epsilon(\mathbf{y})| \leq \frac{\Delta}{2} \end{cases} \tag{6.65}$$

The Bayes estimation is based on the rule that on the average cost is as small as possible. That is, the Bayes estimate is the estimate that minimizes

$$E\{C_t[\epsilon(\mathbf{y})]\} = \int_{-\infty}^{\infty}\int_{-\infty}^{\infty} C_t[\epsilon(\mathbf{y})]p(\mathbf{x},\mathbf{y})d\mathbf{x}d\mathbf{y} \tag{6.66}$$

where $E(\cdot)$ denotes expectation, and $p(\mathbf{x},\mathbf{y})$ is the joint probability density function of $\mathbf{x}$ and $\mathbf{y}$.

For the above two cost functions, the estimates of $\mathbf{x}$ have been computed in [44]. The minimum mean-square error (MMSE) estimate corresponding to the cost

function in (6.64) is given as

$$\hat{\mathbf{x}}(\mathbf{y}) = E\{\mathbf{x}/\mathbf{y}\} \tag{6.67}$$

which indicates that the MMSE estimate is the conditional mean of $\mathbf{x}$ given $\mathbf{y}$. The maximum a posteriori (MAP) estimate corresponding to the cost function in (6.65) is given as the solution of

$$\frac{\partial ln\, p(\mathbf{x}/\mathbf{y})}{\partial \mathbf{x}} |_{\mathbf{x}=\hat{\mathbf{x}}} = 0 \tag{6.68}$$

or

$$\frac{\partial ln\, p(\mathbf{y}/\mathbf{x})}{\partial \mathbf{x}} |_{\mathbf{x}=\hat{\mathbf{x}}} + \frac{\partial ln\, p(\mathbf{x})}{\partial \mathbf{x}} |_{\mathbf{x}=\hat{\mathbf{x}}} = 0 \ . \tag{6.69}$$

In the MAP estimation, the estimate is the values of $\mathbf{x}$ at which the a posteriori density $p(\mathbf{x}/\mathbf{y})$ has its maximum.

In many cases of interest the MAP and MMSE estimates are equal and are optimum, in particular, for the Gaussian a posteriori density. If we know nothing about $\mathbf{x}$ other than the values of $\mathbf{y}$, then $p(\mathbf{x})$ is a constant, and an estimate $\hat{\mathbf{x}}$, called the maximum likelihood (ML) estimate, can be found from the likelihood equation:

$$\frac{\partial ln\, p(\mathbf{y}/\mathbf{x})}{\partial \mathbf{x}} |_{\mathbf{x}=\hat{\mathbf{x}}} = 0 \ . \tag{6.70}$$

The ML estimate corresponds mathematically to the limiting case of a MAP estimate in which the a priori knowledge approaches zero. In the cases where the unknown vector $\mathbf{x}$ is not a random vector, the estimate $\hat{\mathbf{x}}$ is also obtained from the ML estimation in which the likelihood function is maximum.

In our inverse problems, the unknown coefficient vector may be treat as a non-random vector; thus, the ML estimation will be applied to the ship hull problems. In the following, it is assumed that the observation vector $\mathbf{y}$ has a multivariate Gaussian

distribution. The Gaussian conditional probability distribution of $\mathbf{y}$ given $\mathbf{x}$ has the form:

$$p(\mathbf{y}/\mathbf{x}) = \frac{1}{(2\pi)^{\frac{n}{2}}|\mathbf{S}|^{\frac{1}{2}}} exp\{-\frac{1}{2}[\mathbf{y}-\mathbf{f}(\mathbf{x})]^T\mathbf{S}^{-1}[\mathbf{y}-\mathbf{f}(\mathbf{x})]\} \tag{6.71}$$

where n is the dimension of $\mathbf{y}$, and $|\mathbf{S}|$ denotes the determinant of the $n \times n$ covariance matrix $\mathbf{S}$, which is defined as

$$\mathbf{S} = E\{(\mathbf{y}-E[\mathbf{y}])(\mathbf{y}-E[\mathbf{y}])^T\} \ . \tag{6.72}$$

Substituting (6.71) into (6.70) yields

$$\frac{\partial}{\partial \mathbf{x}}(\mathbf{y}-\mathbf{f}(\mathbf{x}))^T\mathbf{S}^{-1}(\mathbf{y}-\mathbf{f}(\mathbf{x}))\ |_{\mathbf{x}=\hat{\mathbf{x}}} = \mathbf{0} \tag{6.73}$$

If a constraint $q(\mathbf{x})$ is included, then the estimate will be found by minimizing

$$Q(\mathbf{x}) = (\mathbf{y}-\mathbf{f}(\mathbf{x}))^T\mathbf{S}^{-1}(\mathbf{y}-\mathbf{f}(\mathbf{x})) + \gamma\, q(\mathbf{x}) \tag{6.74}$$

The above results will be used in the linear ship hull inverse problem described by (6.24) and (6.25) and also in the non-linear ship hull inverse problem which will be discussed in the next subsection. We introduce the following vectors and matrices for the problem given in (6.24) and (6.25):

$$\mathbf{x} \triangleq \begin{bmatrix} \mathbf{c} \\ \mathbf{d} \end{bmatrix} \qquad \mathbf{W}_a \triangleq \begin{bmatrix} \mathbf{W}_R & \\ & \mathbf{W}_I \end{bmatrix}$$

$$\mathbf{y} \triangleq \begin{bmatrix} \mathbf{a}_R \\ \mathbf{a}_I \end{bmatrix} \qquad \mathbf{H}_t \triangleq \begin{bmatrix} \mathbf{H}_c & \mathbf{H}_a \\ \mathbf{H}_a & \mathbf{H}_d \end{bmatrix} .$$

With the above definitions, the problem in (6.24) and (6.25) is described as

$$\mathbf{y} = \mathbf{f}(\mathbf{x}) = \mathbf{W}_a\mathbf{x} \tag{6.75}$$

and the constraint in (6.25) is described as

$$q(\mathbf{x}) = \mathbf{x}^T \mathbf{H}_t \mathbf{x} \,. \tag{6.76}$$

Substituting (6.75) and (6.76) into (6.74) and minimizing the resulting $Q(\mathbf{x})$ yields

$$(\mathbf{W}_a^T \mathbf{S}^{-1} \mathbf{W}_a + \gamma \mathbf{H}_t)\hat{\mathbf{x}} = \mathbf{W}_a^T \mathbf{S}^{-1} \mathbf{y} \,. \tag{6.77}$$

Finally, the estimate $\hat{\mathbf{x}}$ can be obtained by solving this equation. Specifically, when the measurement noise in the components of $\mathbf{y}$ are uncorrelated and have the same variance σ^2, the covariance matrix is given as $\mathbf{S} = \sigma^2 \mathbf{I}$, where $\mathbf{I}$ is an identity matrix, and (6.77) becomes

$$(\mathbf{W}_a^T \mathbf{W}_a + \gamma' \mathbf{H}_t)\hat{\mathbf{x}} = \mathbf{W}_a^T \mathbf{y} \tag{6.78}$$

where $\gamma' \triangleq \sigma^2 \gamma$. Equation (6.78) is the same as (6.60) except that γ in (6.60) has been replaced with γ'. This difference indicates that the choice of the constraining parameter should include the consideration of the noise variance. If large noise is involved in data, large constraining parameter γ' is required.

6.6 Non-Linear inversion

In the above linear inverse problem, it has been assumed that both the real and imaginary parts or, equivalently, both the phase and magnitude of the wave amplitude function $A(\theta)$ are well known. In real situations, however, the phase information of the wave amplitude function may not be available, and only the magnitude $|A(\theta)| = [\,A_R^2(\theta) + A_I^2(\theta)\,]^{\frac{1}{2}}$ is given. For example, the phase information may be lost or can not be recovered fully when ship wave spectra are transformed from remotely sensed images, or when wave spectra are transformed from wave height data without knowing the ship position. If the phase information is not available,

then the inverse problem becomes more complicated since it involves a non-linear problem.

The non-linear inverse problem can be derived from the previously discussed linear problem. By squaring both sides of (6.24) and (6.25) for each k ($k = 1, ..., K$) and then adding the squared values for each k together, a set of non-linear equations is obtained in the form

$$A'_m(\theta_k) = \mathbf{c}^T \mathbf{W}_{ck} \mathbf{c} + \mathbf{d}^T \mathbf{W}_{dk} \mathbf{d} \tag{6.79}$$

$$k = 1, 2, 3, \cdots, K$$

where

$$\begin{aligned} A'_m(\theta_k) &\triangleq A'^2_R(\theta_k) + A'^2_I(\theta_k) \\ \mathbf{W}_{ck} &\triangleq \mathbf{w}_{Rk} \mathbf{w}_{Rk}^T \\ \mathbf{W}_{dk} &\triangleq \mathbf{w}_{Ik} \mathbf{w}_{Ik}^T \end{aligned}$$

$$\begin{aligned} \mathbf{w}_{Rk} &\triangleq [W_{R21k}, W_{R22k}, \cdots, W_{R2Nk}, W_{R41k}, \cdots, W_{R(M'-2)Nk}, W_{RM'1k}, \cdots, W_{RM'Nk}]^T \\ \mathbf{w}_{Ik} &\triangleq [W_{I11k}, W_{I12k}, \cdots, W_{I1Nk}, W_{I31k}, \cdots, W_{I(M''-2)Nk}, W_{IM''1k}, \cdots, W_{IM''Nk}]^T \quad . \end{aligned}$$

To write the above equations in a concise form, let

$$\mathbf{a}_m \triangleq \begin{bmatrix} A'_m(\theta_1) \\ A'_m(\theta_2) \\ \vdots \\ A'_m(\theta_K) \end{bmatrix}$$

$$\mathbf{W}_{mk} \triangleq \begin{bmatrix} \mathbf{W}_{ck} & \\ & \mathbf{W}_{dk} \end{bmatrix} .$$

The problem described in (6.79) then becomes

$$\mathbf{a}_m = \mathbf{f}(\mathbf{x}) = \begin{bmatrix} \mathbf{x}^T\mathbf{W}_{m1}\mathbf{x} \\ \mathbf{x}^T\mathbf{W}_{m2}\mathbf{x} \\ \vdots \\ \mathbf{x}^T\mathbf{W}_{mk}\mathbf{x} \end{bmatrix} . \tag{6.80}$$

Equation (6.80) is a general form for the non-linear hull surface inversion. If the ship hull surface function can be written in the form of separation of variables as in (5.69), then the dimension of the vector to be solved can be reduced from $M \times N$ to $M + N$. This will result in a great reduction of computational efforts, especially for large M and N. Under the assumption of separation of variables, the hull surface function $\zeta(x, z)$ can be expressed in the form

$$\zeta(x,z) = [\sum_{i=1}^{M} a_{xi}\phi_i(x)][\sum_{j=1}^{N} a_{zj}\beta_j(z)] \tag{6.81}$$

where a_{xi} and a_{zj} are the coefficients to be determined, and $\phi_i(x)$ and $\beta_j(z)$ are the basis functions. Substitution of (6.81) into (6.1) gives the equations

$$A_R'(\theta) = [\sum_{i=1}^{M} a_{xi}\, W_{XRi}(\theta)][\sum_{j=1}^{N} a_{zj}\, W_{Zj}(\theta)] \tag{6.82}$$

$$A_I'(\theta) = [\sum_{i=1}^{M} a_{xi}\, W_{XIi}(\theta)][\sum_{j=1}^{N} a_{zj}\, W_{Zj}(\theta)] \tag{6.83}$$

where W_{XRi}, W_{XIi} and W_{Zj} have been defined in (6.8)-(6.10). For K values of θ, there is a set of equations

$$A_R'(\theta_k) = (\mathbf{x}_1^T\, \mathbf{w}_{XRk})(\mathbf{x}_2^T\mathbf{w}_{Zk}) \tag{6.84}$$

$$A_I'(\theta_k) = (\mathbf{x}_1^T\, \mathbf{w}_{XIk})(\mathbf{x}_2^T\mathbf{w}_{Zk}) \tag{6.85}$$

$$k = 1, 2, \cdots, K$$

where

$$\mathbf{x}_1^T \triangleq [a_{x1}, a_{x2}, \ldots a_{xM}]$$

$$
\begin{aligned}
\mathbf{x}_2^T &\triangleq [a_{z1}, a_{z2}, \ldots a_{zN}] \\
\mathbf{w}_{XRk} &\triangleq [W_{XR1}(\theta_k), W_{XR2}(\theta_k), \ldots, W_{XRM}(\theta_k)]^T \\
\mathbf{w}_{XIk} &\triangleq [W_{XI1}(\theta_k), W_{XI2}(\theta_k), \ldots, W_{XIM}(\theta_k)]^T \\
\mathbf{w}_{Zk} &\triangleq [W_{Z1}(\theta_k), W_{Z2}(\theta_k), \ldots, W_{ZN}(\theta_k)]^T \quad .
\end{aligned} \tag{6.86}
$$

By squaring both sides of (6.84) and (6.85) for each k ($k = 1, \ldots, K$) and then adding the squared values for each k together, a vector form of the non-linear equations is obtained in the form

$$
\mathbf{a}_m = \mathbf{f}(\mathbf{x}) = \begin{bmatrix} \mathbf{x}_1^T \mathbf{W}_{X1} \mathbf{x}_1 \mathbf{x}_2^T \mathbf{W}_{Z1} \mathbf{x}_2 \\ \mathbf{x}_1^T \mathbf{W}_{X2} \mathbf{x}_1 \mathbf{x}_2^T \mathbf{W}_{Z2} \mathbf{x}_2 \\ \vdots \\ \mathbf{x}_1^T \mathbf{W}_{XK} \mathbf{x}_1 \mathbf{x}_2^T \mathbf{W}_{ZK} \mathbf{x}_2 \end{bmatrix} \quad . \tag{6.87}
$$

where $\mathbf{W}_{Xk}$ is an $M \times M$ matrix given as

$$
\mathbf{W}_{Xk} \triangleq \mathbf{w}_{XRk} \mathbf{w}_{XRk}^T + \mathbf{w}_{XIk} \mathbf{w}_{XIk}^T
$$

and $\mathbf{W}_{Zk}$ is an $N \times N$ matrix given as

$$
\mathbf{W}_{Zk} \triangleq \mathbf{w}_{Zk} \mathbf{w}_{Zk}^T \quad .
$$

The vector equation in (6.87) can be also written in the form

$$
\mathbf{a}_m = \mathbf{f}(\mathbf{x}) = \begin{bmatrix} \mathbf{x}^T \mathbf{W}_{a1} \mathbf{x} \mathbf{x}^T \mathbf{W}_{b1} \mathbf{x} \\ \mathbf{x}^T \mathbf{W}_{a2} \mathbf{x} \mathbf{x}^T \mathbf{W}_{b2} \mathbf{x} \\ \vdots \\ \mathbf{x}^T \mathbf{W}_{aK} \mathbf{x} \mathbf{x}^T \mathbf{W}_{bK} \mathbf{x} \end{bmatrix} \quad . \tag{6.88}
$$

where

$$
\mathbf{W}_{ak} \triangleq \begin{bmatrix} \mathbf{W}_{Xk} & \mathbf{0}_{MN} \\ \mathbf{0}_{MN} & \mathbf{0}_{NN} \end{bmatrix}
$$

and

$$\mathbf{W}_{bk} \triangleq \begin{bmatrix} \mathbf{0}_{MM} & \mathbf{0}_{MN} \\ \mathbf{0}_{MN} & \mathbf{W}_{Zk} \end{bmatrix} .$$

In the above equations, the subscripts of $\mathbf{0}$ denote the dimension of the null matrices.

So far, we have established the non-linear equations for hull surface inversion; the next step we need to do is to solve the equations to obtain $\mathbf{x}$. Using the method of ML with a constraint $q(\mathbf{x})$, the estimate $\hat{\mathbf{x}}$ can be found by solving the following extremum problem:

$$\begin{aligned} &\textit{minimize}: && (\mathbf{a}_m - \mathbf{f}(\mathbf{x}))^T \mathbf{S}^{-1} (\mathbf{a}_m - \mathbf{f}(\mathbf{x})) \\ &\textit{holding constant}: && q(\mathbf{x}) \ . \end{aligned} \tag{6.89}$$

To solve this extremum problem, several methods of non-linear optimization can be used.

Before we give examples of ship hull estimations, it is worth to have some discussions about the issue of uniqueness. Like many other inverse problems, the uniqueness problem arises in the inversion of a ship's hull shape, that is, whether or not a hull form can be uniquely determined form a free wave spectrum. We may see this problem from two aspects, that is, from physical and mathematical aspects.

In physics, the question is whether different hull shapes have their respective wave patterns. According to Newman's study on this problem [9], there is one and only one equivalent source distribution for a given wave system; however, different physical source distributions can be related to the same equivalent source distribution, different vessels can be responsible for the same wave system, and hence, in general, non-uniqueness exists in the hull inversion. In mathematical processing, the uniqueness problem may also arises even if an original inverse problem is unique.

For example, the non-linear inversion of hull shapes described above may have multiple solutions due to the non-linear operations; thus it is more complicated than the above linear inverse problem of hull shapes.

Because of the above reasons, we must apply proper constraints on hull form to improve problem conditioning. Such constraints may facilitate a unique relation between a free wave spectrum and a hull form [8]. Although we have no idea about a hull's exact shape before we do the inversion for it, we may have some useful knowledge about man-made ship hulls and use it as constraints. For example, hull surface smoothness constraints, closure type constraints and volume constraints are useful in hull inversion. In the following simulations, the hull surface smoothness constraint, especially the third difference smoothness constraint, is used.

6.7 Examples of Ship Hull Estimations

The previous sections have discussed the problems of a ship hull's linear and non-linear inversion and the methods to solve them. This section evaluates the hull model given in (6.32), and gives the simulation results of mathematically well defined hulls and the Quapaw hull.

To evaluate the error performance of the estimated hull surface $\hat{\zeta}(x,z)$, we consider the absolute error $\epsilon_a \triangleq |\hat{\zeta}_{ij} - \zeta_{ij}|$, the relative error $\epsilon_r \triangleq |\hat{\zeta}_{ij} - \zeta_{ij}|/|\zeta_{ij}|$, and the relative overall r.m.s. residual error which is defined as

$$\epsilon_{ro} \triangleq \sqrt{\frac{\int\int[\hat{\zeta}(x,z) - \zeta(x,z)]^2 dx\, dz}{\int\int \zeta^2(x,z) dx\, dz}} \tag{6.90}$$

or, in the discrete form, as

$$\epsilon_{ro} \triangleq \sqrt{\frac{\sum_{i,j}(\hat{\zeta}_{ij} - \zeta_{ij})^2}{\sum_{i,j}\zeta_{ij}^2}} \ . \tag{6.91}$$

There is some difficulty in using the relative error ϵ_r to evaluate the performance on

the edges of the hull surface because the true values on the edges approach zero. The relative overall r.m.s. residual error can be envisaged as the ratio of the volume of the error to the volume of the hull.

In addition to the above criterion on hull surface error performance, we may also consider the residual error due to the inversion operation:

$$\epsilon_{res} \triangleq (\mathbf{a}_R - \mathbf{W}_R\,\hat{\mathbf{c}})^T(\mathbf{a}_R - \mathbf{W}_R\,\hat{\mathbf{c}}) + (\mathbf{a}_I - \mathbf{W}_I\,\hat{\mathbf{d}})^T(\mathbf{a}_I - \mathbf{W}_I\,\hat{\mathbf{d}}) \ . \qquad (6.92)$$

Note that a large error of ϵ_{res} results in a large error of ϵ_{ra}. However, even a very small error of ϵ_{res} never guarantees a small error of ϵ_{ra}, that is, ϵ_{ra} may be very large even for a very small ϵ_{res}.

6.7.1 Evaluation of Hull Surface Models

Before giving the simulation results, we first evaluate the performance of the hull surface model. The basis functions selected from (6.17) and (6.20) consist of only polynomials; thus the hulls defined with polynomials can be exactly expressed when the numbers of basis functions are sufficiently large. So, we do not consider these types of hulls here, but the Wigley-Cosine hull and the Quapaw hull.

For the evaluation of a hull surface model, the model vector is calculated from (6.32) using the least square method given the values of $\zeta(x,z)$, then the resulting model vector $\mathbf{x}_m = [\mathbf{c}_m\ \mathbf{d}_m]^T$ is used to evaluate the hull surface values, $\hat{\zeta}_m(x,z) = \mathbf{h}_o^T(x,z)\hat{\mathbf{c}}_m + \mathbf{h}_e^T(x,z)\hat{\mathbf{d}}_m$.

The Wigley-Cosine hull has length $L = 100$ meters, draft $H = 10$ meters and width $B = 10$ meters. Table 6.1 lists the values of the relative overall r.m.s. residual error ϵ_{ro} for different numbers of basis functions. The relative overall r.m.s. residual error ϵ_{ro} versus the number of basis functions N is shown in Figure 6.4, assuming that the numbers of basis functions in the x- and z-directions are equal, i.e., $M = N$.

$\epsilon_{ro}(\%)$	N=1	2	3	4	5	6	7	8	9	10
M = 1	48.82	21.95	18.14	18.14	18.14	18.14	18.14	18.14	18.14	18.14
M = 2	47.18	16.88	11.37	11.37	11.37	11.37	11.37	11.37	11.37	11.37
M = 3	46.23	13.16	3.96	3.96	3.96	3.96	3.96	3.96	3.96	3.96
M = 4	46.12	12.66	1.61	1.61	1.61	1.61	1.61	1.61	1.61	1.61
M = 5	46.11	12.63	1.33	1.33	1.33	1.33	1.33	1.33	1.33	1.33
M = 6	46.10	12.57	0.51	0.51	0.51	0.51	0.51	0.51	0.51	0.51
M = 7	46.10	12.57	0.51	0.51	0.51	0.51	0.51	0.51	0.51	0.51
M = 8	46.09	12.56	0.26	0.26	0.26	0.26	0.26	0.26	0.26	0.26
M = 9	46.09	12.56	0.26	0.26	0.26	0.26	0.26	0.26	0.26	0.26
M =10	46.09	12.56	0.15	0.15	0.15	0.15	0.15	0.15	0.15	0.15

Table 6.1: The Wigley-Cosine hull's relative overall r.m.s. residual error ϵ_{ro} in the hull approximation using $M \times N$ basis functions.

$\epsilon_{ro}(\%)$	N=1	2	3	4	5	6	7	8	9	10
M = 1	45.62	26.16	21.77	20.67	20.50	20.50	20.40	20.28	20.22	20.21
M = 2	44.46	22.58	17.16	15.34	14.62	14.41	14.32	14.31	14.24	14.23
M = 3	44.33	20.68	11.87	8.99	7.77	7.26	7.02	6.82	6.69	6.63
M = 4	44.32	20.57	11.04	7.89	6.42	5.75	5.44	5.33	5.23	5.13
M = 5	44.21	20.35	10.58	6.85	5.02	4.07	3.61	3.37	3.28	3.17
M = 6	44.15	20.20	10.32	6.27	4.20	2.99	2.33	1.99	1.85	1.69
M = 7	44.14	20.20	10.29	6.25	4.06	2.78	2.04	1.67	1.45	1.40
M = 8	44.13	20.19	10.28	6.24	3.99	2.67	1.89	1.50	1.25	1.19
M = 9	44.13	20.19	10.27	6.22	3.97	2.61	1.81	1.38	1.16	1.05
M =10	44.11	20.16	10.24	6.17	3.91	2.51	1.66	1.17	0.91	0.78

Table 6.2: The Quapaw's relative overall r.m.s. residual error ϵ_{ro} in the hull approximation using $M \times N$ basis functions.

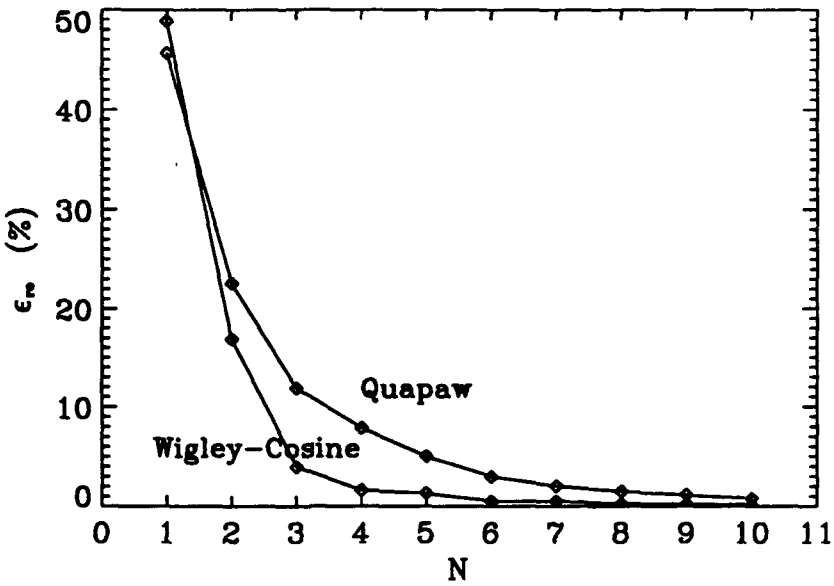

Figure 6.4: The relative overall r.m.s. residual error ϵ_{ro} of the Wigley-Cosine hull and the Quapaw model in the hull approximation using $N \times N$ basis functions.

The Quapaw hull has length $L = 4.953$ meters, draft $H = 0.362$ meters and width $B = 0.978$ meters. Table 6.2 lists the values of the relative overall r.m.s. residual error ϵ_{ro} for different numbers of basis functions. The curve of ϵ_{ro} versus N with the condition of $M = N$ is also plotted in Figure 6.4.

From the above analysis, the hulls can be approximately very well for the sufficiently large numbers of the basis functions. For example, ϵ_{ro} can be less than 3.0% for $M = N = 6$, and less than 1.0% for $M = N = 10$. In actual situations, the noise in the wave amplitude function may result in larger error in the recovered hull surface than this caused by the model approximation.

6.7.2 Estimation of Hull Shape from the Wave Amplitude Function

It is assumed in this subsection that both the real and imaginary parts of the wave amplitude function are fully available. Thus, the model vectors $\mathbf{c}$ and $\mathbf{d}$ are estimated from the linear inversion.

In the following, we consider first a hull defined with polynomials:

$$\zeta(x,z) = \frac{B}{2}(1 - x - x^2 + x^3)(1 - z^2) \qquad x \in [-1,1], z \in [-1,0] \tag{6.93}$$

which is more typical than Wigley's parabolic hull. This hull is not symmetrical in the longitudinal direction, and thus its wave amplitude function contains both real and imaginary parts.

In the simulation, the values of the wave amplitude function $A(\theta)$ are calculated from (5.8) with wave angles θ in $[5°, 80°]$. The basis functions are selected from(6.17) and (6.20). With the basis functions and the given ship length and draft, the kernel matrices $\mathbf{W}_R$ and $\mathbf{W}_I$ can be computed. Once the hull model vector $\mathbf{x} = [\mathbf{c}\ \mathbf{d}]^T$ is determined by solving the linear inversion problem, the hull surface values can be evaluated from (6.32), i.e., $\hat{\zeta}(x,z) = \mathbf{h}_o^T(x,z)\hat{\mathbf{c}} + \mathbf{h}_e^T(x,z)\hat{\mathbf{d}}$. In the calculations below, all the constraints are based on the measures of the sum of the squares of the third differences.

With the above procedures, simulation results can be obtained. As an example, it is assumed that the ship speed is $U = 10$ meters/second, the parameters in (6.93) are $L = 100$ meters, $H = 10$ meters, and $B = 10$ meters. The dotted line shown in Figure 6.6 is the wave amplitude function calculated from (5.8).

When the numbers of basis functions are taken as $M = 4$ and $N = 3$, the constrained ML method gives an exact solution for the containing parameters $\gamma_r = 0$ and $\gamma_s = 10^{-9}$. As the numbers of basis functions increase, the error appears in the

solution, because the kernel matrices become singular. Figure 6.5 shows the curves of ϵ_{ro} and ϵ_{res} versus γ_s when $M = 6$ and $N = 6$. It can be seen from the figure that there is a minimum value 1.0557% of ϵ_{ro} based on the calculation of 11×11 points on the hull surface, associated with a residual error $\epsilon_{res} = 7.4 \times 10^{-8}$. The estimated hull surface is plotted in Figure 6.7 together with the error surface contour plots of ϵ_a and ϵ_r.

To observe the effects of the error in the hull length and draft and the noise in the wave amplitude function on the estimation performance, a couple of assumptions are made: first that there is 10% error in the ship length and draft, that is, $\hat{L} = 110$ and $\hat{H} = 11$ meters are used in the computation of the kernel matrices; second, that there is 10% noise in the real and imaginary parts of the wave amplitude function based on the energy, that is, a 10 dB signal to noise ratio. When the noise is assumed to have a Gaussian distribution with zero mean, the standard deviation is taken as $\sigma_{nR} = \sqrt{0.1(\sigma^2_{A_R} + E[A_R]^2)}$ for the real part, and $\sigma_{nI} = \sqrt{0.1(\sigma^2_{A_I} + E[A_I]^2)}$ for the imaginary part of the wave amplitude function. The wave amplitude function with noise is shown with the solid lines in Figure 6.6. Figure 6.8 shows the estimated hull surface together with the error surface contour plots of ϵ_a and ϵ_r, given $M = N = 6$. In the calculation, both the coefficient constraint and surface constraint are used, with $\gamma_c = 10^{-1}$ and $\gamma_s = 380$. The overall error performances are given as $\epsilon_{ro} = 27.2\%$ and $\epsilon_{res} = 0.482$.

With the same parameters and conditions, we again do the simulation for the Wigley-Cosine Hull. The wave amplitude function and the simulation results are displayed in Figure 6.9 and Figure 6.10. The overall error performances are given as $\epsilon_{ro} = 32.5\%$ and $\epsilon_{res} = 0.55$, with $\gamma_c = 10^{-2}$ and $\gamma_s = 160$. Figure 6.11 shows the curves of ϵ_{ro} and ϵ_{res} verses γ_s, given $\gamma_c = 10^{-1}$ and 10^{-2}, for the modified Wigley

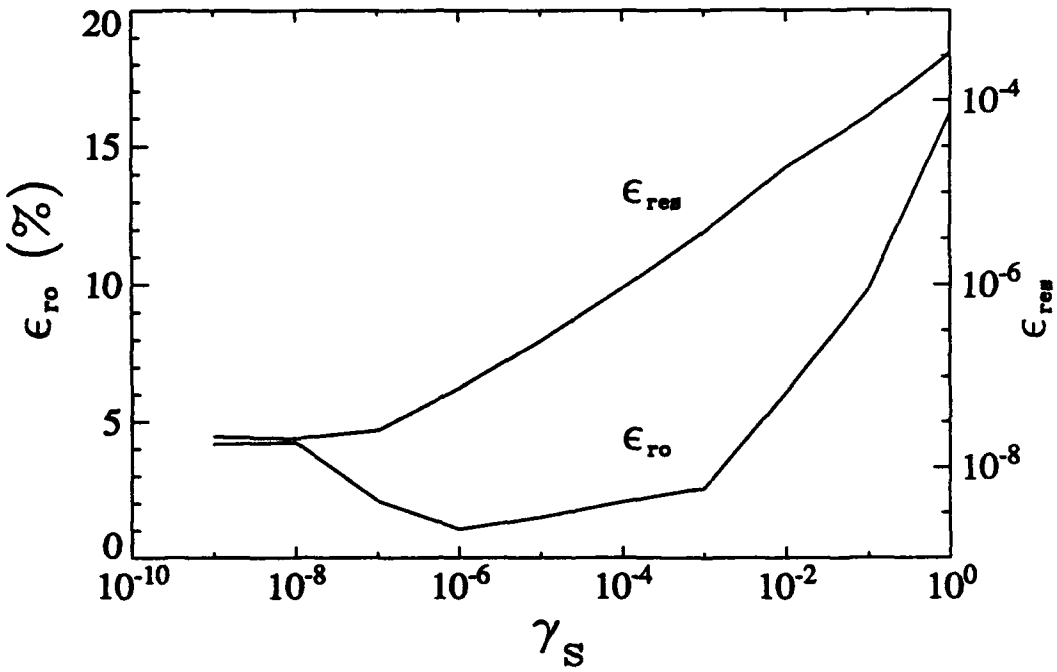

Figure 6.5: Curves of ϵ_{ro} and ϵ_{res} versus γ_s for the modified Wigley hull with $M = N = 6$. No error and noise are present in the input data.

hull described in Eq.(6.93) and the Wigley-Cosine Hull. It is found from the figure that the error of ϵ_{res} has only a small change for different γ_s with a given γ_c. However, ϵ_{ro} has obvious variations for different γ_c.

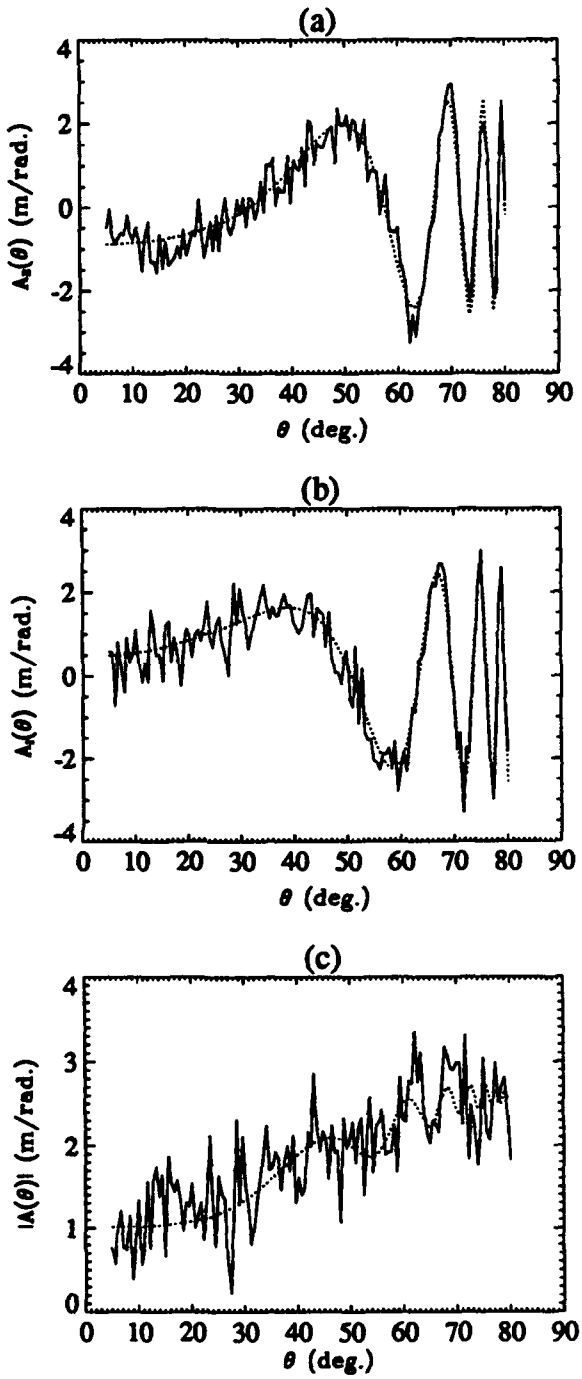

Figure 6.6: (a) the real part, (b) imaginary part, and (c) the magnitude of the wave amplitude function of the modified Wigley hull, given the parameters $L = 100$ m, $H = 10$ m, $B = 10$ m, and $U = 10$ m/s. The dotted lines represent the wave amplitude function with no noise, and solid lines the one with 10% noise.

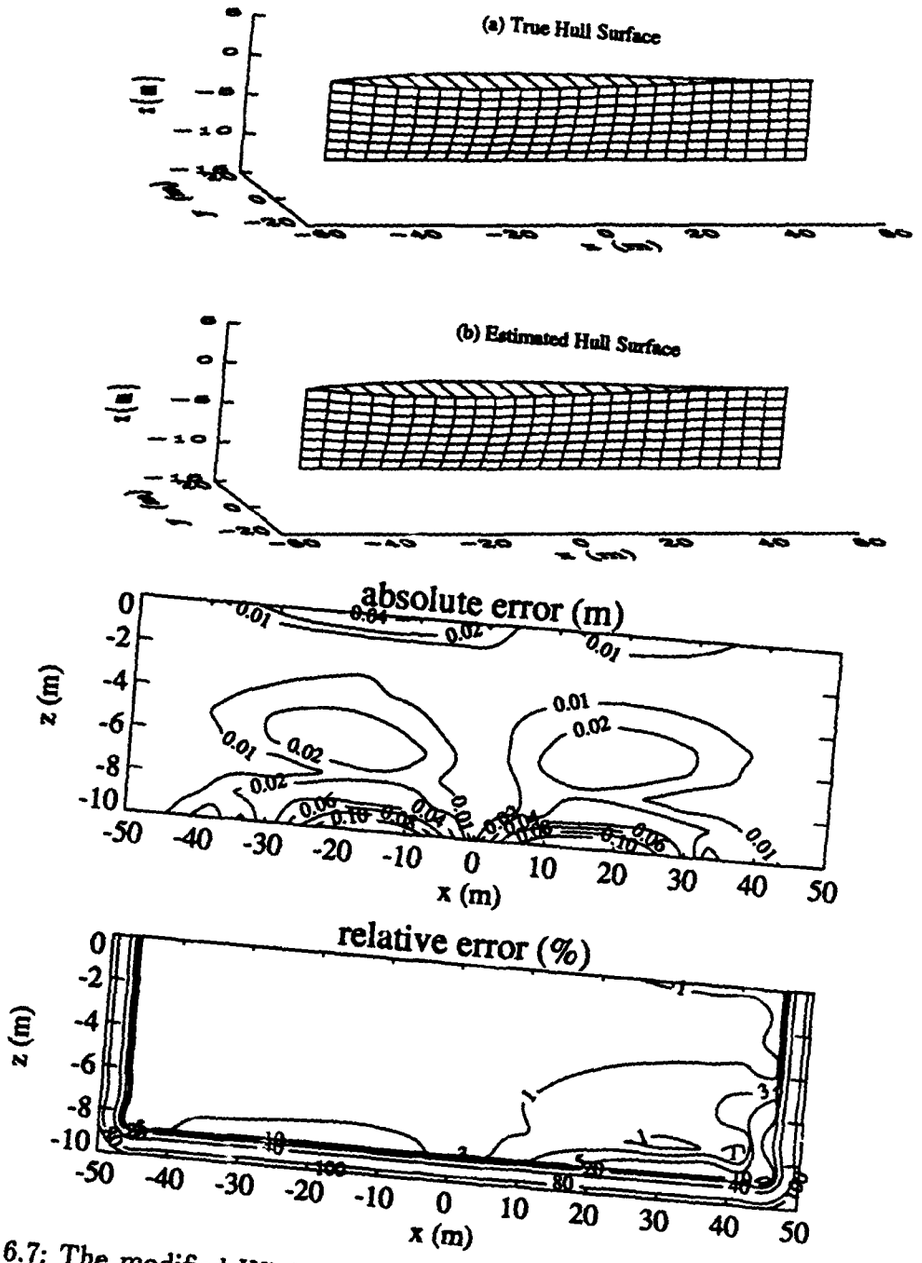

Figure 6.7: The modified Wigley hull recovered from the wave amplitude function with no noise using the constrained ML method, given the parameters $L = 100$ m, $H = 10$ m, $B = 10$ m, $U = 10$ m/s, $M = 6$, $N = 6$, $\gamma_c = 0$. and $\gamma_e = 10^{-6}$

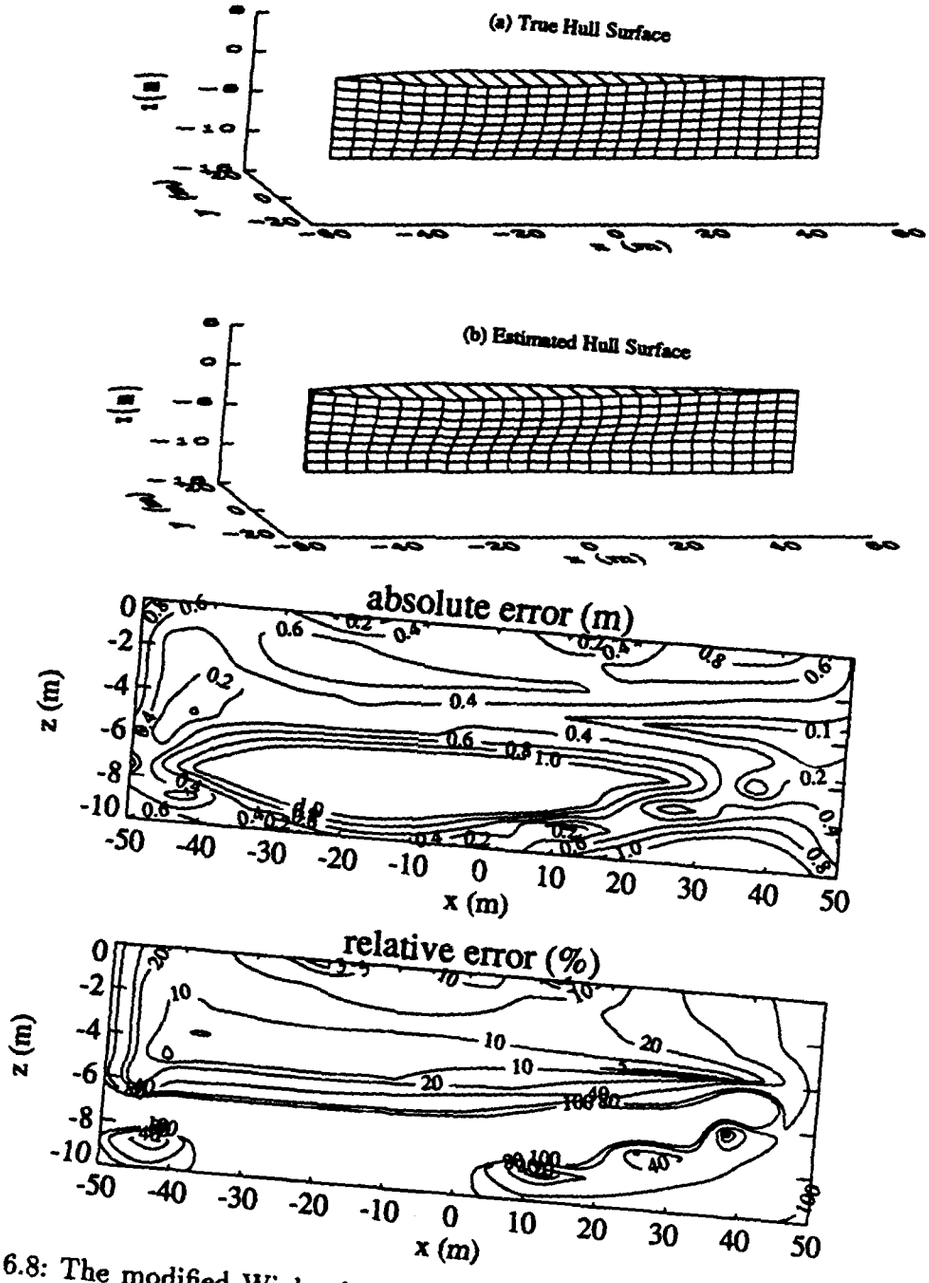

Figure 6.8: The modified Wigley hull recovered from the wave amplitude function with 10% noise using the constrained ML method, given the parameters $L = 100$ m, $H = 10$ m, $B = 10$ m, $U = 10$ m/s, $M = N = 6$, $\gamma_c = 10^{-1}$ and $\gamma_s = 3800$.

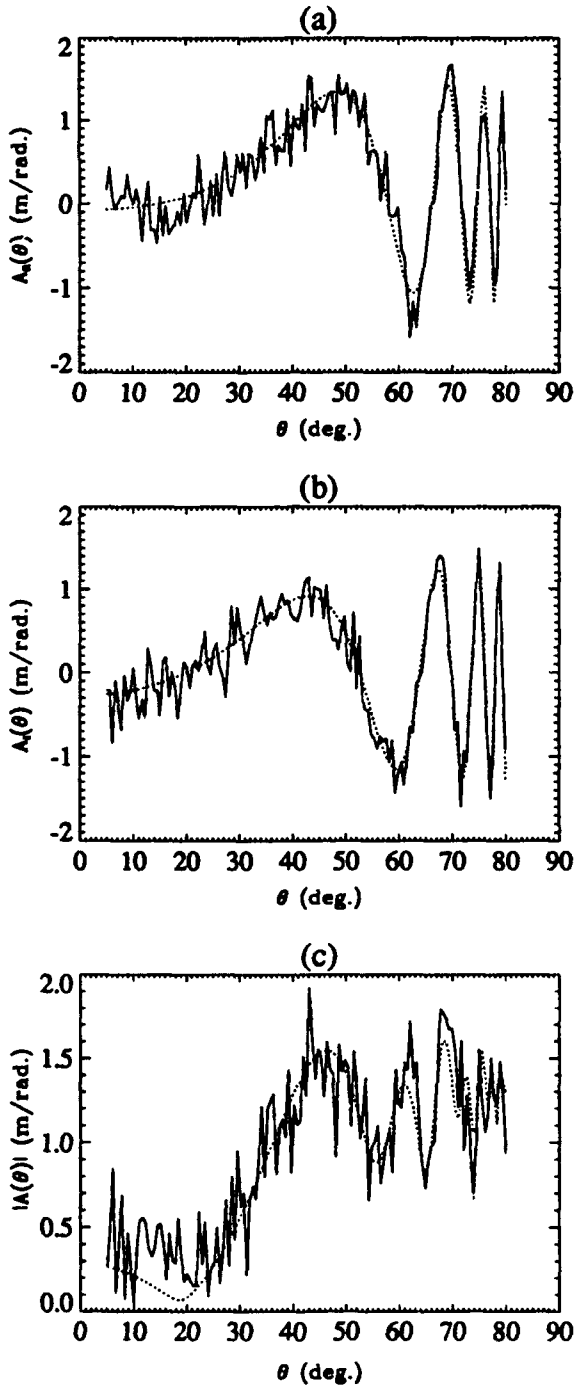

Figure 6.9: (a) The real part, (b) imaginary part, and (c) the magnitude of the wave amplitude function of the Wigley-Cosine hull, given the parameters $L = 100$ m, $H = 10$ m, $B = 10$ m, and $U = 10$ m/s. The dotted lines represent the wave amplitude function with no noise, and solid lines the one with 10% noise.

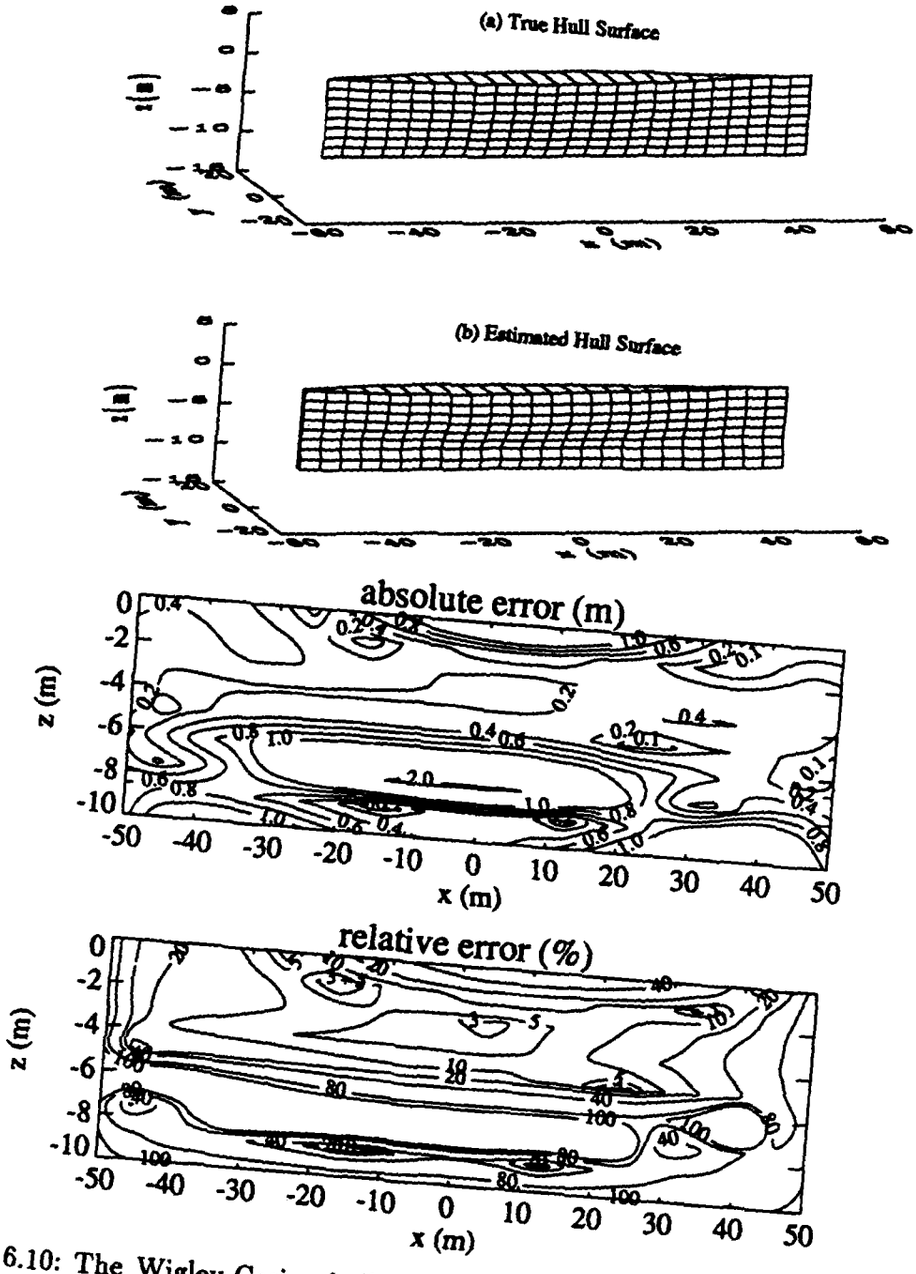

Figure 6.10: The Wigley-Cosine hull recovered from the wave amplitude function with 10% noise using the constrained ML method, given the parameters $L = 100$ m, $H = 10$ m, $B = 10$ m, $U = 10$ m/s, $M = N = 6$, and $\gamma_s = 100$.

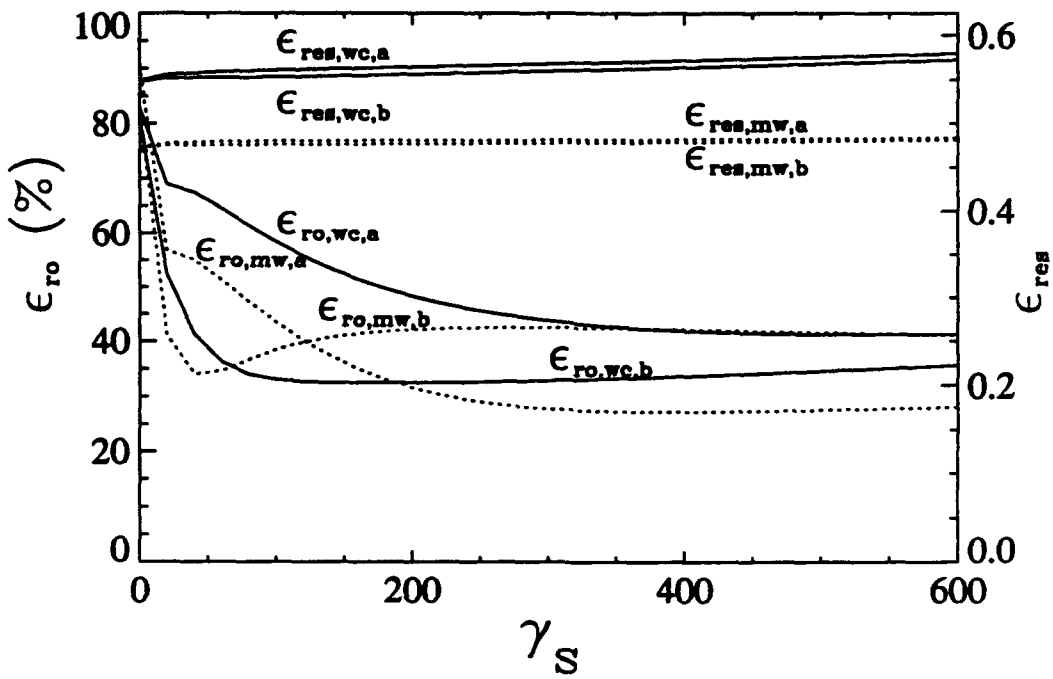

Figure 6.11: Curves of ϵ_{ro} and ϵ_{res} verses γ_s given $\gamma_c = 10^{-3}$ and 10^{-2}, and the parameters $L = 100$ m, $H = 10$ m, $B = 10$ m, $U = 10$ m/s, $M = N = 6$, a 10% noise or error in the input data. In the subscripts of ϵ, "mw" represents the modified Wigley hull, "wc" the Wigley-Cosine hull, "a" denotes $\gamma_c = 10^{-1}$, "b" $\gamma_c = 10^{-2}$.

6.7.3 Estimation of Hull Shape from the Magnitude of the Wave Amplitude Function

It is assumed in this subsection that only the magnitude of the wave amplitude function is available. Thus, the model vectors **c** and **d** will be obtained by solving the extremum problem described in (6.80) and (6.89). In the following, the conjugate gradient method [42] is used to minimize $Q(\mathbf{x}) = (\mathbf{a}_m - \mathbf{f}(\mathbf{x}))^T \mathbf{S}^{-1}(\mathbf{a}_m - \mathbf{f}(\mathbf{x})) + \gamma q_s(\mathbf{x})$, where $q_s(\mathbf{x})$ is a surface smoothness constraint. This multiple-dimensional extremum problem may result in multiple solutions, thus the constraint must be considered. Additionally, an initial vector of **x** needs to be imposed for the conjugate gradient method. To improve problem conditioning, the initial values of the coefficient vector **x** are obtained using the method as shown in Subsection 6.7.1 from a known hull model, given the same hull length and draft and the same numbers of basis functions which will be used in the inversion. In the examples below, the variables of the hull surface functions are assumed not be separable, the numbers of basis functions are taken as $M = 6$ and $N = 6$, and all the constraints are based on the measures of the sum of the squares of the third differences.

The first example is the Wigley-Cosine hull with the same hull parameters as before but with no noise in the input data. The magnitude of the wave amplitude function is shown as a dotted line in Figure 6.9(c). The initial values of the coefficient vector is obtained from the modified Wigley hull given in (6.95), and no constraint is considered. The recovered hull is given in Figure 6.12 together with its error surface contour plots of ϵ_a and ϵ_r. The overall error performances are given as $\epsilon_{ro} = 8.92\%$ and $\epsilon_{res} = 0.0568$.

The next example is the same Wigley-Cosine hull, but 10% noise is considered. The magnitude of the wave amplitude function with noise is shown as a solid line in

$\epsilon_L(\%)$	$\epsilon_H(\%)$	$\epsilon_{A_m}(\%)$	γ_s	ϵ_{res}	ϵ_{ro}
0.0	0.0	0.0	0.0	0.0568	8.92
0.0	0.0	0.0	100.0	0.2845	9.63
10.0	10.0	0.0	0.0	0.5988	24.74
0.0	0.0	10.0	0.0	0.8254	45.32
10.0	10.0	10.0	0.1	0.8977	33.47
10.0	10.0	10.0	100.0	0.8977	28.85

Table 6.3: The error performance of the Wigley-Cosine Hull estimated from the magnitude of the wave amplitude function with $M = N = 6$.

Figure 6.10(c). The hull and draft also have a 10% of error. The initial values of the coefficient vector is obtained from the modified Wigley hull model given in (6.93), and the surface constraint is considered with $\gamma_s = 100$. The recovered hull is shown in Figure 6.13 together with its error surface contour plots of ϵ_a and ϵ_r. The overall error performances are given as $\epsilon_{ro} = 28.85\%$ and $\epsilon_{res} = 0.9037$. Table 6.3 shows the simulation results under different conditions, in which ϵ_L, ϵ_H, ϵ_{A_m} represent the relative errors in L, H and $A_m(\theta)$, respectively.

Finally, we consider the Quapaw hull, a more practical example in which the wave amplitude function is calculated from the spectrum of the wave elevation measured from the tow tank as seen in the previous two chapters. A total of 40 data points of the magnitude of the wave amplitude functions is used in the hull surface estimation, corresponding to wave angles in $[12°, 70°]$. Figure 6.14 shows the magnitude of the wave amplitude function verse wave angles θ for the data RUN5-A and RUN5-B. The hull surface estimated from RUN5-A and RUN5-B are shown in Figure 6.15 and Figure 6.16 together with the error surface contour plots of ϵ_a and ϵ_r for $M = N = 6$. The overall error performances are given as $\epsilon_{ro} = 34.607\%$ and $\epsilon_{res} = 1.335$ for RUN5-

A, and $\epsilon_{ro} = 34.662\%$ and $\epsilon_{res} = 1.250$ for RUN5-B. Figure 6.17 shows the curves of ϵ_{ro} and ϵ_{res} verses γ_s.

In the above, we have demonstrated the examples of ship hull estimation from the wave amplitude functions and their magnitude. From these examples and the simulations with different parameters and conditions, some comments can be made as follows.

(1) When input data are perfect and the hull to be recovered can be exactly expressed using the basis functions, the exact solution of this hull's surface $\zeta(x, z)$ can be obtained in the linear inversion with reasonable numbers of basis functions, for example, $M = 4$ and $N = 3$ for the hull given in (6.93). However, there will be errors in the solution when the input data are not accurate and have noise.

(2) In linear inverse problems, the estimation performance is usually much more sensitive to the noise in the wave amplitude function than the errors on the hull's length and draft. Larger constraining parameters are needed to achieve a better result for larger noise. In addition to a surface constraint, a coefficient constraint is helpful to achieve a stable solution, especially in a severe noise environment.

(3) The smoothness measure based on the sum of the squares of the third differences are more effective than some other measures such as those based on the sum of the squares of the first or second differences.

(4) The error in a hull length L and draft H mainly affects the accuracy of the side edge and bottom edge of the hull in solutions. In general, the relative error in the solutions is larger on the hull's bottom boundary than those on the upper boundary and central part.

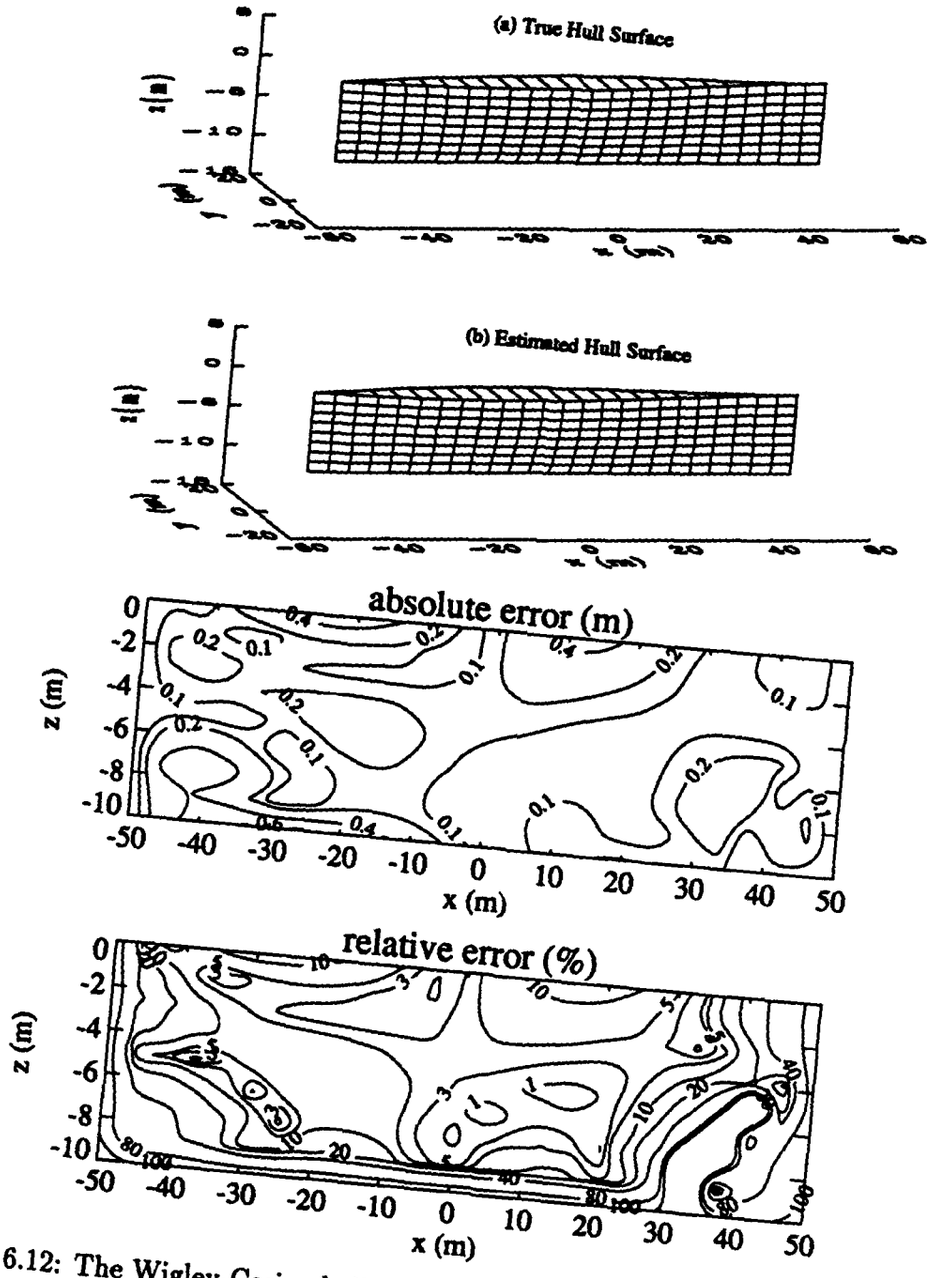

Figure 6.12: The Wigley-Cosine hull recovered from the magnitude of the wave amplitude function with no noise using the conjugate gradient method, given the parameters $L = 100$ m, $H = 10$ m, $B = 10$ m, $U = 10$ m/s and $M = N = 6$, and $\gamma_s = 0$.

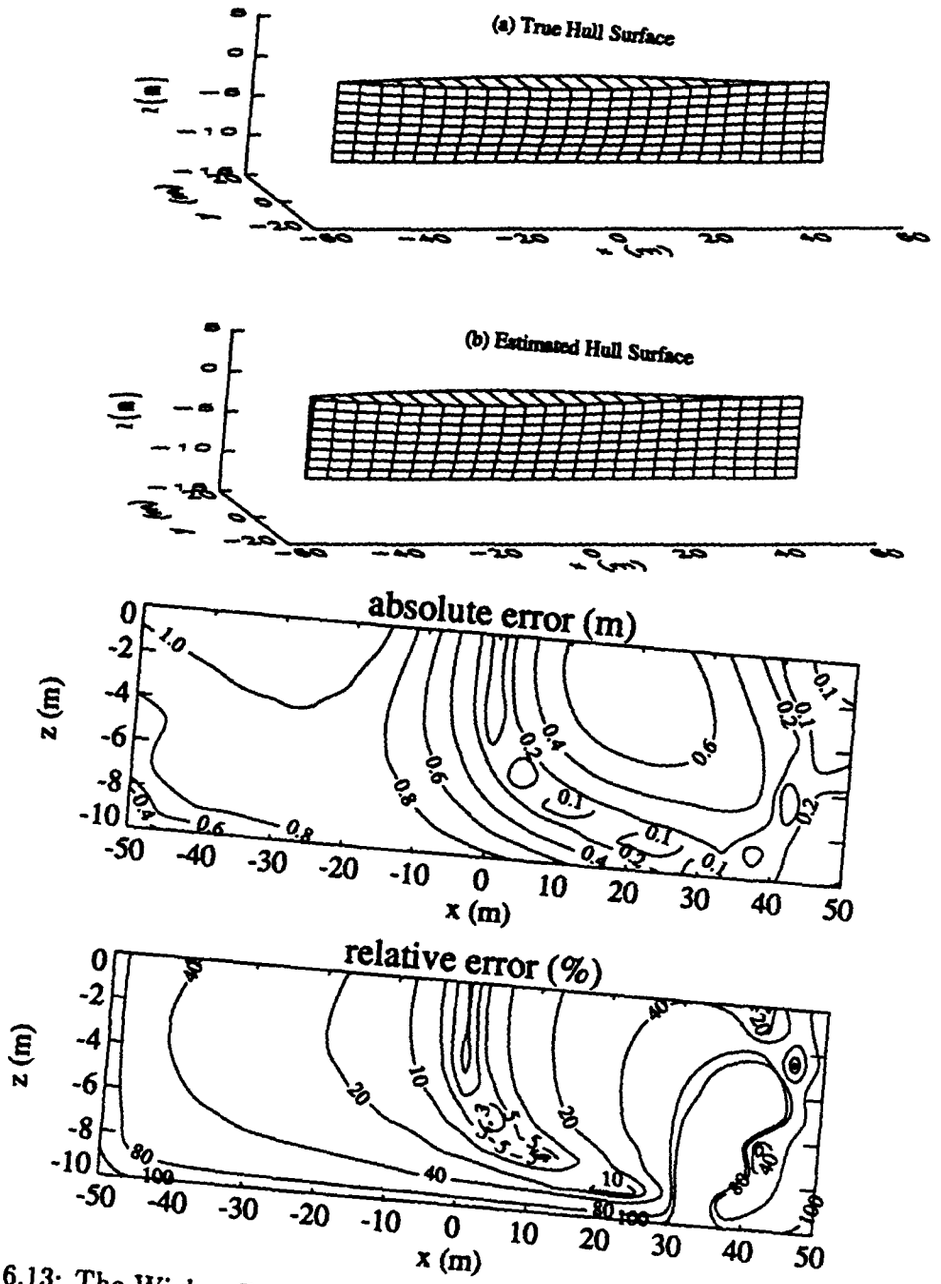

Figure 6.13: The Wigley-Cosine hull recovered from the magnitude of the wave amplitude function with 10% noise, given the parameters $L = 100$ m, $H = 10$ m, $B = 10$ m, $U = 10$ m/s, $M = 6$, $N = 6$, and $\gamma_s = 100$.

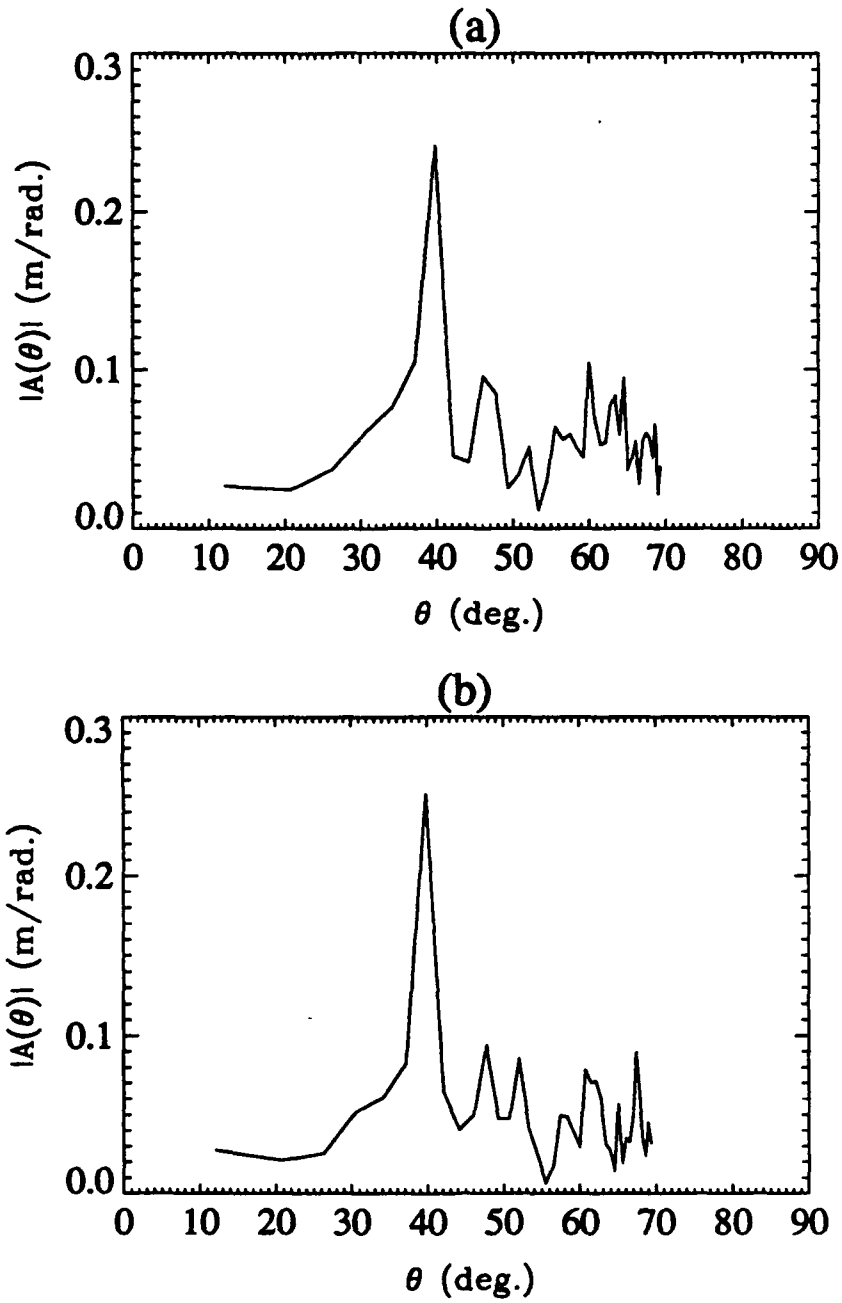

Figure 6.14: The magnitude of the wave amplitude function obtained from the data RUN5-A and RUN5-B for the Quapaw model with $L = 4.953$ m, $H = 0.362$ m, $B = 0.978$ m, and $U = 2.229$ m/s.

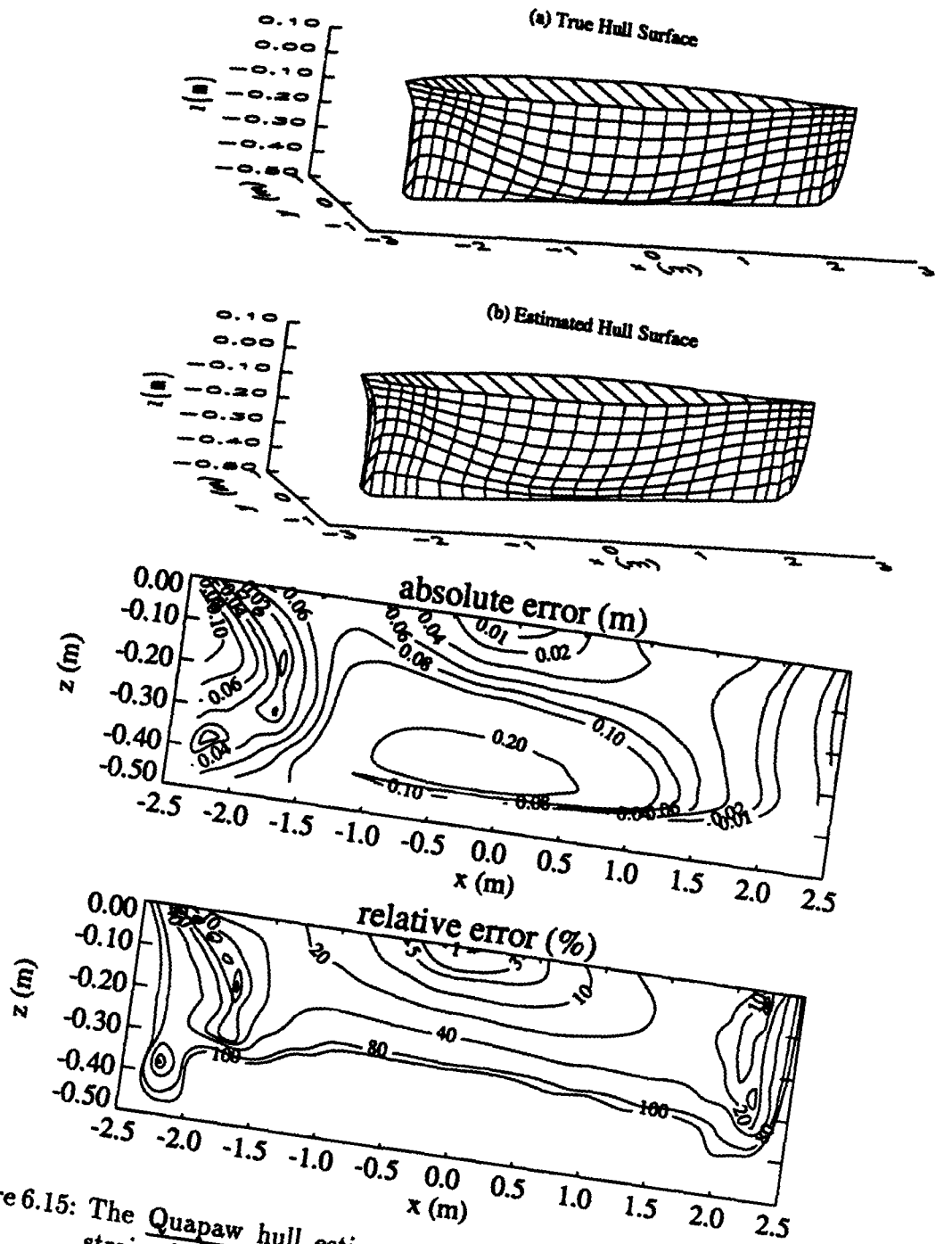

Figure 6.15: The Quapaw hull estimated from the data RUN5-A using the constrained ML method with $M = 6$, $N = 6$, and $\gamma_s = 100$.

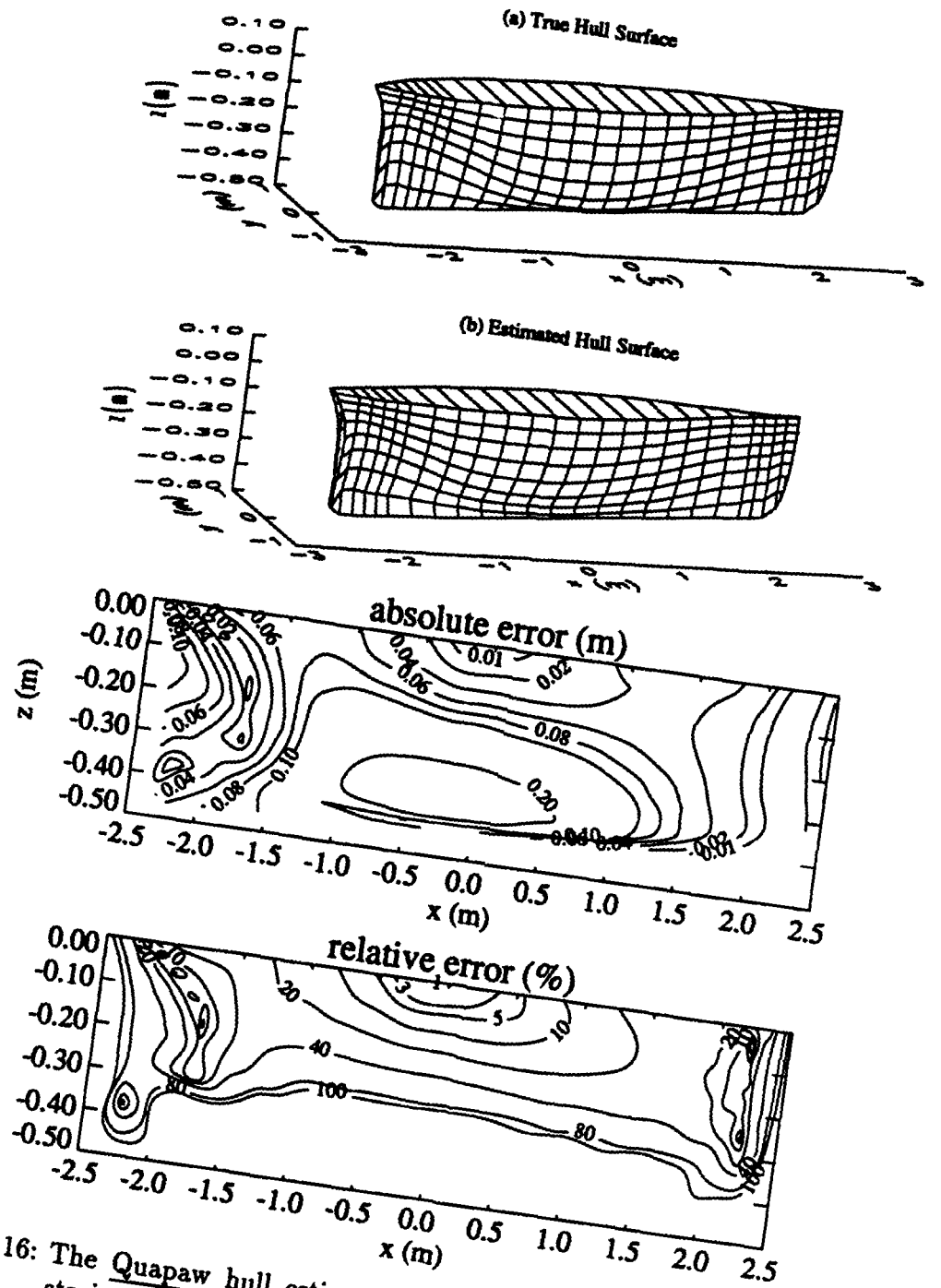

Figure 6.16: The Quapaw hull estimated from the data RUN5-B using the constrained ML method with $M = 6$, $N = 6$, and $\gamma_s = 100$.

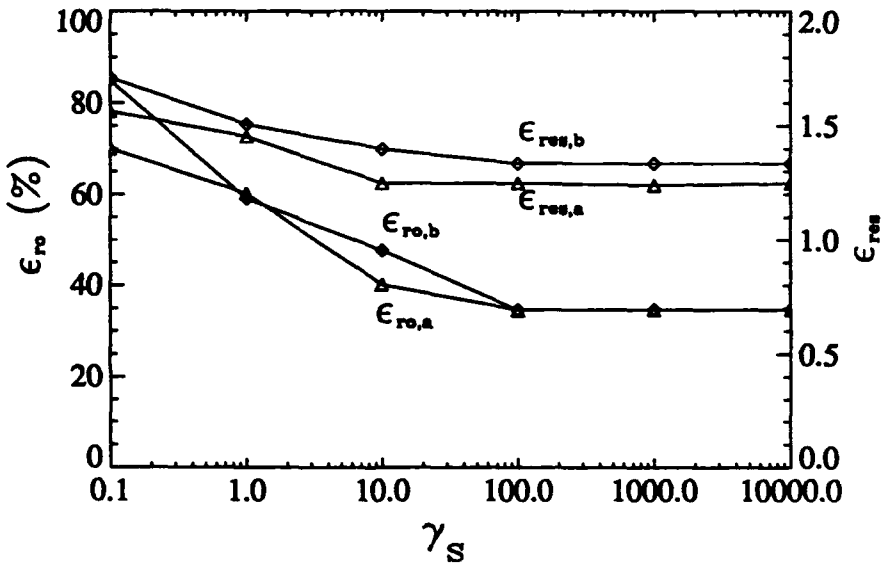

Figure 6.17: Error performance of the Quapaw hull estimated from the data RUN5-A and RUN5-B, given $M = N = 6$. The subscript "a" represents RUN5-A, and "b" RUN5-B.

CHAPTER VII

CONCLUSIONS AND RECOMMENDATIONS

The previous chapters have presented the study on the estimation of a moving ship's speed, direction, length and hull shape from its wave spectra. Deep water, steady waves and the linearized free surface condition are assumed throughout the study.

The estimation of ship speed and direction has relied on the distinct features of the Fourier spectrum of the ship generated waves. The introduction of the concept of the complex wave elevation has been useful in simplifying the derivation of the wave amplitude function from one and two dimensional wave spectra. In general, it is suggested, for high accuracy and the ability to separate background noise, that a ship's speed and direction be estimated from two dimensional wave spectra. However, for high accuracy and easy computation, we suggest that the wave amplitude function be recovered from one dimensional wave spectra.

The extraction of a ship's hull geometry has been based on the relation of the wave amplitude function and the ship geometry under the assumption of the thin-ship theory. The theoretical model developed for the wave amplitude function has explicitly revealed the periodic character of the wave amplitude function and its relation with the ship length. From this model, it is also found that the ship's bow

and stern play a dominant role in the wave amplitude function, and that discontinuities in the hull surface function and its derivatives results in the increase of other frequency components. The real and imaginary parts and the magnitude of the wave amplitude function generally appear to be signals which are both magnitude and angle modulated. The bow and stern's concaveness or convexity have effects on the frequency variation, or the distribution of the zero-crossing points of the wave amplitude function, and may result in over- or underestimation of ship length. The three methods, the spectrum method, zero-crossing method and frequency demodulation method, have shown their effectiveness in the estimation of a ship's length.

The extraction of a ship's geometry information is essentially a linear or nonlinear inverse problem. The ill-conditioning of the kernel matrices is a critical problem in the linear inversion. It has been shown that the constrained maximum likelihood method for hull surfaces or/and coefficients is useful in reducing the effects from this ill-conditioning and the noise present in input data. When the noise components, present in the data of the wave amplitude function, have independent identical Gaussian distributions, the constrained maximum likelihood method and the constrained linear inversion method are equivalent in the case of linear inversion. The uniqueness of the solution is another critical problem in the nonlinear inversion. In addition to holding constraints, the proper choice of the initial coefficient vector has been shown to be helpful in finding the desired solution. In the examples given in Chapter 6, the initial vectors were chosen from the known hull models given the parameters of length and draft. According to simulation results, high accuracy can be achieved when the hulls are recovered from the perfect input data. However, the accuracy decreases, especially at the edges of hulls, when noise is present in input data.

The results from the study show a promising possibility of detecting a moving

ship's characteristics through measuring the ship generated wave pattern. For a practical application of this technique, however, many problems in theory and practice still remain to be investigated and solved. The following are some considerations and recommendations for further study.

(1) The estimation of a ship's length and hull shape given in the study is based on the thin-ship theory. The theory itself has its limitations and weakness. The example of the Quapaw hull has shown that the methods developed under the thin-ship theory are also suitable for fat ships like the Quapaw, however, further investigation of other more general types of hulls will be helpful in understanding the performance and limitation of the methods which have developed.

(2) In the hull inversion, it was assumed that the hull draft was known. However, it is still an open problem - how to estimate the hull draft from ship wave spectra.

(3) The nonlinear inversion described in (6.88) for a variable-separable hull function, having a relatively small size of coefficient vector, has not been tested and needs to be further evaluated.

(4) According to the results of the hull inversion, constraints are important and necessary for obtaining a stable solution with a reasonable accuracy in either linear or nonlinear problems. Thus, we need to search further for an optimal set of constraints, if they exist, to achieve better performance in the hull estimation.

(5) In the above study, constant ship velocity is assumed, thus only a steady ship wave field was considered. However, it may not be always true in practical situations. The effects of a ship's velocity variation and other unsteady effects on the estimations have not been studied. To estimate a ship's characteristics from an unsteady ship wave field, new techniques may need to be developed.

(6) In addition to the techniques developed in this study, another critical problem

existing in the application of remote sensing of a moving ship and extracting its characteristics is how to transform successfully, a remotely sensed image or intensity spectrum to a quantitative wave elevation spectrum. Monaldo and Lyzenga's efforts in the research on the estimation of the wave slope- and height-variance spectra from SAR imagery [5] may be helpful in solving this problem, but further study on it is still needed.

APPENDIX

APPENDIX

WAVE AMPLITUDE FUNCTION WITH ONE DISCONTINUITY

This appendix gives the integration results with the integral

$$A(K_k) = \int_{-1}^{1} F(x) e^{j\nu x} dx \tag{1}$$

and the integrand

$$F(x) = \begin{cases} \sum_{j=0}^{\infty} a_j x^j & \text{for } -1 \le x \le x_b \\ \sum_{j=0}^{\infty} b_j x^j & \text{for } x_b \le x \le 1 \end{cases} . \tag{2}$$

Substituting (2) into (1) yields the results

$$A_R(K_x) = Q_{R_1}(K_x)\cos(\nu - \phi_{R_1}(v)) + Q_{R_2}(K_x, x_b)\cos(x_b\nu - \phi_{R_2}(v, x_b)) \tag{3}$$

$$A_I(K_x) = Q_{I_1}(K_x)\cos(\nu - \phi_{I_1}(v)) + Q_{I_2}(K_x, x_b)\cos(x_b\nu - \phi_{I_2}(v, x_b)) \tag{4}$$

with

$$\begin{aligned} Q_{R_1}(K_x) &= \{[\sum_{i=0}^{\infty}(b_i\, p_{R_i}(\nu, 1) - a_i\, p_{R_i}(\nu, -1))]^2 + \\ &\quad [\sum_{i=0}^{\infty}(b_i\, q_{R_i}(\nu, 1) + a_i\, q_{R_i}(\nu, -1))]^2\}^{\frac{1}{2}} \end{aligned} \tag{5}$$

$$Q_{R_2}(K_x) = \{[\sum_{i=0}^{\infty}(b_i - a_i)\, p_{R_i}(\nu, x_b))]^2 + [\sum_{i=0}^{\infty}(b_i - a_i)\, q_{R_i}(\nu, x_b))]^2\}^{\frac{1}{2}} \tag{6}$$

$$Q_{I_1}(K_x) = \{[\sum_{i=0}^{\infty}(b_i\, p_{I_i}(\nu, 1) - a_i\, p_{I_i}(\nu, -1))]^2 +$$

$$[\sum_{i=0}^{\infty}(b_i\, q_{I_i}(\nu,1) + a_i\, q_{I_i}(\nu,-1))]^2\}^{\frac{1}{2}} \tag{7}$$

$$Q_{I_2}(K_x) = \{[\sum_{i=0}^{\infty}(b_i - a_i)\, p_{I_i}(\nu,x_b))]^2 + [\sum_{i=0}^{\infty}(b_i - a_i)\, q_{I_i}(\nu,x_b))]^2\}^{\frac{1}{2}} \tag{8}$$

$$\phi_{R_1}(\nu) = \tan^{-1}[\frac{\sum_{i=0}^{\infty}[b_i q_{R_i}(\nu,1) + a_i q_{R_i}(\nu,-1)}{\sum_{i=0}^{\infty}[b_i p_{R_i}(\nu,1) - a_i p_{R_i}(\nu,-1)}] \tag{9}$$

$$\phi_{R_2}(\nu,x_b) = \tan^{-1}[\frac{\sum_{i=0}^{\infty}(b_i - a_i) q_{R_i}(\nu,x_b)}{\sum_{i=0}^{\infty}(b_i - -a_i) p_{R_i}(\nu,x_b)}] \tag{10}$$

$$\phi_{I_1}(\nu) = \tan^{-1}[\frac{\sum_{i=0}^{\infty}[b_i q_{I_i}(\nu,1) + a_i q_{I_i}(\nu,-1)}{\sum_{i=0}^{\infty}[b_i p_{I_i}(\nu,1) - a_i p_{I_i}(\nu,-1)}] \tag{11}$$

$$\phi_{I_2}(\nu,x_b) = \tan^{-1}[\frac{\sum_{i=0}^{\infty}(b_i - a_i) q_{I_i}(\nu,x_b)}{\sum_{i=0}^{\infty}(b_i - -a_i) p_{I_i}(\nu,x_b)}] \tag{12}$$

where $p_{R_i}(a,x)$, $q_{R_i}(a,x)$, $p_{I_i}(a,x)$ and $q_{I_i}(a,x)$ are as defined in (5.16)$\sim$ (5.19).

BIBLIOGRAPHY

BIBLIOGRAPHY

[1] William J. Plant, "The microwave measurement of ocean-wave directional spectra," Johns Hopkins APL Technical Digest, Vol.8, No.1, pp. 55-59, 1987.

[2] John F. Vesecky, H. M. Assal, and R. H. Stewart, "Remote sensing of ocean waveheight spectrum using synthetic-aperture-radar images," In: Oceanography From Space, edited by J. F. R. Grow, New YORK: Plenum Press, pp. 449-457, 1981.

[3] John F. Vesecky, and R. H. Stewart, "The Observation of ocean surface phenomena using imagery from the Seasat synthetic aperture radar: An assessment," Journal of Geophysical Research, Vol. 87, pp. 3397-3430, 1982.

[4] John F. Vesecky, R. H. Stewart, R. A. Schuchman, H. M. Assal, E. S. Kasischke, and J. D. Lyden, "On the ability of synthetic aperture radar to measure ocean waves," In: Proceeding IUCRM Symposium on Wave Dynamics and Radio Probing of the Ocean Surface, edited by O. M. Phillips, 1983.

[5] Frank M. Monaldo and David R. Lyzenga, "On the Estimation of wave slope- and height-variance spectra from SAR Imagery," IEEE Trans. on Geoscience and Remote Sensing, Vol. GE-24, No.4, pp. 543-551, July, 1986.

[6] E. O. Tuck, J. I. Collins and W. H. Wells, "On ship wave patterns and their spectra " Journal of Ship Research, Vol. 15, pp. 11-21, 1971.

[7] Part of SAIC (Science Applications International Corporation) Report on inverse Kelvin wake problem, Dec., 1989.

[8] John C. Kuhn, "Considerations of Uniqueness in the Inverse Kelvin Wake Problem," SNAME, H-5 Panel, Analytic Ship Wave Relations, Meeting 90, Jersey City, N.J., Nov., 1990.

[9] John N. Newman, "The inverse ship-wave problem," The Sixth International Workshop on Water Waves and Floating Bodies, MIT, cambridge, Massachusetts, pp. 193-197, April, 1991

[10] Dan E. Dudgeon and Russell M. Mersereau, "Multidimensional digital signal processing," New York: Prentice-Hall, Inc., 1984.

[11] Julius S. Bendat and Allan G. Piersol, "Random data analysis and measurement procedures," 2nd Edition, New York: Wiley-Interscience, John Wiley & Sons, Inc., 1986.

[12] Peter O. Cervenka, "Remote sensing the thermal macrowake," Optical Engineering, Vol. 28, No.7, July, 1989

[13] Jerome H. Milgram "Theory of radar backscatter from short waves generated by ships, with application to radar (SAR) imagery," Journal of Ship Research, Vol. 32, No.1, March, 1988

[14] John N. Newman, "Marine hydrodynamics," Cambridge, Massachusetts: The MIT Press, 1977.

[15] John V. Wehausen and E.V. Laitone, "Surface wave," In Encyclopedia of Physics, Vol.9, Berlin-Gottingen-Heidelberg: Springer-Verlag, 1960.

[16] John V. Wehausen, "The wave resistance of ships," Advances in Applied Mechanics, Vol. 13, pp. 93-245, 1973.

[17] Pao C. Pien and Wilbern L. Moore, "Theoretical and Experimental Study of Wave-Making Resistance of Ships," International Seminar on Theoretical Wave-Resistance, Ann Arbor, Michigan, U.S.A., pp. 131-182, Aug., 1963.

[18] John N. Newman, "The determination of wave resistance from wave measurements and along a partial cut," International Seminar on Theoretical Wave-Resistance, Ann Arbor, Michigan, U.S.A., pp. 351-376, Aug., 1963.

[19] S. D. Sharma, "Some results concerning the wavemaking of a thin ship," Journal of Ship Research, Vol. 15, pp. 72-81, 1969.

[20] W. H. Eggers, S. D. Sharma and L. W. Ward, "An assessment of some experimental methods for determining the wavemaking characteristics of a ship form," Trans. SNAME, Vol. 75, pp. 112-144, 1967.

[21] Ciping Jiang and Shiming Shao, "Ship Resistance," Shanghai, China: Shanghai Jiao Tong University Press, 1984

[22] Carl A. Scragg, Britton Chance, Jr., John C. Talcott and Donald C. Wyatt, "Analysis of wave resistance in the design of the 12-meter yacht Stars & Stripes," Marine Technology, Vol. 24, No. 4, pp. 286-295, Oct. 1987.

[23] T. Inui, T. Takahei, T. Tagori, " A guide note for design of ship model basins with special references to 'wave analysis' work ," International Seminar on Theoretical Wave-Resistance, Ann Arbor, Michigan, U.S.A., pp. 533-555, Aug., 1963.

[24] P. Guevel, G. Delhommeau and J. P. Cordonnier, "Numerical solution of the Newman-Kelvin problem by the method of singularities," 2nd International Conference on Numerical Ship Hydrodynamics, Berkeley, California, pp. 107-123, Sept., 1977.

[25] E. Baba and M. Hara, "Numerical evaluation of a wave-resistance theory for slow ships", 2nd International Conference on Numerical Ship Hydrodynamics, Berkeley, California, pp. 17-29, Sept., 1977.

[26] Francis Nobleses, "A slender-ship theory of wave resistance," Journal of Ship Research, Vol. 27, No.1, pp. 13-33, 1983.

[27] A. Barnell and F. Nobleses "Far field features of the Kelvin wake," 16th Symposium on Naval Hydrodynamic The University of California, Berkeley, California, 1986.

[28] F. Nobleses and D. M. Hendrix, "Near-field nonlinearities and short far-field ship waves," 18th Symposium on Naval Hydrodynamic The University of Michigan, Ann Arbor, Michigan, Aug., 1990.

[29] Fotis A. Papoulias and Robert F. Beck "WAVEAMP: a program for computation of wave elevations created by a ship travelling at a constant speed," Technical Report No. 88-03, Department of Naval Architecture and Marine Engineering, The University of Michigan, Ann Arbor, Michigan, 1988.

[30] Zhijian Wu and Guy A. Meadows, "2-D surface reconstruction of water waves,", IEEE OCEANS'90 Conference Proceeding, Washington, D.C., pp. 416-421, Sept., 1990.

[31] Robert H. Stewart, "Methods of satellite oceanography" Berkeley: University of California Press, 1985.

[32] Simon S. Haykin, "Communication systems," New York: John Wiley & Sons Inc., 2th Edition, 1983.

[33] Lawrence R. Rabiner and Bernard Gold, "Theory and application of digital signal processing," New Jersey: Prentice-Hall, Inc., 1975.

[34] Hildebrand, "Introduction to Numerical Analysis," New York, McGraw Hill, 1974.

[35] Randy S. Roberts, William A. Brown, and Herschel H. Loomis, Jr., "Exploitation of spectral redundancy in cyclostationary signals," IEEE Signal Processing Magazine, pp. 14-36, April 1991.

[36] William A. Gardner, "Computationally efficient Algorithms for cyclic spectral analysis," IEEE Signal Processing Magazine, pp. 38-49, April 1991.

[37] Willianm A. Brown, "On the theory of cyclostationary signals," Ph.D Dissertation, Department of Electrical Engineering and Computer Science, University of California, Davis, 1987.

[38] Steven M. Kay, "Modern Spectral Estimation: Theory and Application," New Jersey: Prentice Hall, 1988.

[39] Y. C. Jenq, "High precision sinusoidal frequency estimator based on weighted least square method," IEEE Trans. on Instrumentation and Measurement, Vol. IM-36,No. 1, March 1987.

[40] John P. Boyd, "Chebyshev & Fourier Spectral methods," Berlin Heidelberg New York: Springer-Verlag, 1989.

[41] A. Messian, "Quantum mechanics," Amsterdam: North-Holland Publishing Company, Vol.1, pp. 468-470, 1961.

[42] William H. Press, P. Flannery, Saul A. Teukosky and William T. Vetterling, "Numerical recipes, the art of scientific computing," New York: Cambridge University Press, 1989.

[43] Azriel Rosenfield and Avinash C. Kak, "Digital Picture Processing," New York: Academic Press, 1982.

[44] Harry L. Van Trees, "Detection, estimation, and Modulation Theory," New York: John Wiley & Sons Inc., 1968

[45] Trung T. Pham, "Maximum likelihood estimation of a class of Non-Gaussian Dendities with Application to l_p Deconvolution," IEEE Trans. on Acoustics, Speech, and Signal Processing, Vol. 37, No. 1, Jan. 1989.

[46] S. Twomey, "Introduction to the mathematics of inversion in remote sensing and indirect measurements," Amsterdam New York: Elsevier Scientific Publishing Company, 1977.

[47] S. Twomey, "Iterative nonlinear inversion methods for Tomographic problems," Journal of the Atmospheric Sciences, Vol. 44 No. 23, Dec., 1987.

[48] E. Yee, K. V. Paulson and G. G. Spepherd, "Minimum cross-entropy inversion of satellite photometer data," Applied Optics Vol. 26, No. 11, pp. 2106-2110, 1987.

[49] C. D. Rodgers, "Retrieval of atmospheric temperature composition from remote measurements of thermal radiation," Reviews of Geophysics and Space Physics, Vol. 14, No. 4, pp. 609-624, 1976.

[50] Stanley C. Solomon, P. B. Hays, and Vincent J. Abreu, "Tomographic inversion of satellite photometry," Applied Optics, Vol. 23, No. 19, pp. 3409-3414, Oct. 1984.

[51] Monson H. Hays, J. S. Lim, and A. V. Oppenheim, "Signal reconstruction from phase or magnitude," IEEE Trans. on Acoustics, Speech, and Signal Processing, Vol. 28, No. 4, pp. 672-680, Dec. 1980.

[52] Monson H. Hays, "The reconstruction of a multidimensional sequence from the phase or magnitude of its Fourier," IEEE Trans. on Acoustics, Speech, and Signal Processing, Vol. 30, No. 2, pp. 140-154, April 1982.

[53] M. Bernabini, P. Carrion, G. Jacovitti, F. Rocca, S. Treitel, and M. Worthington, "Deconvolution and inversion," Blackwell Scientific Publication, 1987.

[54] William Menke, "Geophysical data analysis: discrete inverse theory," San Diego: Academic Press, Inc., 1989.